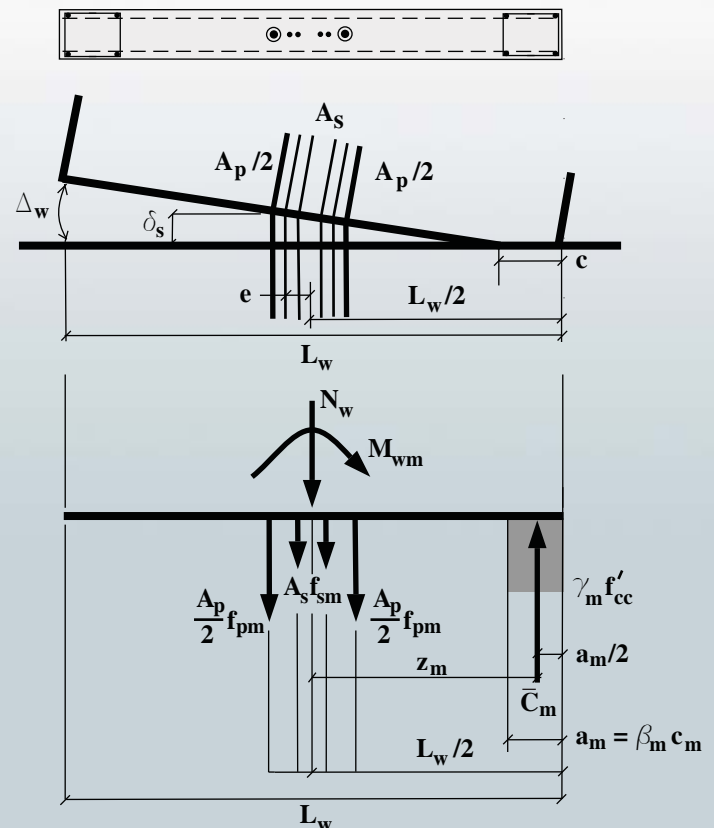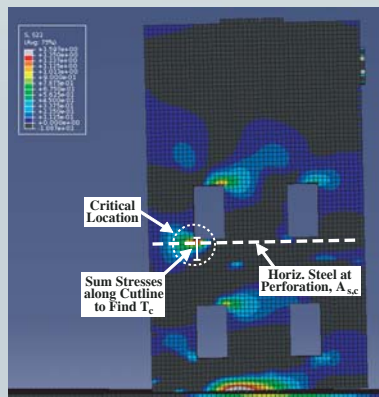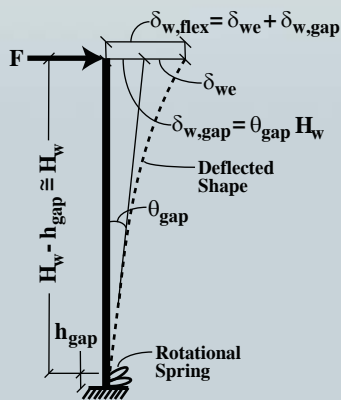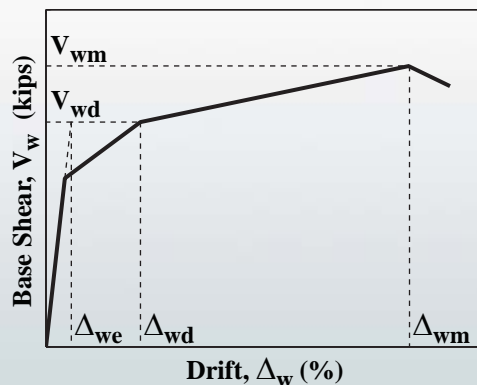# Seismic Design Guidelines for Special Hybrid Precast Concrete Shear Walls

## June 2012

Brian J. Smith and Yahya C. Kurama

## Structural Engineering Research Report

## Department of Civil Engineering and Geological Sciences

### University of Notre Dame

### Notre Dame, Indiana
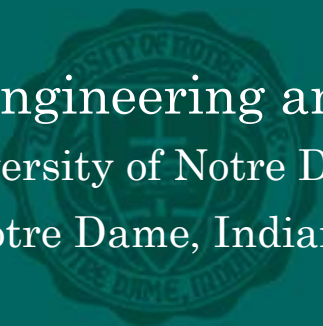
This page intentionally left blank.

# Seismic Design Guidelines for Special Hybrid Precast Concrete Shear Walls

by

## Brian J. Smith

Graduate Research Assistant
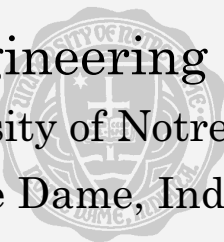
## Yahya C. Kurama

Professor

University of Notre Dame

Structural Engineering Research Report

Department of Civil Engineering and Geological Sciences

University of Notre Dame

Notre Dame, Indiana

This page intentionally left blank.

**TABLE OF CONTENTS**

# ACKNOWLEDGEMENTS

This page intentionally left blank.

# ABSTRACT

This document provides recommended, validated seismic design and analysis guidelines for special unbonded post-tensioned hybrid precast concrete shear walls based on the experimental and analytical results from a research project entitled "*Hybrid Precast Wall Systems for Seismic Regions*" at the University of Notre Dame (Smith et al. 2012a). The most pressing U.S. market need related to hybrid precast walls is code validation subject to the requirements of the American Concrete Institute (ACI). In accordance with this need, the primary goal of this project was to develop the required experimental validation and the associated design and analytical studies for the classification of the hybrid system as "special" reinforced concrete shear walls for use in moderate and high seismic regions of the U.S. The project aimed to develop a structure with improved performance while utilizing practical construction details through the active guidance of a relevant industry advisory panel.

The design and analysis guidelines in this document were validated using the measured behaviors from six 0.4-scale wall test specimens (four solid and two perforated walls) subjected to service-level gravity loads combined with reversed-cyclic lateral loading. The analytical tools intentionally incorporate simplifying assumptions appropriate for the design office. The behavior of the test specimens was measured using conventional data acquisition techniques as well as full-field three-dimensional digital image correlation (a non-contact optical technique), providing unprecedented information on the wall performance. Ultimately, the recommendations contained in this document are aimed to allow practicing engineers and precast concrete producers to design ACI-compliant special hybrid shear walls with predictable and reliable seismic behavior. A detailed design example demonstrating a step-by-step application of the design procedure is also provided.

This page intentionally left blank.

# CHAPTER 1

# INTRODUCTION

This document provides seismic design guidelines, including a design example, for special unbonded post-tensioned hybrid precast concrete shear walls based on the experimental and analytical results from a research project entitled *"Hybrid Precast Concrete Shear Walls for Seismic Regions"* conducted at the University of Notre Dame. The design procedures include specific recommendations and analysis tools to ensure that the structure can achieve the required lateral strength, displacement capacity, energy dissipation, and self-centering without undergoing undesirable failure mechanisms under seismic loads. The design of rectangular perforations within the wall panels is also addressed. The design and analysis guidelines outlined in the document have been validated using the measured and predicted behaviors of six 0.40-scale wall specimens that were tested as part of the project, which can be found in the Final Project Report (Smith et al. 2012a).

## 1.1 DESCRIPTION OF STRUCTURAL SYSTEM

Since the early 1990s, researchers have been investigating the behavior and design of precast concrete structures subjected to seismic loading. Two distinct construction concepts have been studied, namely "emulative" and "non-emulative" precast structures. Emulative precast systems are designed and detailed such that their behavior under lateral loading is similar to the behavior of conventional monolithic cast-in-place reinforced concrete structures. Unlike these systems, the behavior of non-emulative precast concrete structures under lateral loads is governed by the opening and closing of gaps at the joints between the precast members, resulting in distinctly different characteristics. The hybrid precast shear wall structure discussed in this document is a type of non-emulative system. As specified in Section 21.10.3 of ACI 318 (2011), the minimum experimental evidence needed to achieve code-validation for hybrid walls as "special" reinforced concrete shear walls is described in ACI ITG-5.1 (2007). Guidelines and recommendations for the design of special unbonded post-tensioned precast shear walls can be found in ACI ITG-5.2 (2009).

Hybrid precast walls offer high quality production, relatively simple construction, and excellent seismic characteristics by providing self-centering to restore the building towards its original undisplaced position (i.e., the wall returns to its undisplaced "plumb" position after a large earthquake) as well as energy dissipation to control the lateral displacements during an earthquake. As shown in Figure 1.1, the system investigated in this project is constructed by stacking rectangular precast wall panels along horizontal joints above the foundation and at the floor levels. Fiber-reinforced non-shrink dry-pack grout is used at these joints for the alignment/bearing of the wall panels and to allow for construction tolerances during erection. The term "hybrid" reflects that a combination of mild (i.e., Grade 60) reinforcing steel and high-strength unbonded post-tensioning (PT) steel is used for lateral resistance across the joints. The PT force is provided by multi-strand tendons placed inside ungrouted ducts (to prevent bond between the steel and concrete) through the wall panels and the foundation. The PT force, in

combination with the gravity loads acting on the wall, provides the system with self-centering capability while the mild steel bars crossing the base joint are designed to yield and dissipate energy, thus creating an efficient structure. To prevent significant gap opening at the upper panel-to-panel joints, a small amount of mild steel reinforcing bars, designed to remain linear-elastic with short unbonded lengths, are placed at the panel ends as shown in Figure 1.1.

Under the application of lateral loads into the nonlinear range, the primary mode of displacement in a well-designed hybrid precast wall occurs through gap opening at the horizontal joint between the base panel and the foundation (i.e., the base joint or base-panel-to-foundation joint). In comparison, the flexural and shear deformations of the wall panels do not contribute significantly to the lateral displacements of the structure. In other words, the wall essentially behaves as a rigid body rotating above its foundation. This behavior results in a smaller amount of concrete cracking in the hybrid shear wall system than the cracking that would be expected in a conventional monolithic cast-in-place reinforced concrete wall system at a similar lateral displacement.
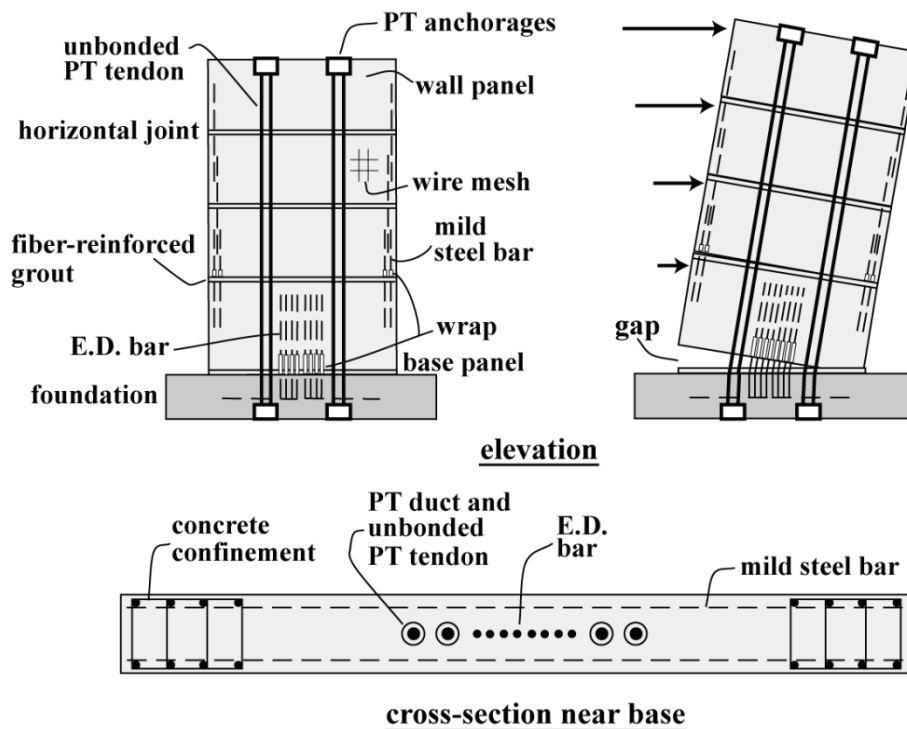


**Figure 1.1  Elevation, Exaggerated Displaced Position, and Cross Section of Hybrid Wall**

Upon unloading, the PT steel provides a vertical restoring force (in addition to the gravity load acting on the wall) to close the gap at the base joint, thus significantly reducing the residual (i.e., permanent) lateral displacements of the structure after a large earthquake. The PT tendons are connected to the structure only at the end anchorages. The use of unbonded tendons reduces the strand strains as well as the tensile stresses transferred to the concrete as the tendons elongate under lateral loading (thus, preventing or delaying the yielding of the strands and reducing the cracking of the concrete in the wall panels). Further, the tendons are placed near the centerline (i.e., mid-length) of the wall to minimize the strand elongations and to keep the tendons outside of the critical confined concrete regions at the wall toes.

The mild steel bars crossing the base joint, referred to as energy dissipating (E.D.) steel in this document, are designed to yield in tension and compression, and provide energy dissipation through the gap opening/closing behavior of the wall under reversed-cyclic loading. A pre-determined length of these bars is unbonded at the base joint (by wrapping the bars with plastic sleeves) to limit the steel strains and prevent low-cycle fatigue fracture. The E.D. bars should be designed and detailed to develop the maximum steel strains and stresses (including strain hardening) that are expected to occur during a large earthquake.

While the gap opening behavior designed at the base joint of hybrid precast walls leads to a reduced amount of concrete cracking, localized compression damage should be expected at the toes of the base panel (about which the wall rotates at the base). Under a large ground motion, the cover concrete at the wall toes will be damaged and possibly spall. This damage is deemed acceptable and should be repairable if necessary. However, excessive deterioration of the core concrete is undesirable, and accordingly, confinement reinforcement in the form of closed hoops should be placed at the ends of the base panel to prevent the compression failure of the core concrete. The dry pack grout placed at the base joint should also be made ductile by utilizing fibers within the grout mix design.


## 1.2 INTENT AND APPLICATION OF DOCUMENT

This document contains specific seismic design, detailing, and analysis guidelines and recommendations to be used by practicing engineers and precast concrete producers for the application of hybrid precast concrete walls as special reinforced concrete shear walls in moderate and high seismic regions of the U.S. The document can be used to design hybrid walls with height-to-length ($H_w/L_w$) aspect ratios equal to or greater than 0.5 in low to mid-rise structures with a practical height limitation of 120-ft (approximately eight to ten stories tall). The design procedure is applicable to both single-panel wall systems (featuring only the base-panel-to-foundation joint) as well multi-panel wall systems (featuring the base-panel-to-foundation as well as upper panel-to-panel joints) with our without panel perforations.

The document makes specific recommendations discussing key design aspects and material assumptions as well as critical steel reinforcing bar placement and details across the horizontal joints and within the wall panels. Both a performance-based design procedure and a prescriptive design procedure are provided. Where appropriate, ACI 318 (2011) design requirements for conventional monolithic cast-in-place reinforced concrete structures are utilized to help in the adoption of the hybrid wall design guidelines by practicing engineers. Furthermore, applicable references and suggested revisions to the design recommendations and requirements in ACI ITG-5.2 (2009) are included. A detailed design example demonstrating a step-by-step application of the design process is provided in Appendix A.

The design and analysis guidelines outlined in this document were validated using the measured and predicted behaviors of six 0.4-scale wall test specimens (four solid and two perforated walls) subjected to service-level gravity loads combined with quasi-static reversed-cyclic lateral loading (Smith et al. 2012a). The analytical modeling tools include a linear-elastic effective stiffness model and a basic finite element model for nonlinear monotonic pushover analysis as design

aids. The finite element model is especially needed for the design of walls with panel perforations. The analytical modeling recommendations intentionally incorporate simplifying assumptions appropriate for the design office. The document also describes a detailed fiber element model that can be used to conduct reversed-cyclic and dynamic analyses of hybrid walls; however, this model is not a necessary tool for seismic design.


## 1.3 ORGANIZATION OF DOCUMENT

The remainder of this document is organized as follows:

- Chapter 2 provides a brief overview of background information relevant to hybrid precast concrete shear wall systems.
- Chapter 3 presents analytical modeling guidelines and recommendations.
- Chapter 4 describes the performance-based seismic design and detailing methodology.
- Chapter 5 presents the prescriptive seismic design and detailing methodology.
- Chapter 6 describes a methodology for the design of perforations within the wall panels.
- Finally, the end of the report provides a list of references, important definitions, and notations (i.e., symbols), as well as a detailed design example (Appendix A).

# CHAPTER 2

## BACKGROUND

This chapter provides a brief overview on the emergence of precast concrete shear wall structures for seismic regions, including previous research on hybrid precast walls. Since the 1990s, several research programs have investigated the seismic behavior and design of non-emulative precast shear walls. Earlier studies focused on fully post-tensioned walls with no E.D. steel reinforcement crossing the horizontal joints (Kurama et al. 1999a,b, 2002; Rahman and Restrepo 2000; Perez et al. 2003, 2007; Restrepo 2003). The biggest limitation for the use of fully post-tensioned walls in seismic regions is that the energy dissipation of these structures is very small; and thus, their lateral displacements during an earthquake can be considerably larger than the displacements of a comparable monolithic cast-in-place wall with the same lateral strength and stiffness. Therefore, a number of researchers have investigated the use of supplemental energy dissipation, such as friction dampers, fluid dampers, and yielding metal dampers, to reduce the seismic displacements of fully post-tensioned precast walls (Priestley et al. 1999; Kurama 2000, 2001; Ajrab et al. 2004; Perez et al. 2004a,b).

Previous research on precast concrete shear walls featuring panel perforations is extremely limited. Mackertich and Aswad (1997) developed a linear-elastic finite element analytical model for precast walls with rectangular panel perforations. Using a nonlinear finite element model, Allen and Kurama (2002) investigated the design of rectangular perforations in fully post-tensioned walls under combined gravity and lateral loads. The research identified the critical regions of the wall panels around the perforations and proposed a methodology to design the reinforcement in these regions so that the perforations would not affect the seismic performance of the wall.

Previous studies are also available on hybrid precast walls that use yielding mild (E.D.) steel reinforcing bars for energy dissipation. Three hybrid walls were tested under quasi-static reversed-cyclic lateral loading in New Zealand as follows. Rahman and Restrepo (2000) tested two identical specimens, with the exception that gravity load was applied on one wall but not the other. An additional hybrid wall, which used steel-fiber reinforced concrete and carbon fiber PT tendons, was tested by Holden et al. (2001, 2003). This specimen had a faulty construction detail near the critical joint at the base and did not produce desirable results. However, one of the walls tested by Rahman and Restrepo (2000) showed excellent behavior, sustaining drifts in excess of ±3.0% while maintaining its lateral strength, energy dissipation, and ability to self-center. The observed concrete damage after the test was limited to cover concrete spalling at the toes of the wall and minimal cracking near the base. The study concluded that hybrid precast walls can resist lateral loads with a reduced amount of structural damage during a major earthquake, with adequate energy dissipation and the absence of significant post-earthquake residual drifts.

These previous experimental studies on hybrid precast walls featured specimen configurations using a single panel over the entire height of the structure; and therefore, the tests focused on the behavior at the base joint and did not explore the behavior at the upper panel-to-panel joints that would be needed in multi-panel systems. The specimens were solid walls and did not include any

panel perforations, which are common for utility and/or security purposes in U.S. building practice (e.g., in the case of a parking garage). Also, ACI code validation was not an objective of the previous experiments; and thus, the wall specimens were not necessarily designed and tested to satisfy the validation requirements prescribed in ACI ITG-5.1 (2007).

Additional experimental studies on building structures with solid hybrid precast shear walls are described in Fleischman et al. (2005a,b) and Nagae et al. (2011). The project described by Fleischman et al. (2005a,b) focused on the development of a seismic design methodology for precast concrete floor diaphragms. The research combined finite element analyses of diaphragms, full-scale component experiments, and shake-table tests of a half-scale three-story structure that featured hybrid walls with a single joint at the base. Nagae et al. (2011) tested two full-scale, four-story buildings on the NIED E-Defense shake table in Japan. One specimen utilized a conventional cast-in-place reinforced concrete structural system with shear walls and moment frames, and the other specimen utilized solid hybrid precast concrete shear walls (featuring multiple wall panels post-tensioned together across horizontal joints) and precast frames. The goal of the project was to develop comparative shake table data on the response of conventional and precast concrete structures over a spectrum of earthquake intensities, including near-collapse. While the experimental portions of both of these major research projects have been completed, detailed results from the studies have not yet been published.

The research that formed the basis for this Design Procedure Document specifically focused on the ACI requirements for the use of hybrid precast walls as special reinforced concrete shear walls in seismic regions. In accordance with Section 21.10.3 of ACI 318 (2011), the primary objective of the project was to experimentally and analytically validate the hybrid wall system according to the guidelines, prerequisites, and requirements in ACI ITG-5.1 (2007). To achieve this objective, six 0.40-scale wall specimens were tested under quasi-static reversed-cyclic lateral loading combined with gravity loads. The measured behavior of the walls, which featured multiple horizontal joints and panel perforations, demonstrated that the hybrid precast wall system can satisfy all of the requirements for special reinforced concrete shear walls in seismic regions with improved performance, while also revealing important design, detailing, and analysis considerations to prevent undesirable failure mechanisms. Full details from the research can be found in Smith and Kurama (2009, 2010a,b) and Smith et al. (2010, 2011a,b,c, 2012a,b,c,d).

The analytical study conducted as part of this project built upon previous research by Kurama (2002), which developed a model with fiber elements to represent the precast wall panels. The unbonded PT steel and the unbonded lengths of the E.D. bars were modeled with truss elements. Using this model, Kurama (2002) conducted a parametric study to investigate the seismic behavior of hybrid walls with varying amounts of E.D. and PT steel reinforcement. Based on nonlinear dynamic time-history analyses, it was shown that the yielding of the E.D. reinforcement results in a considerable reduction in the lateral displacements of the walls, with no significant effect on the self-centering capability. A subsequent study (Kurama 2005) proposed a seismic design approach for the hybrid wall system based on the analyses of two prototype walls designed for different seismic performance objectives. Overall, these previous analytical studies revealed several important advantages of hybrid precast walls subjected to earthquake loading as compared to fully post-tensioned walls with no E.D. steel reinforcement.

# CHAPTER 3

## ANALYTICAL DESIGN TOOLS

This chapter provides general recommendations and guidelines on three different analysis tools that can be used in the seismic design and analysis of hybrid precast concrete shear walls: (1) a linear-elastic effective stiffness model; (2) a simplified nonlinear finite element model; and (3) a detailed fiber element model. The linear-elastic effective stiffness model can be used as part of the equivalent lateral force procedure in ASCE 7 (2010). The finite element model can be used for the design of panel perforations as well as to conduct nonlinear pushover analyses. The fiber element model can be used to conduct reversed-cyclic and dynamic analyses of the walls.

The analytical models intentionally incorporate several simplifying assumptions appropriate for the design office and have been validated based on the results from the experimental program. The finite element and fiber element models were developed using the ABAQUS (Hibbitt et al. 2009) and DRAIN-2DX (Prakash et al. 1993) programs, respectively. As a result, some of the modeling terminology may be specific to these programs. However, the assumptions, guidelines, and philosophies used in the creation of these models could be successfully applied to other analysis platforms as well, such as SAP2000 (CSI 2008), OpenSees (Mazzoni et al. 2007), and ANSYS (ANSYS Inc. 2009).

## 3.1 LINEAR-ELASTIC EFFECTIVE STIFFNESS MODEL

The lateral displacements of a hybrid precast concrete shear wall after the initiation of gap opening but prior to the significant nonlinear behavior of the concrete at the wall toes and significant yielding of the E.D. reinforcement crossing the base joint can be modeled using a reduced, linear-elastic, effective stiffness model. The total roof displacement of the wall can be written as:

$$\delta_w = \delta_{w,flex} + \delta_{w,sh} \tag{3.1}$$

where, $\delta_w$=total displacement at the top of the wall; $\delta_{w,flex}$=wall displacement due to flexural deformations; and $\delta_{w,sh}$=wall displacement due to shear deformations. The flexural displacements of the linear-elastic effective stiffness model can be calculated using Section 3.1.1 and the shear deformations can be calculated using Section 3.1.2.

### 3.1.1 Effective Flexural Stiffness

The flexural displacements of a hybrid wall after gap opening at the base but before significant material nonlinearity can be modeled using an effective moment of inertia, $I_e$ of the wall cross section that accounts for the extent of gap opening. An expression for $I_e$ is developed using the model in Figure 3.1, where the lateral displacements of the wall due to gap opening are represented by a rotational spring. The total flexural roof displacement can be written as:

$$\delta_{w,flex} = \delta_{we} + \delta_{w,gap} \tag{3.2}$$

where, $\delta_{we}$=component of $\delta_{w,flex}$ due to linear-elastic flexural deformations over the wall height; and $\delta_{w,gap}$=component of $\delta_{w,flex}$ due to gap opening at the wall base.
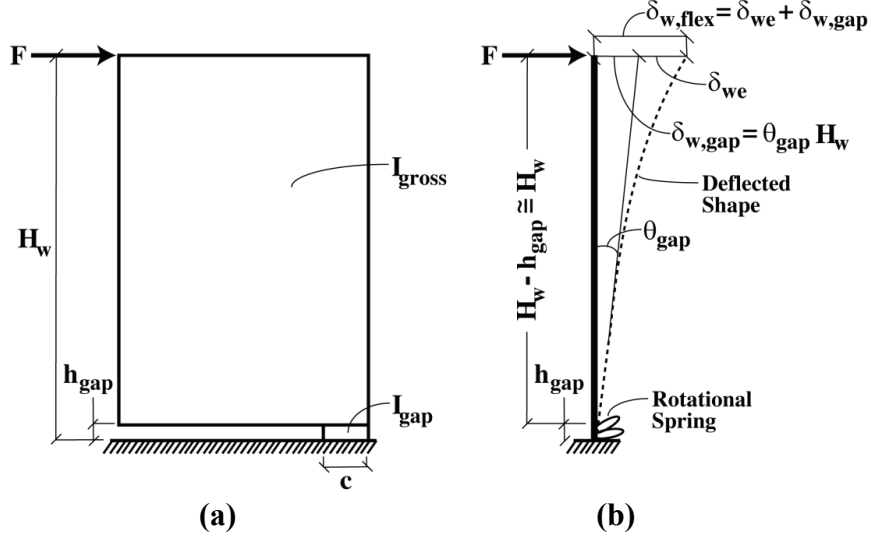


**Figure 3.1 Linear-Elastic Effective Stiffness Model:**
**(a) Elevation View of Idealized Wall; (b) Idealized Deflected Shape**

Using the deflection equation for a linear-elastic cantilever, $\delta_{we}$ can be determined as:

$$\delta_{we} = \frac{FH_w^3}{3E_cI_{gross}} \tag{3.3}$$

where, $F$=applied lateral force at the top of the wall; $H_w$=wall height; $E_c$=Young's modulus for concrete; and $I_{gross}$=moment of inertia of the gross wall cross section [see Figure 3.1(a)]. For perforated walls, $I_{gross}$ should be calculated based on the cross-section of the wall at the location of the panel perforations.

The rotation, $\theta_{gap}$ of the wall due to gap opening at the base can be idealized by considering the cross section in compression (i.e., the contact region at the base joint) over an assumed height, $h_{gap}$. Then, using the rotation equation for a linear-elastic cantilever

$$\theta_{gap} = \frac{Fh_{gap}^2}{2E_cI_{gap}} \tag{3.4}$$

where, $I_{gap}$=moment of inertia of the wall base in contact with the foundation. An expression for $I_{gap}$ can be written as:

$$I_{gap} = \frac{t_wc^3}{12} \tag{3.5}$$

14

where, $t_w$=wall thickness; and $c$=contact length (or neutral axis length) of the wall at the base. The corresponding displacement at the top of the wall can be determined as

$$\delta_{w,gap} = \theta_{gap}H_w \tag{3.6}$$

Equating $\delta_{w,flex}$ to the top deflection of a linear-elastic wall with an effective moment of inertia, $I_e$, it can be written that:

$$\frac{FH_w^3}{3E_cI_{gross}} + \frac{Fh_{gap}^2H_w}{2E_cI_{gap}} = \frac{FH_w^3}{3E_cI_e} \tag{3.7}$$

Finally, using Eqn. 3.7, the effective moment of inertia, $I_e$, can be written as:

$$I_e = \frac{2I_{gross}I_{gap}H_w^3}{3I_{gross}h_{gap}H_w^2 + 2I_{gap}H_w^3} \tag{3.8}$$

Figure 3.2 plots $I_e/I_{gross}$ versus $c/L_w$ (where, $L_w$=wall length) for one of the solid wall specimens tested as part of this project. The thin curves, which are plotted using Eqn 3.8 for different values of $h_{gap}$ ranging from $0.02H_w$ to $0.10H_w$, are compared with the results (thick red curve) obtained from a detailed fiber element model of the wall (this model is described subsequently in Section 3.3). It can be seen that Eqn. 3.8 with $h_{gap}=0.06H_w$ provides a reasonable estimate to the behavior from the fiber element model.

Assuming, for design purposes, that the gap opening extends over 82.5% of the wall length (i.e., $c=0.175L_w$), the linear-elastic effective flexural stiffness of the structure can be determined using Eqn. 3.8 and $h_{gap}=0.06H_w$ as:

$$I_e = 0.50I_{gross} \tag{3.9}$$
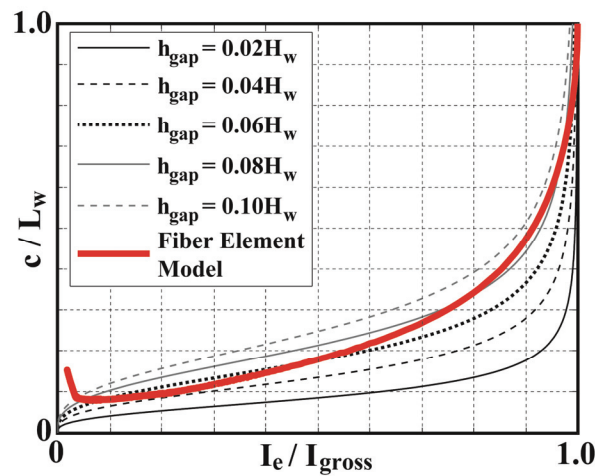


**Figure 3.2** $I_e/I_{gross}$ versus $c/L_w$ for Linear-Elastic Effective Stiffness Model

### 3.1.2 Effective Shear Stiffness

Since concrete cracking remains small, the shear deformations of a hybrid precast concrete wall are typically significantly less than the flexural deformations. However, shear deformations should still be accounted for within the linear-elastic effective stiffness model, especially for walls with aspect ratios, $H_w/L_w$ less than 4.0 and for walls with panel perforations. The wall roof displacement due to shear deformations, $\delta_{w,sh}$ can be determined using the deflection equation for a linear-elastic cantilever, such that:

$$\delta_{w,sh} = \frac{FH_w}{G_c A_{sh}}$$

(3.10)

where, $G_c$=concrete shear modulus; and $A_{sh}$=shear area of the wall cross section. For design purposes, the concept of an effective shear area can be utilized, with the following assumption for solid walls:

$$A_{sh} = 0.8 A_{gross}$$

(3.11)

where, $A_{gross}=L_w t_w$=gross area of the wall cross section.

For perforated walls, the shear deformations are considerably increased and the effective shear area, $A_{sh}$ should be taken as the gross cross-sectional area of only the exterior vertical chord on the compression side of the base panel (i.e., the compression vertical chord located outside of the perforations) without the 0.8 factor. The other vertical chords located on the tension side of the wall and in between the perforations do not contribute significantly to the shear stiffness; and thus, should not be included in the effective shear area. This is because the exterior vertical chord on the tension side of the wall carries only a small portion of the total wall shear force and the central chord in between the perforations will likely undergo considerable shear cracking. Therefore, most of the shear stiffness of a perforated wall is provided by the compression vertical chord, which should sustain relatively little cracking during the lateral displacements of the structure.

### 3.1.3 Linear-Elastic Effective Flexural Stiffness versus Gross Stiffness

To provide a visual assessment of the effective flexural stiffness recommendations in Section 3.1.1, Figure 3.3 plots the base shear, $V_w$ (i.e., applied lateral force, $F$) versus the lateral drift, $\Delta_w$ (i.e., relative lateral displacement, $\delta_w$ at the top of the wall divided by the wall height from the top of the foundation, $H_w$) for one of the solid wall specimens tested as part of this project. The results from the linear-elastic effective stiffness model (flexure plus shear deformations) are compared with the results obtained from a fiber element model of the wall (described in Section 3.3). The flexural deformations of the fiber model in the initial linear-elastic range are based on the gross moment of inertia, $I_{gross}$ of the structure, where the impact of the reduced moment of inertia, $I_e$ (Eqn. 3.9) used in the effective linear-elastic model can be seen. Note that as described in Section 3.3, the shear deformations in the fiber model are based on the effective shear area given by the linear-elastic effective stiffness model in Eqn. 3.11 (i.e., the shear stiffness is assumed to remain constant at the effective stiffness); and thus, the differences between the two models in Figure 3.3 are due to the flexural deformations only.

16
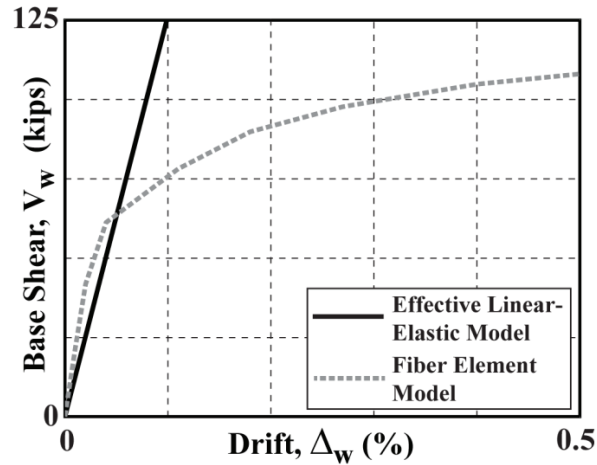
**Figure 3.3  Base Shear versus Wall Drift for Linear-Elastic Effective Stiffness Model**

## 3.2 SIMPLIFIED NONLINEAR FINITE ELEMENT MODEL

The overall modeling philosophy for the nonlinear finite element model is to create a basic analysis tool that incorporates simplifying assumptions appropriate for the design office. The model can be used to conduct nonlinear pushover analyses of hybrid walls under lateral loading combined with gravity loads. As an example, Figure 3.4 shows the exaggerated lateral displaced shape of the finite element model for one of the perforated hybrid walls tested as part of this project. The model, which was created using ABAQUS (Hibbitt et al. 2009), utilizes the following features:

- Three-dimensional eight-node stress/displacement solid elements (type C3D8R in ABAQUS) are used for the concrete in the wall panels and the foundation.
- Three-dimensional stress/displacement truss elements (type C3D8R in ABAQUS) are used for the PT steel. The anchored ends of the PT tendons are embedded within the solid elements for the wall and foundation concrete. The initial stresses in the PT steel after all short-term and long-term losses (but before lateral displacements of the wall) are simulated by placing an initial tension force in the truss elements.
- Three-dimensional stress/displacement truss elements are used for the E.D. bars crossing the base joint as well as the mild steel bars crossing the upper panel-to-panel joints. These truss elements are partitioned into bonded and unbonded regions. The bonded regions are embedded within the solid elements for the wall and foundation concrete while the unbonded regions are not constrained, thereby allowing a uniform strain distribution to form over the unbonded length of the steel.
- "Hard contact" surfaces are used at the horizontal joints to allow for gap opening. These surfaces are defined with "rough" friction, which prevents joint slip when the surfaces are in contact.

A major simplification adopted in the model is that the bonded mild steel reinforcement contained within the wall panels and the foundation (except for the bonded regions of the reinforcement crossing the horizontal joints) is not modeled explicitly. Instead, the effect of the

17

bonded steel reinforcement inside each wall component is captured using linear-elastic tension properties for the concrete. It is assumed (and ensured through design) that the wall panels and the foundation are reinforced with a sufficient amount of bonded mild steel to limit the size of the cracks and that this reinforcement does not yield. Note that as a result of using linear-elastic tension properties for the concrete, the redistribution of stresses due to cracking cannot be modeled. However, in a properly designed and detailed hybrid precast wall with sufficient and well-distributed reinforcement, the concrete cracks remain small and do not significantly affect the global behavior of the structure. The largest "crack" in a hybrid wall is the gap that forms at the base joint, which is appropriately included in the model by using hard contact surfaces at this joint.
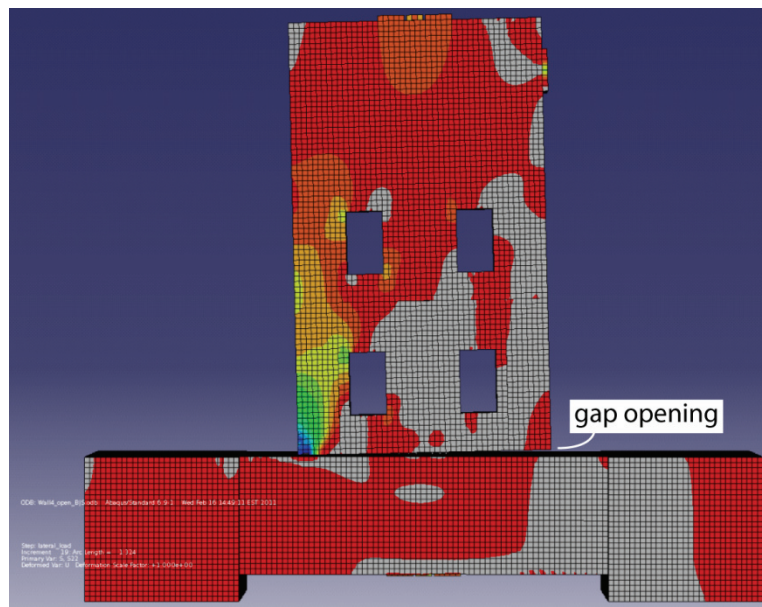


**Figure 3.4  Finite Element Model of a Perforated Hybrid Wall Test Specimen**

Additional assumptions and approximations incorporated into the finite element wall model are:

- The total unbonded length modeled for the E.D. bars includes an additional length of "debonding," which is assumed to occur during a large earthquake (see Section 4.4.4). This increased unbonded length is assumed to remain constant from the beginning to the end of the analysis using a debonding coefficient of $\alpha_s$=2.0 as described in Section 4.4.4.
- The nonlinear material properties for the concrete in compression and steel are modeled using multiple-point approximations of the measured or expected monotonic stress-strain behaviors (utilizing both "elastic" and "plastic" regions as defined in ABAQUS).
- For the confined concrete regions at the wall toes, the confinement reinforcement is not modeled explicitly but rather represented by incorporating the effect of the confinement on the uniaxial stress-strain relationship of the concrete in compression. The effects of the multi-axial stresses that develop in the three-dimensional solid elements for the concrete are ignored.
- The grout pads at the horizontal joints are not modeled explicitly. Instead, the grout thickness is modeled as part of the wall panels assuming that the grout and panel concrete behave similarly.

18

Further simplification of the finite element model can be achieved by: (1) appropriately lumping the areas of the PT steel and E.D. steel rather than modeling the individual PT tendons and E.D. bars; and (2) not modeling the upper panel-to-panel horizontal joints, since gap opening at these joint is expected to be negligible by design. Note that if a lumped steel model is used, it would not be possible to check the strains and stresses of the individual E.D. bars or PT tendons. Also, when excluding the upper panel-to-panel joints from the model, a separate check should be conducted to ensure that no significant gap opening occurs at the joint locations (which can be achieved by monitoring the development of vertical tension stresses at these locations).

## 3.3 DETAILED FIBER ELEMENT MODEL

The fiber element model described in this section is a research tool to conduct nonlinear reverse-cyclic and dynamic response history analyses of hybrid walls under seismic loading. The goal is to accurately reproduce the hysteretic behavior of the structure including gap opening/closing at the horizontal joints and hysteretic stress-strain behaviors for the materials. As an example, Figure 3.5 shows a schematic of the fiber element model for one of the solid hybrid walls tested as part of this project. The analysis of walls with perforations follows a similar approach by removing the concrete fibers from the perforated regions of the wall panels; however, it should be noted that unlike the finite element model described in Section 3.2, the fiber element model is not capable of capturing the local behavior around the perforations. The model, created using DRAIN-2DX (Prakash et al. 1993), utilizes the following features:

- Fiber beam-column elements are used to represent the axial-flexural behavior of the precast wall panels. The shear stiffness of the panels is assumed to remain constant at the effective stiffness given by the linear-elastic effective stiffness model described in Section 3.1.
- The foundation is assumed to be fixed. To simulate the effect of gap opening at the base joint, the tension strength of the concrete fibers at the bottom of the base panel is set to zero over a height, $h_{cr}$, which is equal to the confined concrete thickness of the wall. Outside these regions, the wall concrete is assumed to be linear-elastic in tension (i.e., similar to the finite element model, the cracking of the concrete is ignored and the bonded mild steel reinforcement contained within each wall panel is not modeled explicitly).
- Truss elements are used for the unbonded PT steel. The PT anchors can be modeled by kinematically constraining the ends of the truss elements to corresponding fiber element nodes for the wall panels at the same elevation. The initial PT stresses are simulated by placing an initial tension force in the truss elements.
- The unbonded regions of the E.D. bars are also modeled using truss elements so as to capture the uniform strains over the unbonded length of the steel. Similar to the finite element model, an additional debonding length (see Section 4.4.4) is incorporated into the total unbonded length modeled for the E.D. bars. This increased unbonded length is assumed to remain constant throughout the analysis. The bonded regions of the bars are modeled by kinematically constraining the end nodes of the truss elements to corresponding fiber element nodes for the wall panels at the same elevation (the actual bonded lengths of the E.D. bars are not modeled).

19

▪ Similar to the base joint, the effect of gap opening at the upper panel-to-panel joints (albeit small) can be modeled by using "compression-only" material properties for the concrete fibers (i.e., the tension strength of the concrete is taken as zero) over a short height at the bottom of each upper wall panel. The compression-only concrete fibers above each panel-to-panel joint extend over a height equal to the unbonded length of the mild steel bars crossing the upper panel-to-panel joints. Even though these mild steel bars are not bonded to the concrete, they are modeled as part of the fiber cross section representation of these regions. Concrete with linear-elastic tension properties is used to model the remaining height of each wall panel.
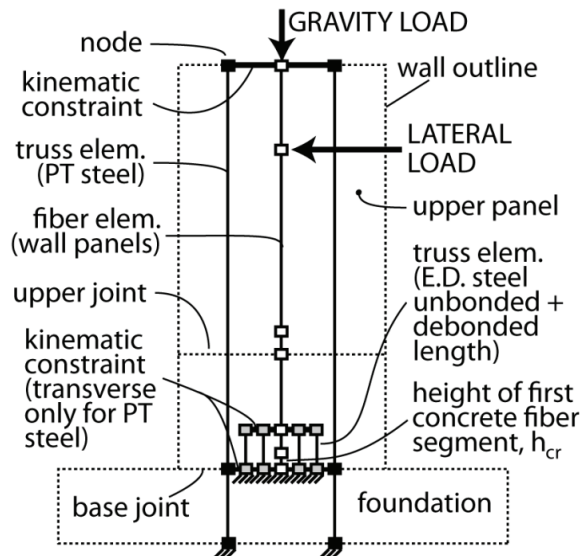


**Figure 3.5  Fiber Element Model of a Hybrid Wall**

The concrete under compression is modeled using a multiple-point approximation of the measured or expected uniaxial stress-strain behavior. For the confined concrete regions at the wall toes, the confinement reinforcement is not modeled explicitly, but is represented by incorporating the effect of the confinement on the concrete compression stress-strain relationship. The grout pads at the horizontal joints are also not modeled explicitly. Instead, the grout thickness is modeled as part of the wall panel concrete assuming that the grout and the panel concrete behave similarly.

The behavior of the steel reinforcement crossing the horizontal joints is also modeled using a multiple-point approximation of the measured or expected stress-strain behavior. In modeling the E.D. bars crossing the base joint, Bauschinger effect of the steel should be included so as not to over-estimate the energy dissipation of the wall. The mild steel bars across the upper panel-to-panel joints can be modeled as linear-elastic; however, the resulting steel strains should be checked to ensure that the yield strain is not exceeded. For the PT steel, the strand stiffness from the measured or expected material stress-strain relationship should be reduced to account for the localized concrete and anchorage deformations at the tendon ends, since these local deformations cannot be captured by the fiber elements modeling the wall panels. This can be done by reducing the initial PT strand stiffness in the linear-elastic range by a factor of 0.75 and by reducing the PT stress at the maximum expected wall displacement by a factor of 0.85.

## CHAPTER 4

## PERFORMANCE-BASED DESIGN OF HYBRID WALLS

This chapter provides recommendations and guidelines for the performance-based seismic design of hybrid precast concrete shear walls. These guidelines include the determination of the seismic design forces, lateral drift demands, flexural and shear design of the horizontal joints, design and detailing of the wall reinforcement, and various design checks to ensure satisfactory performance of the structure through the expected drift demands. A detailed design example is given in Appendix A.

### 4.1 SEISMIC DESIGN FORCES

The design of a hybrid wall should be conducted under all of the applicable load combinations prescribed by ASCE-7 (2010), including the use of a redundancy factor and torsional effects from accidental and applied eccentricities. The design base shear force can be obtained using any of the procedures allowed in ASCE-7, such as the equivalent lateral force procedure or the modal analysis procedure. The most basic approach is the equivalent lateral force procedure, in which the wall design base shear force, $V_{wd}$ is determined by dividing the first mode linear-elastic force demand under the design-basis earthquake (DBE) with the prescribed response modification factor, $R$. When selecting $R$ using Table 12.2-1 in ASCE-7, the seismic force-resisting system for hybrid walls can be classified as "special reinforced concrete shear walls." Therefore, the response modification factors should be taken as $R$=5.0 and 6.0 for bearing wall systems and building frame systems, respectively. Once the design base shear force, $V_{wd}$ is established, the design base moment, $M_{wd}$ and the other design forces (e.g., story shear forces and bending moments) can be found from a linear-elastic analysis of the structure under the vertical distribution of the design base shear force from ASCE-7.

### 4.2 WALL DRIFT DEMANDS AND EXPECTED PERFORMANCE

As shown in Figure 4.1 adopted from ACI ITG-5.1 (2007), the wall drift, $\Delta_w$ is defined as the relative lateral displacement at the top of the wall divided by the wall height, $H_w$ from the top of the foundation. While only the gap opening rotation at the wall base and the flexural deformations of the wall panels are shown in Figure 4.1, ACI ITG-5.1 requires that all lateral deformations and rotations of the wall due to flexure, shear, and horizontal shear slip are included in the calculation for $\Delta_w$. Since the design of a wall includes provisions to prevent significant shear slip across the horizontal joints and gap opening across the upper panel-to-panel joints, these displacement components can be ignored in the design process.

The design is conducted at two drift levels: (1) the design-level wall drift, $\Delta_{wd}$ corresponding to the design basis earthquake (DBE); and (2) the maximum-level wall drift, $\Delta_{wm}$ corresponding to the maximum considered earthquake (MCE). Appropriate analytical techniques, such as nonlinear dynamic response history analyses under properly selected DBE and MCE ground

motion sets, can be used to determine these drifts. Alternatively, the ASCE-7 guidelines in Section 12.8.6 can be used to determine the design-level drift by multiplying the linear-elastic drift, $\Delta_{we}$ under the design base shear force, $V_{wd}$ with the prescribed deflection amplification factor, $C_d$. The linear-elastic wall drift, $\Delta_{we}$ (flexural plus shear displacements corresponding to $V_{wd}$) can be calculated using the effective linear-elastic stiffness model given in Section 3.1. When selecting the deflection amplification factor, $C_d$ from Table 12.2-1 in ASCE-7, the seismic force-resisting system for hybrid walls should be classified as "special reinforced concrete shear walls," resulting in $C_d$=5.0.
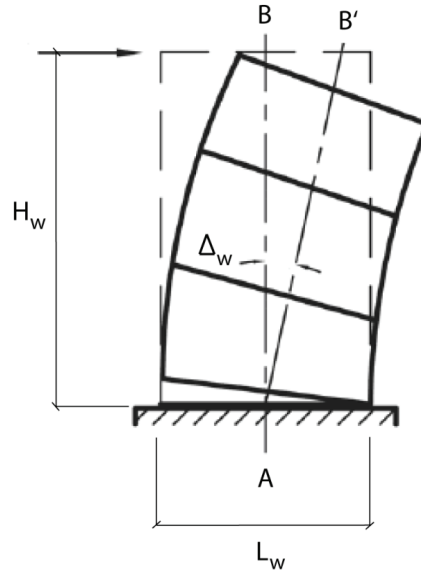


**Figure 4.1  Definition of Wall Drift, $\Delta_w$ (adopted from ACI ITG-5.1)**

Unless nonlinear dynamic response history analyses are conducted under MCE ground motion sets, the maximum-level wall drift, $\Delta_{wm}$ can be calculated as:

$$\Delta_{wm} = 0.95\Delta_{wc} \tag{4.1}$$

with:

$$\Delta_{wc} = 0.9\% \leq \left(\frac{H_w}{L_w}\right)0.8\% + 0.5\% \leq 3.0\% \tag{4.2}$$

where, Eqn. 4.2 is adopted from ACI ITG-5.1 (2007) as the minimum drift capacity of special unbonded post-tensioned precast concrete shear walls.

Alternatively, approximate methods that consider the unique hysteretic characteristics of hybrid walls (in particular, the reduced energy dissipation and increased self-centering) can be used to estimate the nonlinear displacement demands of the structure.

The idealized base shear force versus roof drift behavior of a wall subjected to these drift demands is shown in Figure 4.2. The corresponding expected wall performance is as follows:

At $\Delta_{wd}$:

- Gap opening at the base joint but no gap opening or nonlinear material behavior at the upper panel-to-panel joints.
- No residual vertical uplift of the wall upon removal of lateral loads (i.e., the gap at the base joint fully closes upon unloading).
- No shear slip at the horizontal joints.
- Yielding of the E.D. bars.
- PT steel remaining in the linear-elastic range.
- Minor hairline cracking in the base panel (for perforated walls, cracking may extend into the upper panels).
- No observable concrete damage in compression, but cover concrete on the verge of spalling.

At $\Delta_{wm}$:

- Increased gap opening at the base joint but no significant gap opening or nonlinear material behavior at the upper panel-to-panel joints.
- No significant residual vertical uplift of the wall upon removal of lateral loads.
- No significant shear slip at the horizontal joints.
- Significant yielding but no fracture of the E.D. bars.
- PT steel in the nonlinear range but with strains not exceeding 0.01 in./in.
- Well distributed, still hairline, cracking of the concrete.
- Cover concrete spalling at the wall toes, with the confined core concrete on the verge of crushing.
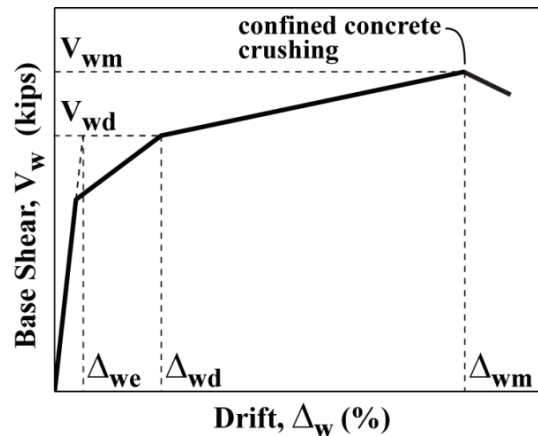


**Figure 4.2  Expected Base Shear versus Roof Drift Behavior**

## 4.3 PRELIMINARY PROPORTIONING OF WALL CROSS SECTION GEOMETRY

The preliminary proportioning of a hybrid wall can be done by limiting the nominal shear stress at the design-level drift, $\Delta_{wd}$, such that:

$$\frac{V_{wd}}{A_{gross}} \leq 4\sqrt{f_c'}$$
(4.3)

where, $V_{wd}$=design base shear force; $A_{gross}$=gross area of wall cross section (taken at section with perforations in case of perforated walls); and $f_c'$=design compressive strength of the panel concrete.

It is also recommended that:

$$\frac{V_{wm}}{A_{gross}} < 4.5\sqrt{f_c'}$$
(4.4)

where, $V_{wm}$= base shear resistance of the wall at $\Delta_{wm}$ (see Figure 4.2 and Section 4.4.2). The nominal shear stress in the base panel of the wall specimens tested as part of this project ranged from $2.0\sqrt{f_c'}$ to $4.0\sqrt{f_c'}$ at $\Delta_{wd}$ and from $2.1\sqrt{f_c'}$ to $4.5\sqrt{f_c'}$ at $\Delta_{wm}$. These shear stress values were calculated using the measured concrete strength for each specimen and considering the reduced area from the perforations in the perforated specimens.


## 4.4 DESIGN OF BASE JOINT

This section describes the design of the base joint with respect to the E.D. and PT steel areas, probable (maximum) base moment strength of the wall, contact length and confinement reinforcement at the wall toes, E.D. steel strains and stresses (including the determination of the unbonded length for the E.D. bars), and PT steel strains and stresses (including the determination of the PT stress losses). In presenting the design steps, is assumed that:

- The overall dimensions of the wall and the individual wall panels (i.e., height, length, and thickness) have been determined for a trial structure (the guidelines given in Section 4.3 can be used for this purpose). The length and thickness of the wall panels remain constant over the height of the structure.
- The design forces (axial, shear, and bending moment) and design-level and maximum-level drift demands ($\Delta_{wd}$ and $\Delta_{wm}$) have been determined.
- The material properties for the PT steel, mild steel, and concrete have been selected. For the steel reinforcement, design approximations for the nonlinear stress-strain relationships including strain hardening are available (e.g., see Figure 4.3). Stress-strain properties of the E.D. steel need to be defined accurately.

### 4.4.1 PT and E.D. Steel Areas

The PT and E.D. steel areas, $A_p$ and $A_s$, respectively, are determined to satisfy the wall design base moment, $M_{wd}$ (corresponding to $V_{wd}$) at the design-level drift, $\Delta_{wd}$. As shown in a free-body diagram of the wall base in Figure 4.4, the wall behavior at $\Delta_{wd}$ can be estimated using fundamental concepts of reinforced and prestressed concrete mechanics (equilibrium, compatibility/kinematics, and design constitutive relationships). The PT and E.D. steel

24

reinforcement should be placed in a symmetrical layout and located outside of the confined concrete boundary (toe) regions of the base panel.
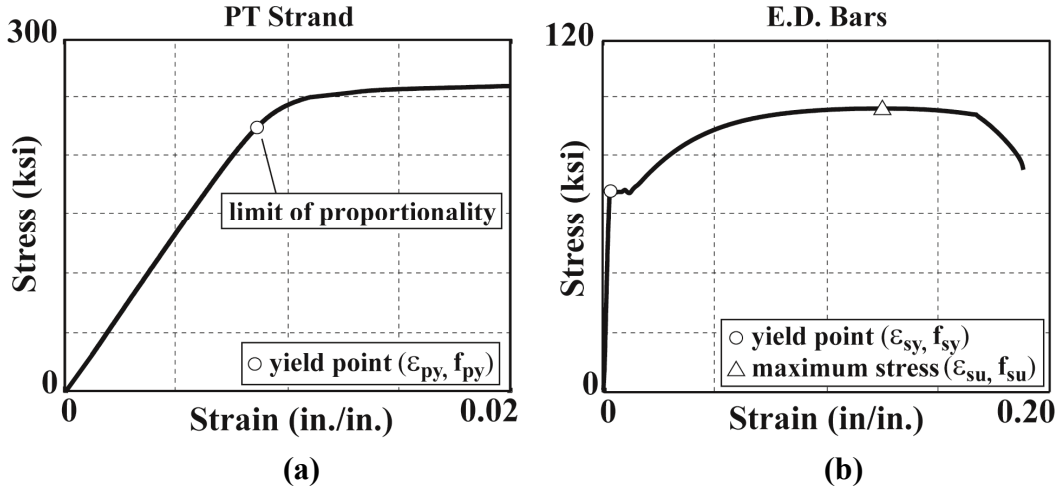


**Figure 4.3  Stress-Strain Behavior: (a) PT Steel Strand; (b) E.D. Bar**

To simplify the presentation of the design process below, the PT and E.D steel areas are assumed to be lumped at the wall centerline, resulting in equal PT steel stresses and equal E.D. steel stresses on the "compression-side" and "tension-side" of the wall centerline (see Figure 4.4) and leading to the following equations:

$$\bar{C}_d = A_s f_{sd} + A_p f_{pd} + N_w \tag{4.5}$$

$$\bar{C}_d = 0.85 f_c' t_w \beta_1 c_d \tag{4.6}$$

$$\frac{M_{wd}}{\phi_f} = \bar{C}_d z_d \tag{4.7}$$

with:

$$z_d = \frac{L_w}{2} - \frac{\beta_1 c_d}{2} \tag{4.8}$$

Note that the different stresses in the individual PT tendons and E.D. bars should be incorporated in the final design of the wall. Further, the steel areas should not be lumped at the wall centerline if the reinforcement is placed outside the middle one-quarter of the wall length, $L_w$ (i.e., if the distance from the wall centerline to the extreme PT tendon or E.D. bar is greater than $0.125L_w$). In Eqns. 4.5-4.8, $\bar{C}_d$=concrete compressive stress resultant at the wall base; $A_p$, $A_s$=total PT and E.D. steel areas, respectively, lumped at the wall centerline; $f_{pd}$, $f_{sd}$=corresponding PT and E.D. steel stresses, respectively, when $\Delta_{wd}$ is reached; $N_w$=design gravity axial force at the wall base (for the design load combination being considered); $f_c'$=compression strength of the unconfined concrete; $t_w$=wall thickness; $c_d$=neutral axis length (i.e., contact length) when $\Delta_{wd}$ is reached; $\beta_1$=ACI 318 factor that relates $c_d$ to the length, $a_d$ of the equivalent rectangular concrete compression stress block; $\phi_f$=axial-flexural capacity reduction factor from ACI 318; $M_{wd}$=design base moment corresponding to $V_{wd}$; and $z_d$=distance between the tension and compression stress resultants at $\Delta_{wd}$.
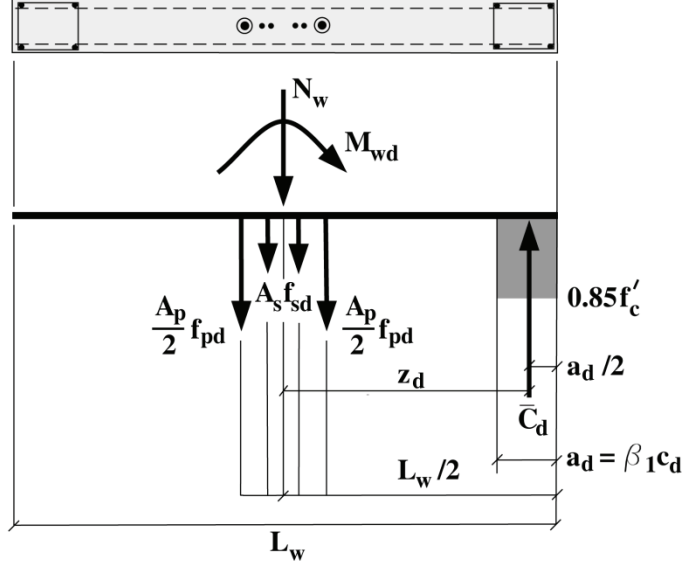
**Figure 4.4 Free Body Diagram of Base Joint at $\Delta_{wd}$**

Let $M_{ws}$, $M_{wp}$, and $M_{wn}$ be the contributions of the E.D. steel, PT steel, and axial force, $N_w$, respectively, to satisfy $M_{wd}$. The corresponding design requirement can be written as:

$$M_{wd} = \phi_f\left(M_{ws} + M_{wp} + M_{wn}\right) \tag{4.9}$$

with

$$M_{ws} = A_s f_{sd} z_d \tag{4.10}$$
$$M_{wp} = A_p f_{pd} z_d \tag{4.11}$$
$$M_{wn} = N_w z_d \tag{4.12}$$

To determine the required steel areas, the "E.D. steel moment ratio," $\kappa_d$ is defined as:

$$\kappa_d = \frac{M_{ws}}{M_{wp} + M_{wn}} \tag{4.13}$$

For lumped steel areas, $\kappa_d$ can be written as:

$$\kappa_d = \frac{A_s f_{sd}}{A_p f_{pd} + N_w} \tag{4.14}$$

An appropriate value for $\kappa_d$ should be selected for design. The $\kappa_d$ ratio is a relative measure of the resisting moments from of the energy dissipating force provided by the E.D. steel reinforcement ($A_s f_{sd}$) and the vertical restoring (i.e., self-centering) force provided by the PT steel reinforcement ($A_p f_{pd}$) plus the gravity axial load ($N_w$) in the wall. If $\kappa_d$ is too small, the energy dissipation of the wall may be very small. Conversely, if $\kappa_d$ is too large, the self-centering capability of the wall may not be sufficient to yield the tensile E.D. bars back in compression and close the gap at the base joint upon the removal of lateral loads.

Based on the performance of the specimens tested as part of this project, the $\kappa_d$ ratio used in design should not exceed 0.80 (to ensure sufficient self-centering) and should not be less than 0.50 (to ensure sufficient energy dissipation). Specimens with $\kappa_d$ ratios close to both of these limits were tested (Smith et al. 2012a), demonstrating that walls with $\kappa_d$<0.50 may not satisfy the relative energy dissipation requirement of ACI ITG-5.1 (2007) and walls with $\kappa_d$>0.80 may fail due to excessive in-plane or out-of-plane shear slip across the base joint associated with the uplift of the wall from the foundation (i.e., a gap forms along the entire base joint when the wall is unloaded to $\Delta_w$=0%). Wall uplift and shear slip across the base joint can develop quickly with little warning and can ultimately result in the failure of the wall through the buckling of the E.D. bars and/or splitting of the wall panel concrete.

After selecting the design $\kappa_d$ ratio, the required E.D. steel area, $A_s$, and PT steel area, $A_p$, as well as the concrete compressive stress resultant, $\bar{C}_d$, and the neutral axis length, $c_d$, at $\Delta_{wd}$ can be determined using equilibrium (as shown in Figure 4.4). For lumped steel areas, Eqns. 4.6-4.8 can be directly solved for $\bar{C}_d$ and $c_d$. The resulting $c_d$ can then be used to determine the E.D. steel and PT steel strains and stresses, $\varepsilon_{sd}$, $f_{sd}$, $\varepsilon_{pd}$, and $f_{pd}$, respectively, using the gap opening displacements at the wall base (as described in Sections 4.4.4 and 4.4.6), the steel stress-strain relationships, selected unbonded lengths ($l_{su}$ and $l_{pu}$ for the E.D. and PT steel, respectively), and selected locations of the bars and tendons from the wall centerline ($e_s$ and $e_p$ for the E.D. and PT steel, respectively). Finally, the required $A_s$ and $A_p$ can be found by solving Eqns. 4.5 and 4.14. Once the remaining design steps in Sections 4.4.2, 4.4.3, 4.4.4, and 4.4.6 are completed, the selections for the steel locations and unbonded lengths should be checked. This process is demonstrated in the design example in Appendix A.

Note that if the E.D bars and PT tendons cannot be lumped at the wall centerline, the design process to determine the steel areas requires iteration by assuming an initial value for the neutral axis length, $c_d$, to determine the E.D. steel and PT steel strains and stresses, $\varepsilon_{sd}$, $f_{sd}$, $\varepsilon_{pd}$, and $f_{pd}$, respectively, using the gap opening displacements at the wall base (as described in Sections 4.4.4 and 4.4.6). An initial value of $c_d$=0.175$L_w$ can be used as the starting point for the iteration, with the process completed when the calculated $c_d$ from equilibrium is sufficiently close to the value used at the beginning of the step to determine the steel strains and stresses.

### 4.4.2 Probable Base Moment Strength

The probable maximum base moment strength of the wall, $M_{wm}$, determined at the maximum-level drift, $\Delta_{wm}$, is needed to establish the maximum demands on the wall (e.g., maximum base shear force and the forces at the upper panel-to-panel joints). As shown in the free-body diagram of the wall base in Figure 4.5, $M_{wm}$ is calculated with $A_p$ and $A_s$ determined in Section 4.4.1 and using equilibrium considering material strain hardening at $\Delta_{wm}$. This process requires iterative steps with an assumed neutral axis length, $c_m$ at $\Delta_{wm}$, and the resulting confined concrete, E.D. steel, and PT steel strains and stresses $f'_{cc}$, $\varepsilon_{sm}$, $f_{sm}$, $\varepsilon_{pm}$, and $f_{pm}$, respectively, as described in Sections 4.4.3, 4.4.4, and 4.4.6. As a starting point for the iteration, $c_m$=0.9$c_d$ can be selected, with the process repeated until the calculated $c_m$ from the axial force equilibrium at the wall base is sufficiently close to the assumed $c_m$ value.
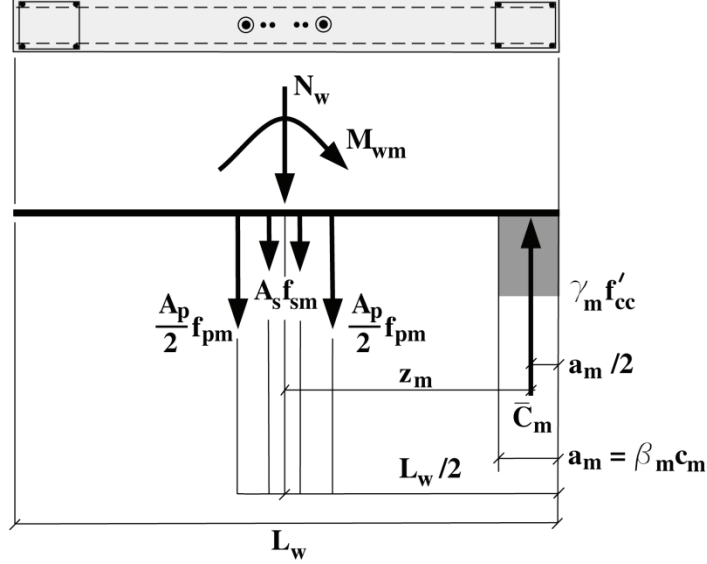
**Figure 4.5  Free Body Diagram of Base Joint at $\Delta_{wm}$**

Once convergence on $c_m$ has been satisfied, $M_{wm}$ can be calculated as:

$$M_{wm} = \bar{C}_m z_m \tag{4.15}$$

with:

$$\bar{C}_m = A_s f_{sm} + A_p f_{pm} + N_w \tag{4.16}$$

$$\bar{C}_m = \gamma_m f'_{cc} t_w \beta_m c_m \tag{4.17}$$

$$z_m = \frac{L_w}{2} - \frac{\beta_m c_m}{2} \tag{4.18}$$

where, $f'_{cc}$=confined concrete compression strength; and $z_m$=distance between the tension and compression stress resultants at $\Delta_{wm}$. The confined concrete in compression is represented using a modified rectangular stress block (see Figure 4.5), with the concrete strength parameter and the stress block length parameter, $\gamma_m$=0.92 and $\beta_m$=0.96, respectively, as given in Section 5.6.3.8(a) of ACI ITG-5.2 (2009). These $\gamma_m$ and $\beta_m$ values were used in the design and analysis of the wall specimens tested as part of this project (Smith et al. 2012a), demonstrating reasonable comparisons with the measured behavior of the walls. Note that to maintain simplicity, the above design process makes no distinction for the thickness of the unconfined cover concrete, which is ineffective at $\Delta_{wm}$. If necessary, the cover concrete can be excluded from the wall length and thickness in the design calculations at $\Delta_{wm}$.

### 4.4.3 Contact Length and Confinement Reinforcement at Wall Toes

Confinement reinforcement is required at the ends of the base panel to prevent premature crushing and failure of the core (i.e., inner) concrete prior to the maximum-level drift, $\Delta_{wm}$. The confinement reinforcement ratio, $\rho_h$ should be designed to satisfy the estimated maximum concrete compression strain, $\varepsilon_{cm}$ at $\Delta_{wm}$. According to Sections 5.6.3.5 through 5.6.3.9 of ACI ITG-5.2 (2009), $\varepsilon_{cm}$ can be determined as:

$$\varepsilon_{cm} = \varphi_{wm}c_m \tag{4.19}$$

with

$$\varphi_{wm} = \frac{\Delta_{wm}}{h_p} \tag{4.20}$$

$$h_p = 0.06H_w \tag{4.21}$$

where, $\varphi_{wm}$=plastic curvature; and $h_p$=assumed plastic hinge height over which the plastic curvature is uniformly distributed at the wall base. Based on the extent of the cover concrete spalling in the wall specimens tested as part of this project, the confined concrete region at the wall toes should extend vertically over a height of the base panel not less than the plastic hinge height, $h_p$. Horizontally, the confined region should extend from each end of the base panel over a distance not less than $0.95c_m$ and not less than 12 in., as required by ACI ITG-5.2.

The determination of $\varepsilon_{cm}$ is conducted as part of the iterative process for the estimation of $M_{wm}$ in Section 4.4.2 (as a starting point for the iteration, $c_m$=0.9$c_d$ can be selected). Once $f'_{cc}$ and $c_m$ have been determined, the confinement hoop layout and spacing can be designed according to Sections 5.6.3.5 through 5.6.3.9 in ACI ITG-5.2. This process is demonstrated in the design example in Appendix A. The design and detailing of the wall toes should also satisfy the applicable requirements for special boundary regions in Section 21.9.6.4 of ACI 318 (2011) as well as the bar spacing and concrete cover requirements in ACI 318. Note that the requirement in Section 21.9.6.4(d) of ACI 318 does not apply since the vertical reinforcement in the boundary regions of a hybrid precast wall does not continue into the foundation.

The above guidelines were used in the design of the wall specimens tested in this project with satisfactory behavior of the confined concrete at the wall toes. The height of the first confinement hoop from the base of the wall is critical to the performance of the confined concrete. The first hoop should be placed at a distance from the bottom of the base panel no greater than the minimum concrete cover required by ACI 318. Additionally, for rectangular confinement hoops, the length-to-width aspect ratio of the hoop (measured center-to-center of bar) should not exceed 2.50. Note that this requirement is slightly more conservative than but similar to past seismic design code specifications for boundary zone confinement reinforcement [e.g., see Section 1921.6.6.6 of the Uniform Building Code (ICBO 1997)], which have since been removed from the code requirements in the U.S. As observed from the performance of the wall specimens tested in this project, a large length-to-width ratio for the confinement hoops can cause the bowing of the longer hoop legs in the out-of-plane direction, reducing the confinement effectiveness. Further, the experiments showed that intermediate crossties are ineffective in preventing the bowing of the longer hoop legs, since in typical construction, the crossties do not directly engage the hoop steel (rather, the crossties engage the vertical reinforcement within the hoops). In general, crossties not directly engaging the hoop steel should be considered ineffective in providing confinement to the concrete.

### 4.4.4 E.D. Steel Strains, Stresses, and Unbonded Length

The iterative processes to determine $A_p$ and $A_s$ at $\Delta_{wd}$ and $M_{wm}$ at $\Delta_{wm}$ require the estimation of the E.D. and PT steel strains based on the assumed neutral axis lengths, $c_d$ and $c_m$, respectively.

As shown in Figure 4.6, the elongations, $\delta_s$ of the E.D. bars can be found by lumping all of the lateral displacements of the wall at $\Delta_w$ to the gap opening rotation at the base, resulting in:

$$\delta_s = \Delta_w(0.5L_w - c \pm e_s) \tag{4.22}$$

where, $c$=neutral axis length (equal to $c_d$ at $\Delta_w=\Delta_{wd}$ and $c_m$ at $\Delta_w=\Delta_{wm}$); and $e_s$=distance of each bar from the wall centerline. Then, the E.D. bar strains can be determined as:

$$\varepsilon_s = \frac{\delta_s}{l_{sw} + \alpha_s d_s} \tag{4.23}$$

where, $l_{sw}$=wrapped length of the E.D. bars; $\alpha_s$=coefficient defined in ACI ITG-5.2 (2009) to estimate the additional length of "debonding" that is expected to develop during the reversed-cyclic lateral displacements of the structure; and $d_s$=bar diameter. It can be assumed that $\alpha_s=0$ and $\alpha_s=2.0$ at $\Delta_{wd}$ and $\Delta_{wm}$, respectively. Concrete cores were taken through the thickness of the base panel around the end of the wrapped length of the E.D. bars in two of the specimens tested as part of this project, supporting the use of $\alpha_s=2.0$ at $\Delta_{wm}$. The wrapped length can be located in either the bottom of the base panel or the top of the foundation; in either configuration, the E.D. bars should also be isolated from the grout through the thickness of the grout pad at the base joint (i.e., the wrapped length should include the grout pad).
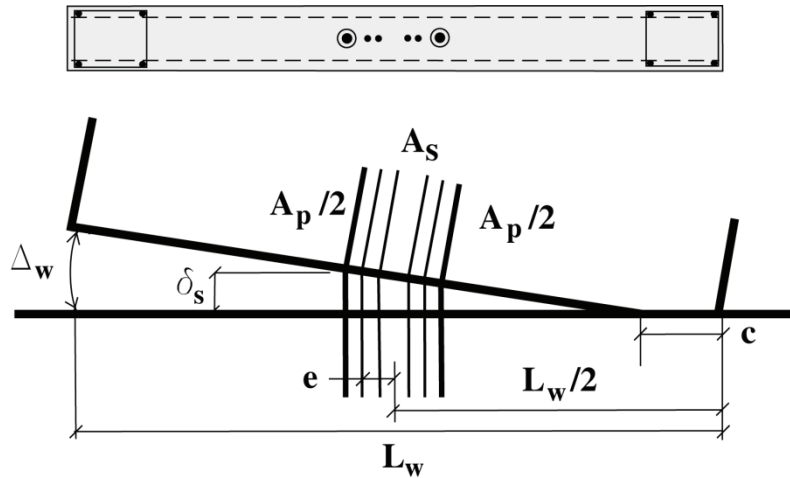


**Figure 4.6  Gap Opening at Base Joint**

Once the unbonded lengths, $l_{su}$ (i.e., wrapped length, $l_{sw}$ plus additional debonding length, $\alpha_s d_s$), and locations, $e_s$ of the E.D. bars have been selected in Section 4.4.1, Eqns. 4.22 and 4.23 can be used to determine the bar strains and, in turn, the bar stresses from an assumed steel stress-strain relationship (including strain hardening) for both $\Delta_w=\Delta_{wd}$ (with $c=c_d$) and $\Delta_w=\Delta_{wm}$ (with $c=c_m$). Note that this process tends to overestimate the steel strains (and thus, stresses) since it ignores the flexural and shear deformations of the wall panels over the height of the structure. It is recommended that the resulting $\varepsilon_{sm}$ be greater than $0.5\varepsilon_{su}$ to ensure sufficient energy dissipation (where, $\varepsilon_{su}$ is the monotonic strain capacity of the steel at peak strength as shown in Figure 4.3). Furthermore, per ACI ITG-5.2, the maximum E.D. bar strains should not exceed $0.85\varepsilon_{su}$ to prevent low-cycle fatigue fracture of the bars. The selected unbonded lengths,

$l_{su}$ of the bars can be checked by limiting $\varepsilon_{sm}$ to an allowable strain, $\varepsilon_{sa}$ between $0.5\varepsilon_{su}$ and $0.85\varepsilon_{su}$. Strain limits ranging from $\varepsilon_{sa}=0.5\varepsilon_{su}$ to $0.85\varepsilon_{su}$ were used in the design of the test specimens in this research, with adequate energy dissipation and no bar fracture observed during the experiments. The design of the unbonded length of the bars should consider the wall displaced in both directions of loading.

The stress-strain properties of the E.D. steel should be defined accurately for design. The E.D. reinforcement should satisfy Section 21.1.5 of ACI 318 (2011). In general, the steel should comply with ASTM A706, Grade 60 reinforcement specifications. However, ASTM A615, Grade 60 reinforcement should be permitted for the E.D. bars if, for all the reinforcement in the precast wall panels and present on the jobsite, "(a) the actual yield strength (i.e., measured yield strength, $f_{sy}$) based on mill tests does not exceed the specified yield strength (i.e., 60 ksi design yield strength) by more than 18,000 psi; and (b) the ratio of the actual tensile strength (i.e., measured ultimate strength, $f_{su}$) to the actual yield strength (i.e., measured $f_{sy}$) is not less than 1.25." This requirement should be applied to all the reinforcement on the jobsite to avoid potential confusion and misplacement between the ASTM A615 reinforcement that has been approved and reinforcement that has not been approved as a substitute for the ASTM A706 E.D. bars.

### 4.4.5 Development Length and Splices of E.D. Bars

Sufficient development length should be provided at both ends of the wrapped unbonded region of the E.D. bars. Due to the large cyclic steel strains expected through $\Delta_{wm}$, Type II mechanical splices specified in Section 21.1.6 of ACI 318 (2011) and permitted by Section 5.4.2 of ACI ITG-5.2 should not be used for the E.D. bars in hybrid precast walls in seismic regions unless the splices have been tested and validated under cyclic loading up to a steel strain of at least $0.85\varepsilon_{su}$. In one of the specimens tested as part of this project, pullout of the E.D. bars from the foundation occurred due to the failure of the grout within Type II splice connections prior to $\Delta_{wm}$. The pullout caused the E.D. bar elongations and strains to be smaller than designed, resulting in smaller lateral strength and energy dissipation of the wall. While the splices satisfied all ACI 318 and AC133 (ICC 2010) performance requirements for Type II mechanical connectors and the grout used inside the splices satisfied the splice manufacturer's specifications, the E.D. bars were subjected to greater strains and over a significantly larger number of cycles than required to classify a Type II connection per ACI 318 and AC133, resulting in the pullout of the bars.

In validating Type II connectors for use in E.D. bar splices, it is recommended that the bars be first subjected to 20 cycles of loading through $+0.95\varepsilon_{sy}$ and $-0.5\varepsilon_{sy}$, where $\varepsilon_{sy}$=yield strain of the steel, as required by AC133. Beyond this point, 6 cycles should be applied at each load increment, with the compression strain amplitude kept constant at $-0.5\varepsilon_{sy}$ and the tension strain amplitude increased to a value not less than 5/4 times and not more than 3/2 times the strain amplitude from the previous load increment. Testing should continue until the tension strain amplitude reaches or exceeds $+0.85\varepsilon_{su}$ over 6 cycles. These requirements would result in similar cyclic loading conditions during the validation testing of the splices as the loading conditions that can develop during the validation testing of hybrid shear walls based on ACI ITG-5.1 (2007). The requirement to subject the splices to 6 cycles at each load increment considers that

the E.D. bars will likely be placed near the wall centerline; and thus, the bars will undergo tensile strains in each of the positive and negative directions of lateral wall displacement.

In lieu of using Type II mechanical splices, the full development length of the E.D. bars can be cast or grouted (during the construction process) into the base panel and the foundation. This connection technique was successfully used in this project, with no pullout of the bars from the concrete. The development length of bars cast inside the concrete should be designed according to Section 21.9.2.3(c) of ACI 318 (2011). For bars that are grouted inside corrugated metal ducts, a reduced development length of $25d_s$, where $d_s$=E.D. bar diameter, can be used according to Section 5.4.3 of ACI ITG-5.2 (2009).

### 4.4.6 PT Steel Strains and Stresses

Figure 4.6 can also be utilized to determine the elongation, $\delta_p$ of the PT strands due to gap opening (as the wall is displaced to $\Delta_w = \Delta_{wd}$ or $\Delta_{wm}$) by using the distance, $e_p$ of each tendon from the wall centerline as:

$$\delta_p = \Delta_w \left(0.5L_w - c \pm e_p\right) \tag{4.24}$$

Then, the strand strains due to gap opening can be calculated by dividing the strand elongations with the unbonded length, $l_{pu}$ of the strands, taken as the tendon length between the anchorages. The total strand strains, $\varepsilon_p$ are determined by summing the gap opening strains with the initial strains from $f_{pi}$ (including all short-term and long-term losses) as:

$$\varepsilon_p = \frac{f_{pi}}{E_p} + \frac{\delta_p}{l_{pu}} \tag{4.25}$$

where, $E_p$=Young's modulus of the strand. The calculated strand strains can be used to determine the PT steel stresses from an assumed strand stress-strain relationship [e.g., see Figure 4.3(a)].

The anchorage system for the PT tendons should be capable of allowing the strands to reach the predicted stresses and strains at $\Delta_{wm}$ without strand wire fracture or wire slip. Unless the PT anchors have been qualified for greater strand strains under cyclic loading, the total maximum strand strains, $\varepsilon_p$ (which include prestrain) should be limited to a maximum of 0.01 in./in. at $\Delta_{wm}$. As discussed in detail by Walsh and Kurama (2010, 2012), strand wire fractures can occur if the tendon strains exceed 0.01 cm/cm (0.01 in./in.). With this strain limit, which was used in the design of the specimens tested as part of this project, no strand wire fracture or slip was observed and the tendons remained mostly in the linear-elastic range through $\Delta_{wm}$. Significant nonlinear straining of the PT steel should be prevented to limit the prestress losses at $\Delta_{wm}$.

A small amount of PT stress loss will occur as the wall is displaced to $\pm\Delta_{wm}$ under fully-reversed and repeated cyclic loading and the strand strains exceed the limit of proportionality (i.e., as the stress-strain behavior of the strand becomes nonlinear). Figure 4.7 displays the stress-strain relationship of two PT steel tendons (located to the left and right of the wall centerline as

shown in Figure 4.6) as the wall is cyclically displaced at $\pm\Delta_{wm}$. Let the stresses in the "tension-side" and "compression-side" tendons (i.e., the tendons farther from and closer to the compression toe of the wall, respectively) upon first loading to $+\Delta_{wm}$ be $f_{pm,1}$ and $f_{pm,2}$, respectively. Upon reversed loading of the wall to $-\Delta_{wm}$ and reloading back to $+\Delta_{wm}$, the tension-side tendon will return to the same point on the stress-strain relationship (i.e., the stress and strain of the tendon will equal $f_{pm,1}$ and $\varepsilon_{pm,1}$, respectively) and the tendon will not experience any stress loss due to the nonlinear material behavior. The compression-side tendon will also return to the same strain (i.e., $\varepsilon_{pm,2}$) but it will incur stress losses because of the greater strain (equal to $\varepsilon_{pm,1}$) that it experiences in the reverse loading direction (i.e., when the wall is subjected to $-\Delta_{wm}$).
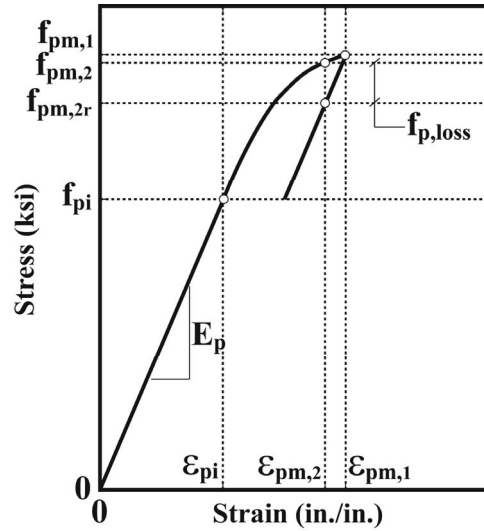


**Figure 4.7  PT Steel Stress-Strain Relationship under Repeated Cycles to $\pm\Delta_{wm}$**

The stress loss, $f_{p,loss}$ in the compression-side PT tendon can be calculated as:

$$f_{p,loss} = f_{pm,2} - f_{pm,2r} \tag{4.26}$$

with

$$f_{pm,2r} = f_{pm,1} - E_p\left(\varepsilon_{pm,1} - \varepsilon_{pm,2}\right) \tag{4.27}$$

where, $f_{pi}$, $\varepsilon_{pi}$=initial strand stress and strain, respectively, after all short-term and long-term stress losses but before any lateral displacements of the wall; $f_{pm,1}$, $\varepsilon_{pm,1}$=stress and strain, respectively, in the tension-side PT tendon at both the initial and repeated loading to $+\Delta_{wm}$ (as determined using Eqn. 4.25); $f_{pm,2}$=stress in the compression-side tendon at initial loading to $+\Delta_{wm}$ (also determined using Eqn. 4.25); $f_{pm,2r}$=stress in the compression-side tendon after repeated loading to $+\Delta_{wm}$; $\varepsilon_{pm,2}$=strain in the compression-side tendon at both the initial and repeated loading to $+\Delta_{wm}$; and $f_{p,loss}$=stress loss in the compression-side tendon due to nonlinear material behavior associated with cyclic loading of the wall to $\pm\Delta_{wm}$.

Note that the above PT stress losses should not be considered during the design steps in Sections 4.4.1 through 4.4.4, which are based on the first-time monotonic loading of the wall through $\Delta_{wd}$

and $\Delta_{wm}$. However, the losses should be incorporated into the design steps in Sections 4.5, 4.6, and 4.8.1, which consider the effects of repeated reversed-cyclic loading of the wall on the PT forces.

**4.4.7 Grout Pad at Base Joint**

The grout pad placed at the base joint is a very important component in the design and construction of the wall. The design 28-day compressive strength of the grout should be within ±20% of the design 28-day strength of the unconfined concrete in the base panel to provide a matching bearing bed for the wall. This strength range, which was used for the grout in the specimens tested as part of this project, resulted in satisfactory behavior at the base. The placement of the grout at each joint should be completed in a single application. The grout should be reinforced with polypropylene microfilament fibers (in amounts per fiber manufacturer's recommendations) to ensure sufficient ductility and toughness. Further, the E.D. bars and the PT tendons should be isolated from the grout so that the deformations of the steel during the lateral displacements of the wall do not deteriorate the integrity of the grout pad.

**4.5 FLEXURAL DESIGN OF UPPER JOINTS**

The E.D. bars crossing the base joint do not continue into the upper panel-to-panel joints, resulting in a significant reduction in the lateral strength of the wall at these locations. The philosophy behind the flexural design of the upper panel-to-panel joints is to prevent significant gap opening and nonlinear behavior of the material through $\Delta_{wm}$. Except for the base joint where the wall is designed to rotate about the foundation, the structure should behave essentially as a rigid body through $\Delta_{wm}$. Thus, the design of the upper panel-to-panel joint is conducted for the maximum joint moment demand, $M_{wm,u}$ corresponding to the probable base moment strength, $M_{wm}$ of the wall (determined in Section 4.4.2).

To prevent significant gap opening at the upper panel-to-panel joints, mild steel reinforcement should be designed at the panel ends as shown in Figures 1.1 and 4.8. The design of this reinforcement is based on the principles of equilibrium, linear material models, and a linear strain distribution (i.e., plane sections assumption). The panel-to-panel reinforcement should be placed in a symmetrical layout. To simplify the presentation of the design process, the PT tendon areas can be lumped at the wall centerline, resulting in the following equations:

$$\bar{C}_{m,u} = A_{s,u}f_{s,u} - A'_{s,u}f'_{s,u} + A_p(f_{pm} - 0.5f_{p,loss}) + N_{w,u} \qquad (4.28)$$

$$\bar{C}_{m,u} = 0.5f_{c,u}t_w c_{m,u} \qquad (4.29)$$

$$\frac{M_{wm,u}}{\phi_{f,u}} = \bar{C}_{m,u}\left(\frac{L_w}{2} - \frac{c_{m,u}}{3}\right) + A_{s,u}f_{s,u}\left(\frac{L_w}{2} - d\right) + A'_{s,u}f'_{s,u}\left(\frac{L_w}{2} - d'\right) \qquad (4.30)$$

with

$$f_{s,u} = \left(\frac{E_s}{E_c}\right)f_{c,u}\left(\frac{L_w - c_{m,u} - d}{c_{m,u}}\right) \qquad (4.31)$$

$$f'_{s,u} = \left(\frac{E_s}{E_c}\right) f_{c,u} \left(\frac{c_{m,u} - d'}{c_{m,u}}\right) \tag{4.32}$$

where, $\bar{C}_{m,u}$=concrete compressive stress resultant at the upper panel-to-panel joint when $\Delta_{wm}$ is reached; $c_{m,u}$=neutral axis length (i.e., contact length) at the upper panel-to-panel joint; $d$, $d'$=centroid location of the tension and compression mild steel bars crossing the upper panel-to-panel joint, respectively (note that $d=d'$); $A_{s,u}$, $A'_{s,u}$=tension and compression mild steel areas crossing the upper panel-to-panel joint, respectively (note that $A_{s,u}=A'_{s,u}$); $f_{s,u}$, $f'_{s,u}$=stresses in the tension and compression mild steel, respectively; $N_{w,u}$=design axial force at the upper panel-to-panel joint (for the design load combination being considered); $f_{c,u}$=maximum concrete compression stress at the upper panel-to-panel joint; $E_s$, $E_c$=Young's modulus of mild steel and concrete, respectively; and $\phi_{f,u}$=0.90 is the capacity reduction factor for the flexural design of the upper panel-to-panel joints.
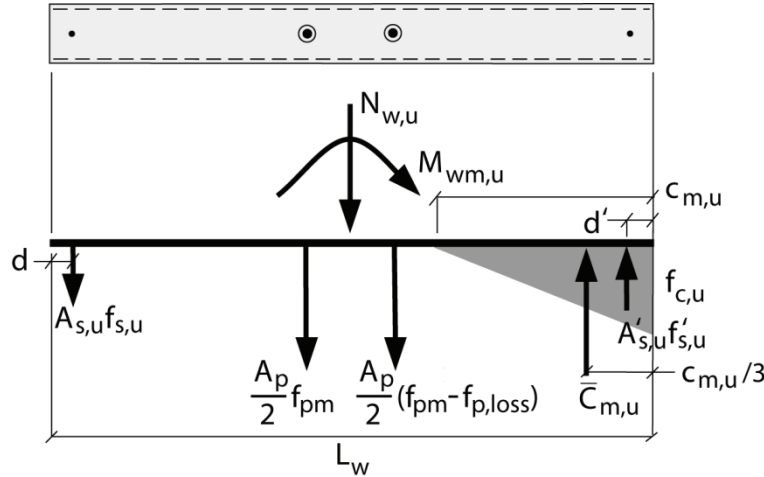


**Figure 4.8  Free Body Diagram of Upper Panel-to-Panel Joint at $\Delta_{wm}$**

In Eqns. 4.28-4.32, the total PT force including losses, $A_p(f_{pm}\text{-}0.5f_{p,loss})$, is a known quantity from the design of the base joint in Sections 4.4.1, 4.4.2, and 4.4.6. By making an initial assumption for the mild steel area, $A_{s,u}$ and the centroid location of the tension and compression bars, $d$ and $d'$, respectively, Eqns. 4.28-4.32 can be solved for $\bar{C}_{m,u}$, $c_{m,u}$, $f_{c,u}$, $f_{s,u}$, and $f'_{s,u}$. The design requires that the tension steel strain be limited to $\varepsilon_{sy}$ (to limit gap opening) and the maximum concrete compressive stress, $f_{c,u}$ be limited to $0.5f'_c$ (to keep the concrete linear elastic). Therefore, the design process is iterated (by revising the mild steel area, $A_{s,u}=A'_{s,u}$) until the steel strain and concrete stress limitations are adequately satisfied. The steel strain limit will control in most cases. These material limits were used in the design of the wall specimens tested as part of this project, with no undesirable behavior developing in the upper panel-to-panel joints.

The upper panel-to-panel joint reinforcement should be placed as close to the panel ends as possible with adequate concrete cover. To prevent strain concentrations in the steel, a short prescribed length of the bars (approximately 4 to 6 in.) should be unbonded at each joint. The

unbonded length can be located in either panel and should include the thickness of the grout pad placed at the joint. Note that reinforcement at joints higher up in the structure may not be required if the PT and gravity forces are large enough to prevent gap opening at these locations. However, a nominal amount of steel should still be used (minimum one No. 3 bar at each panel end) for alignment purposes during the erection of the structure. This minimum amount of reinforcement does not need to be unbonded.


## 4.6 SHEAR DESIGN ACROSS HORIZONTAL JOINTS

To prevent significant horizontal slip of the wall during loading up to the maximum-level drift, $\Delta_{wm}$, the shear friction capacity at the horizontal joints, $V_{ss}$ should be greater than the joint shear force demand, $V_{jm}$. The resulting design equation can be written as:

$$\phi_s V_{ss} > V_{jm} \tag{4.33}$$

where, $\phi_s$=0.75 represents a capacity reduction factor against shear slip failure. The joint shear forces, $V_{jm}$ should be calculated from the maximum base shear force, $V_{wm}$ corresponding to the probable base moment strength, $M_{wm}$ of the wall at $\Delta_{wm}$. Using the compressive force at the wall base to determine the shear friction capacity, $V_{ss}$, Eqn. 4.33 for the base joint can be written as:

$$\phi_s \mu_{ss}(\bar{C}_m - 0.5A_p f_{p,loss}) > V_{wm} \tag{4.34}$$

where, $\mu_{ss}$=0.5 is the shear friction coefficient for the base joint as recommended by Section 5.5.3 of ACI ITG-5.2 (2009). It is assumed that the wall has an adequate amount of restoring force (i.e., self-centering capability) to ensure that the gap at the base joint is fully closed upon removal of the lateral load (see Section 4.8.1).

At the upper panel-to-panel joints, Eqn. 4.33 can be written as:

$$\phi_s \mu_{ss}[(A_{s,u} + A'_{s,u})f_{sy} + A_p(f_{pm} - 0.5f_{p,loss}) + N_{w,u}] > V_{wm,u} \tag{4.35}$$

where, $\mu_{ss}$=0.6 for the upper panel-to-panel joints as recommended by Section 5.5.3 of ACI ITG-5.2; and $V_{wm,u}$=upper joint shear force corresponding to $V_{wm}$. The larger value of $\mu_{ss}$ for the upper joints as compared with the base joint is because deterioration to the grout and concrete at the base joint could lead to reduced slip strength. Note also that unlike the base joint, the concrete compressive stress resultant is not used in Eqn. 4.35 for the upper joints. Instead, $V_{ss}$ at the upper joints is determined by combining the shear friction strength from the axial force due to the PT steel and the gravity load with the shear friction strength from the yielding of the mild steel bars placed at both ends of the wall (similar to the shear friction design method in Section 11.6 of ACI 318).

The specimens tested as part of this project were designed using the above approach. No appreciable slip was measured or observed in the upper joints of the test specimens. For walls that satisfied the axial restoring force requirement in Section 4.8.1, only a small amount of shear

36

slip occurred along the base joint. In some instances, base slip of up to 0.15 in. was measured, exceeding the allowable limit of 0.06 in. per Section 7.1.4(3) of ACI ITG-5.1. However, this slip did not result in any undesirable behavior of the structures. Therefore, the shear slip limit in ACI ITG-5.1 can be increased to 0.15 in. without affecting the wall performance.

## 4.7 DESIGN OF PANEL REINFORCEMENT

This section discusses the reinforcement contained within the individual wall panels (i.e., the panel reinforcement that is not continued across the horizontal joints).

### 4.7.1 Distributed Reinforcement in Wall Panels

Based on the performance of the specimens tested as part of this project, the base panel of a hybrid precast wall is expected to develop diagonal cracking; and thus, distributed vertical and horizontal reinforcement is necessary. The distributed reinforcement in the base panel of solid walls (i.e., without perforations) should be designed following the applicable requirements in Sections 21.9.2 and 21.9.4 of ACI 318 (2011). In addition, the requirements in Section 21.9.6.4(e) of ACI 318 should be satisfied for the development of the wall horizontal reinforcement in the confined boundary regions at the wall toes. The wall specimens in this project were designed using these requirements, resulting in well distributed hairline cracking in the base panel. Horizontal bars that were not developed inside the confined boundary regions reduced the effectiveness of these bars, causing increased spalling and delamination of the cover concrete at the base.

The design of the shear reinforcement in the base panel should be conducted for the maximum base shear force, $V_{wm}$, calculated from $M_{wm}$ at $\Delta_{wm}$. A capacity reduction factor of $\phi_s$=0.75 against shear failure should be used in the design. The reduced capacity reduction factor of 0.60 in Section 9.3.4 of ACI 318 does not apply since the shear design is carried out based on the probable flexural strength of the wall, $M_{wm}$.

The upper panels of the solid walls tested as part of this project developed no cracking; and thus, the distributed reinforcement in the upper panels can be reduced following the requirements in Section 16.4.2 of ACI 318 (2011). Note that this exception does not apply for perforated wall systems. Pre-tensioned wall panels can also be designed with reduced distributed reinforcement by incorporating the effect of the prestressing force on the shear resistance.

Perforated wall panels should be designed according to Chapter 6 of this document.

### 4.7.2 Edge Reinforcement in Wall Panels

Reinforcement should be placed around the entire perimeter of each wall panel using mild steel bars placed parallel to each panel edge. As required by Section 4.4.10 of ACI ITG-5.2 (2009), the mild steel reinforcement along the bottom edge of the base panel should provide a nominal tensile strength of not less than 6000 lbs per horizontal foot along the length of the panel. The bottom edge bars should be anchored using a standard 90° hook at the panel corners with

sufficient development length from the critical location at the neutral axis (i.e., at a distance $c_m$ from each end of the wall). The objective of this reinforcement is to control concrete cracking initiating from the bottom of the base panel near the tip of the gap (see Allen and Kurama 2002); and thus, the bars should be placed as close to the bottom of the panel as practically possible, while also satisfying the ACI 318 concrete cover and spacing requirements. The bottom edge reinforcement in the walls tested as part of this project was designed using this approach. Strain gauges placed on the bars indicated strains reaching approximately $0.85\varepsilon_{sy}$ at $\Delta_{wm}$, where $\varepsilon_{sy}$=yield strain of the steel, supporting the design requirement.

The top and side edges of the base panel as well as all four edges of the upper panels can be reinforced with a reduced amount of perimeter steel, which can be designed by the precast concrete producer to support the temporary loads during the casting, lifting, and transportation operations.

Perforated wall panels should be designed according to Chapter 6 of this document.

### 4.7.3 Other Panel Reinforcement

All other panel reinforcement, including but not limited to any additional reinforcement to control temperature and shrinkage cracks as well as to support lifting inserts, should be designed according to Chapter 16 of ACI 318 (2011).

## 4.8 DESIGN CHECKS

### 4.8.1 Wall Restoring Force

Hybrid precast walls must maintain an adequate amount of axial restoring force (i.e., self-centering capability) to ensure that the gap at the base joint is fully closed upon removal of the lateral load after tensile yielding of the E.D. bars. This restoring force is comprised of the gravity axial force, $N_w$ and the total PT force including losses, $A_p(f_{pm}\text{-}0.5f_{p,loss})$ at $\Delta_{wm}$. Experiments conducted as part of this project (Smith et al. 2012a) demonstrated rapid deterioration of the wall lateral strength and stiffness if significant plastic tensile strains are allowed to accumulate in the E.D. bars and uplift of the wall occurs over the entire base joint upon return of the structure to the zero drift position.

The design requirement is demonstrated in Figure 4.9, which shows an idealized stress-strain relationship for the E.D. steel. As the wall is displaced from the initial position (close to Point A), the E.D. bars yield in tension (Point B) and reach the maximum strain, $\varepsilon_{sm}$ (Point C) at $\Delta_{wm}$. Upon unloading of the wall, the restoring force must be able to yield the tensile E.D. bars back in compression (Point D) and return the bars to essentially zero strain (Point E), requiring a total force reversal of approximately $A_s(f_{sm} + f_{sy})$ such that no significant plastic tensile strains accumulate in the steel.
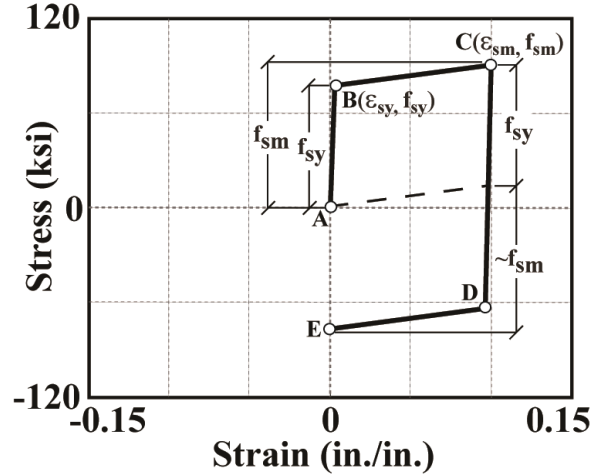
**Figure 4.9 Idealized E.D. Steel Stress-Strain Relationship upon Unloading from $\Delta_{wm}$**

The following equation should be satisfied to provide an adequate amount of axial restoring force through $\Delta_{wm}$:

$$\phi_r \left[ A_p (f_{pm} - 0.5 f_{p,loss}) + N_w \right] > A_s (f_{sm} + f_{sy}) \tag{4.36}$$

where, $\phi_r$=0.90 represents a capacity reduction factor against loss of self-centering. Note that Eqn. 4.36 assumes lumped steel areas; the stresses in the individual bars and tendons should be considered separately if the steel cannot be lumped. Note also that this equation is more demanding than the recommendation in Section 5.3.1 of ACI ITG-5.2 (2009). The restoring force in one of the hybrid wall specimens tested as part of this project was close to the limit given by Section 5.3.1 of ACI ITG-5.2, but was not sufficient to overcome $A_s (f_{sm} + f_{sy})$. This wall developed excessive residual uplift at the base joint due to a lack of sufficient restoring force and the resulting accumulation of plastic tensile strains in the E.D. bars. The wall ultimately failed through significant out-of-plane displacements at the base and buckling of the E.D. bars. The deterioration of the wall occurred very rapidly and before $\Delta_{wm}$ was reached, underscoring the importance of the design requirement given in Eqn. 4.36.

### 4.8.2 Yielding of E.D. Steel

As required by Section 5.3.2 of ACI ITG-5.2, the E.D. steel should reach the yield stress, $f_{sy}$ before the PT steel stress reaches $0.95 f_{py}$, where $f_{py}$=yield strength of the PT steel, determined at the limit of proportionality point on the strand stress-strain relationship (see Figure 4.3). All of the walls that were tested in this project satisfied this requirement.

This page intentionally left blank.

# CHAPTER 5

## PERSCRIPTIVE DESIGN OF HYBRID WALLS

This chapter provides prescriptive simplifications to the performance-based methodology in Chapter 4 for the seismic design of hybrid precast concrete walls as special reinforced concrete shear walls.

The primary objective of the prescriptive design approach is to avoid the iteration steps associated with the performance-based design methodology, while ensuring similar behavior of the walls through the design-level and maximum-level drifts, $\Delta_{wd}$ and $\Delta_{wm}$, respectively. In presenting the prescriptive recommendations, is assumed that:

- The overall dimensions of the wall and the individual wall panels (i.e., height, length and thickness) have been determined for a trial structure. The length and thickness of the wall panels remain constant over the height of the structure.
- The design forces (axial, shear, and bending moment) have been determined.
- The design strengths for the mild steel and concrete have been selected.

The design base shear force, $V_{wd}$, corresponding design base moment, $M_{wd}$, and design-level wall drift, $\Delta_{wd}$, should be determined according to Sections 4.1 and 4.2. The maximum-level wall drift, $\Delta_{wm}$, can be determined using Eqn. 4.1. The preliminary proportioning of the wall geometry can be conducted as described in Section 4.3. As an important limitation, the prescriptive methodology requires that the PT and E.D. steel reinforcement be placed in a symmetrical layout and located within a distance $0.125L_w$ on either side from the wall centerline (i.e., all PT and E.D. steel is placed within the middle $0.25L_w$ of the wall). This requirement is needed to allow for the material stress recommendations below by lumping all PT and E.D. steel reinforcement at the wall centerline.

The design of the PT and E.D. steel areas, $A_p$ and $A_s$, respectively, at the base joint should be conducted to satisfy the design base moment, $M_{wd}$, using fundamental concepts in reinforced and prestressed concrete mechanics. Unlike the performance-based procedure in Section 4.4.1, the prescriptive design approach requires no iteration. Instead, once an appropriate $\kappa_d$ ratio is selected, Eqns. 4.5-4.8 and 4.14 are solved for $A_p$, $A_s$, $\bar{C}_d$, and $c_d$ by assuming that:

$$f_{pd}=1.1f_{pi} \text{ and } f_{sd}=f_{sy}$$

where, $f_{pi}$=initial stress of the PT steel after all short-term and long-term losses (but before any lateral displacements of the wall); and $f_{sy}$=yield strength of the E.D. steel. The value of $\kappa_d$ used in design should not exceed 0.80 and should not be less than 0.50.

Similarly, in lieu of the iterative process required in the performance-based procedure to determine the probable base moment strength, $M_{wm}$, and neutral axis length, $c_m$, at $\Delta_{wm}$, the following series of assumptions can be used, in accordance with Sections 4.4.2 and 4.4.3, to determine the required confined concrete strength and confinement reinforcing details:

41

$$M_{wm}=1.4M_{wd}; \; f_{pm}=0.95f_{py}; \; f_{sm}=1.4f_{sy}; \text{ and } c_m=0.9c_d$$

These assumptions should also be used to determine the E.D. steel unbonded length per Section 4.4.4, E.D. steel development length per Section 4.4.5, PT stress losses per Section 4.4.6, reinforcement at the upper panel-to-panel joints per Section 4.5, design for shear across horizontal joints per Section 4.6, design of panel reinforcement per Section 4.7, and the additional design checks per Section 4.8.

# CHAPTER 6

## DESIGN OF PANEL PERFORATIONS

This chapter provides guidelines for the design of rectangular panel perforations in hybrid precast concrete shear walls. The focus is on the design of the reinforcement contained within the individual wall panels (i.e., reinforcement that is not continued across the horizontal joints). Other aspects of the wall design (e.g., amounts of E.D. and PT steel reinforcement) should be conducted following Chapter 4 or 5.

As shown by the perforated specimens tested as part of this project (Smith et al. 2012a), the presence of perforations in the wall panels results in increased concrete cracking, including cracks that occur in the upper panels. The general design philosophy is to provide an adequate amount of mild steel reinforcement in the vertical and horizontal chords around each perforation such that the presence of the perforations does not negatively affect the performance of the wall through the expected drift demands. The perforated specimens tested in this project were designed using this philosophy, resulting in minimal effect of the perforations on the overall wall behavior.

## 6.1 LOCATION AND SIZE OF PANEL PERFORATIONS

The perforations should be located outside the calculated neutral axis (i.e., contact) length, $c_d$ for the base joint. This will ensure that the perforations are away from the critical compression regions at the toes of the wall. Additionally, the placement of the PT ducts and E.D. steel within the wall panels must be considered when determining the locations of the panel perforations. These two requirements will control the length of the perforations and will typically lead to the use of two perforations in each panel (see Figure 6.1) to allow for the placement of the PT tendons near the wall centerline. The height of the perforations designed using the guidelines in this chapter should be limited to $0.5H_p$, where $H_p$=wall panel height.

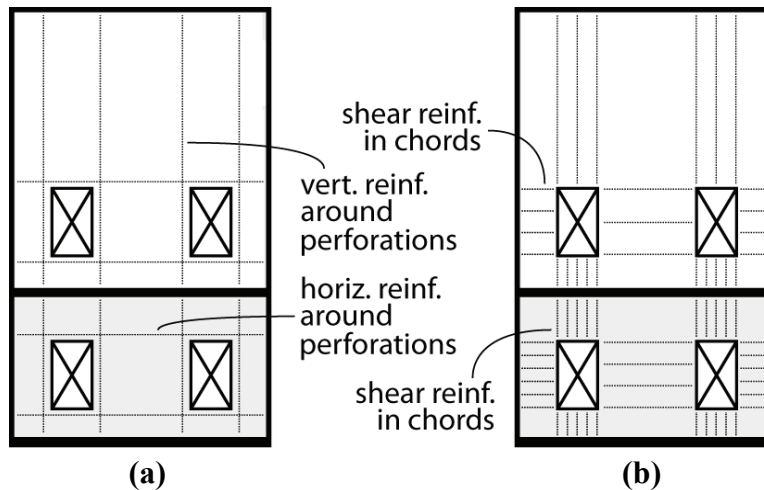## 6.2 DESIGN OF PANEL REINFORCEMENT AROUND PERFORATIONS

The recommended design approach is based on a finite element analytical model of the wall subjected to monotonic pushover analysis through the maximum-level wall drift, $\Delta_{wm}$. The modeling guidelines in Section 3.2 should be followed when creating this model, which uses "hard-contact" surfaces at the horizontal joints to allow for gap opening and linear-elastic tension properties for the concrete, ignoring any cracking. The resulting concrete stresses can then be used to design the horizontal and vertical steel reinforcement as well as the shear reinforcement in the chords around the panel perforations (Figure 6.1).

The horizontal, vertical, and shear stresses in the concrete elements of the finite element model should be used in the design. As an example, Figure 6.2 shows the *x*-direction (i.e., horizontal) stresses, *y*-direction (i.e., vertical) stresses, and shear stresses from the pushover analysis to $\Delta_{wm}$

of one of the perforated walls tested as part of this project. For clarity, only the critical regions of the wall where tensile $x$-direction and $y$-direction stresses and positive shear stresses develop in the concrete are displayed in color, with the other regions colored in black. As shown in Figures 6.2(a) and 6.2(b) for the $x$ and $y$-directions, respectively, the required area, $A_{s,c}$ of the horizontal and vertical mild steel reinforcement around each perforation can be designed by summing the tensile stresses along a cutline (or critical path) to determine the total tensile force, $T_c$. The required steel area, $A_{s,c}$ in each critical region can be then determined as:

$$A_{s,c} = \frac{T_c}{\phi_c f_{sy}}$$

(6.1)

where, $T_c$=total tensile force at cutline; $\phi_c$=capacity reduction factor of 0.75; and $f_{sy}$=design yield strength of the steel.



shear reinf. in chords

vert. reinf. around perforations

horiz. reinf. around perforations

shear reinf. in chords

(a)                                        (b)

**Figure 6.1  Panel Reinforcement Around Perforations:**
**(a) Horizontal and Vertical Reinforcement; (b) Shear Reinforcement**

This process should be repeated for each edge of each panel perforation in the $x$ and $y$-directions and should consider the wall displaced in both directions of loading to the maximum-level wall drift, $\Delta_{wm}$. Alternatively, the reinforcement can be designed at only the most critical location (i.e., the location with the largest tensile force at any edge of the perforations). This reinforcement would then be specified at all edges of each perforation, thus, resulting in a more conservative design. The reinforcement should be placed as close to the edges of the perforations as practically possible, while also satisfying the ACI 318 concrete cover and spacing requirements. Sufficient development length should be provided beyond each critical location (i.e., cutline) to achieve the yield strength, $f_{sy}$ of the bars following the requirements in Section 21.9.2.3 of ACI 318 (2011). Applicable requirements for boundary regions and wall piers in Sections 21.9.6.4 and 21.9.8, respectively, of ACI 318 should also be satisfied. Note that the requirements for coupling beams in Section 21.9.7 of ACI 318 do not apply to the horizontal chords around the perforations since the chord reinforcement is designed not to yield (i.e., unlike a coupling beam, no significant yielding is allowed in the horizontal chords).

The above process can also be used to design the edge reinforcement along the outer perimeter of each wall panel. The bottom edge reinforcement for the base panel should not be less than the amount calculated using Section 4.7.2.

A similar procedure can be followed to calculate the critical shear forces in the horizontal and vertical chords around the perforations [see Figure 6.2(c)]. Unlike the solid wall specimens that were tested as part of this project, the perforated specimens developed diagonal cracking in the upper panels; and thus, shear reinforcement should be designed at the upper levels of the structure as well. Once the maximum chord shear forces are found from the finite element model, the required shear reinforcement areas should be determined following the applicable requirements in Sections 21.9.2 and 21.9.4 of ACI 318 (2011). A capacity reduction factor of $\phi_c$=0.75 should be used for the shear design of the chords.
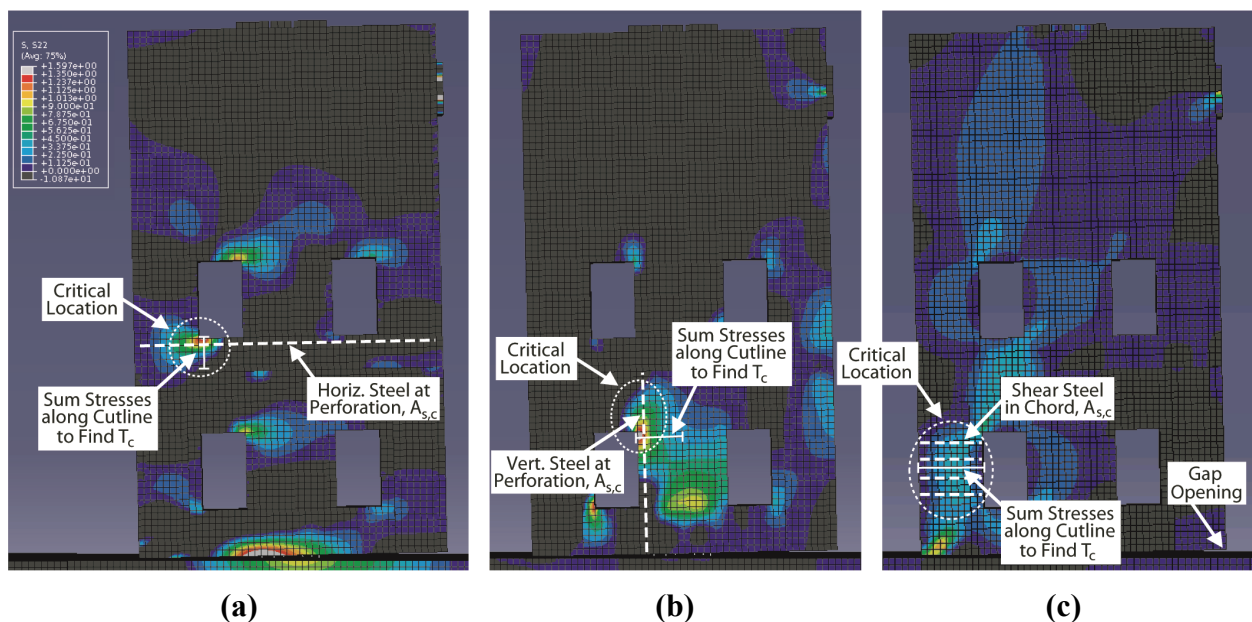


**Figure 6.2  Representative Finite Element Analysis Results:**
**(a) *X*-Direction Tensile Stresses; (b) *Y*-Direction Tensile Stresses; (c) Shear Stresses**

In order to satisfy the maximum limit for the shear strength of a horizontal wall segment in Section 21.9.4.5 of ACI 318, the two adjacent horizontal chords located above the base panel perforation and below the upper panel perforation (or other adjacent horizontal chords at the upper levels of the structure) can be considered as a combined single deep chord. This is acceptable since the upper panel-to-panel joint is designed to be closed between these two chords (i.e., the panels are in contact). As shown in Figure 6.2(c), where the structure has been laterally displaced to the left (gap opening at the base joint can be seen on the right side of the wall), the upper panel-to-panel joint between the critical perforations on the left side of the wall remains closed, resulting in a flow of shear stresses across the joint. Note that while the depths of the two horizontal chords can be combined to satisfy the maximum shear strength limit in Section 21.9.4.5 of ACI 318, each chord should still be designed and reinforced as a separate component using the individual chord depth and shear stresses in that chord.

The design approach outlined above for the reinforcement around the panel perforations has limitations. First, minor localized yielding of the reinforcement can occur due to the redistribution of stresses associated with the cracking of the wall panels, which is not included in the analytical model. Based on the experimental results from the wall specimens tested as part of this project, a small amount of yielding in the reinforcement around the perforations is not expected to impact the local or global performance of the wall. Additionally, as can been seen in Figure 6.2(a), the finite element analysis results indicate that the $x$-direction tensile stresses are larger (i.e., more critical) around the upper panel perforations than around the base panel perforations. However, the test results from this project have shown that the horizontal bars in the base panel are subjected to larger strains, possibly due to the larger amount of cracking that occurs in the base panel. Therefore, the design procedure has a tendency to slightly underestimate the required steel area in the base panel and overestimate the steel area in the upper panels due to the assumptions and simplifications incorporated in the finite element model (i.e., the use of linear elastic properties for the concrete in tension).

The design of the confined boundary regions at the wall toes should follow the requirements in Section 4.4.3. The confined concrete region should extend vertically over a height of the base panel not less than the plastic hinge height, $h_p$.

# CHAPTER 7

# REFERENCES

1. ACI. (2007). "ACI ITG-5.1-07 Acceptance Criteria for Special Unbonded Post-Tensioned Precast Structural Walls Based on Validation Testing and Commentary." ACI Innovation Task Group 5.

2. ACI. (2009). "ACI ITG-5.2-09 Design of a Special Unbonded Post-Tensioned Precast Shear Wall Satisfying ACI ITG-5.1 Requirements." ACI Innovation Task Group 5.

3. ACI. (2011). "ACI 318-11 Building Code Requirements for Structural Concrete (ACI 318-11) and Commentary." ACI Committee 318.

4. Ajrab, J., Pekcan, G., and Mander, J. (2004). "Rocking Wall-Frame Structures with Supplemental Tendon Systems." *Journal of Structural Engineering*, 130(6), 895-903.

5. Allen, M. and Kurama, Y. (2002). "Design of Rectangular Openings in Precast Walls Under Combined Vertical and Lateral Loads." *PCI Journal*, 47(2), 58-83.

6. ANSYS, Inc. (2009). "ANSYS LS-DYNA User's Guide." ANSYS, Inc.

7. ASCE. (2010). "Minimum Design Loads for Buildings and Other Structures." ASCE/SEI 7-10.

8. CSI. (2008). "CSI Analysis Reference Manual for SAP2000, ETABS, and SAFE." Computer and Structures, Inc.

9. Fleischman, R., Naito, C., Restrepo, J., Sause, R., Ghosh, S., Wan, G., Schoettler, M., and Cao, L. (2005a). "Precast Diaphragm Seismic Design Methodology (DSDM) Project, Part 2: Research Program." *PCI Journal*, 50(6), 14-31.

10. Fleischman, R., Naito, C., Restrepo, J., Sause, R., and Ghosh, S. (2005b). "Precast Diaphragm Seismic Design Methodology (DSDM) Project, Part 1: Design Philosophy and Research Approach." *PCI Journal*, 50(5), 68-83.

11. Hibbitt, Karlsson, and Sorenson. (2009). "ABAQUS User's Manual - Version 6.9." Hibbitt, Karlsson & Sorenson, Inc.

12. Holden, T., Restrepo, J., and Mander, J. (2001). "A Comparison of the Seismic Performance of Precast Wall Construction: Emulation and Hybrid Approaches." University of Canterbury, Research Report 2001-4.

13. Holden, T., Restrepo, J., and Mander, J. (2003). "Seismic Performance of Precast Reinforced and Prestressed Concrete Walls." *Journal of Structural Engineering*, 129(3), 286-296.

14. ICBO. (1997). "Uniform Building Code, Volume 2: Structural Engineering Design Provisions." International Conference of Building Officials.

15. ICC. (2010). "Acceptance Criteria for Mechanical Connector Systems for Steel Reinforcing Bars." AC133, ICC Evaluation Services.

16. Kurama, Y. (2000). "Seismic Design of Unbonded Post Tensioned Precast Walls with Supplemental Viscous Damping." *ACI Structural Journal*, 97(4), 648-658.

17. Kurama, Y. (2001). "Simplified Seismic Design Approach for Friction Damped Unbonded Post Tensioned Precast Walls." *ACI Structural Journal*, 98(5), 705-716.

18. Kurama, Y. (2002). "Hybrid Post-Tensioned Precast Concrete Walls for Use in Seismic Regions." *PCI Journal*, 47(5), 36-59.

19. Kurama, Y. (2005). "Seismic Design of Partially Post-Tensioned Precast Concrete Walls." *PCI Journal*, 50(4), 100-125.

20. Kurama, Y., Pessiki, S., Sause, R., and Lu, L.W. (1999a). "Seismic Behavior and Design of Unbonded Post-Tensioned Precast Concrete Walls." *PCI Journal*, 44(3), 72-89.

21. Kurama, Y., Sause, R., Pessiki, S., and Lu, L.W. (1999b). "Lateral Load Behavior and Seismic Design of Unbonded Post-Tensioned Precast Concrete Walls." *ACI Structural Journal*, 96(4), 622-632.

22. Kurama, Y., Sause, R., Pessiki, S., and Lu, L.W. (2002). "Seismic Response Evaluation of Unbonded Post-Tensioned Precast Walls." *ACI Structural Journal*, 99(5), 641-651.

23. Mackertich, S., and Aswad, A. (1997). "Lateral Deformations of Perforated Shear Walls for Low and Mid-Rise Buildings." *PCI Journal*, 42(1), 30-41.

24. Mazzoni, S., McKenna, F., Scott, M., and Fenves G. (2007). "OpenSees Command Language Manual." University of California, Berkeley.

25. Nagae, T., Tahara, K., Matsumori, T., Shiohara, H., Kabeyasawa, T., Kono, S., Nishiyama, M., Wallace, J., Ghannoum, W., Moehle, J., Sause, R., Keller, W., and Tuna, Z. (2011). "Design and Instrumentation of 2010 E-Defense Four-Story Reinforced Concrete and Post-Tensioned Concrete Buildings." University of California, Berkeley, Pacific Earthquake Engineering Research Center (PEER) Report 2011/103.

26. Perez, F., Pessiki, S., Sause, R., and Lu, L.W. (2003). "Lateral Load Tests of Unbonded Post-Tensioned Precast Concrete Walls in Large-Scale Structural Testing." ACI Special Publication SP-211.

27. Perez, F., Pessiki, S., and Sause, R. (2004a). "Seismic Design of Unbonded Post-Tensioned Precast Concrete Walls with Vertical Joint Connectors." *PCI Journal*, 49(1), 58-79.

28. Perez, F., Pessiki, S., and Sause, R. (2004b). "Lateral Load Behavior of Unbonded Post-Tensioned Precast Concrete Walls with Vertical Joints." *PCI Journal*, 49(2), 48-64.

29. Perez, F. J., Sause, R., and Pessiki, S. (2007). "Analytical and Experimental Lateral Load Behavior of Unbonded Posttensioned Precast Concrete Walls." *Journal of Structural Engineering*, 133(11), 1531-1540.

30. Prakash, V., Powell, G., and Campbell, S. (1993). "DRAIN-2DX Base Program Description and User Guide; Version 1.10." University of California, Berkeley, Research Report UCB/SEMM-93/17.

31. Priestley, M., Sritharan, S., Conley, J., and Pampanin, S. (1999). "Preliminary Results and Conclusions from the PRESSS Five-Story Precast Concrete Test Building." *PCI Journal*, 44(6), 42-67.

32. Rahman, A. and Restrepo, J. (2000). "Earthquake Resistant Precast Concrete Buildings: Seismic Performance of Cantilever Walls Prestressed Using Unbonded Tendon." University of Canterbury, Research Report 2000-5.

33. Restrepo, J. (2003). "Self-Centering Precast Post-Tensioned Cantilever Walls – Theory and Experimental Work." *Proceeding of the 2003 ASCE Structures Congress*, Seattle, WA.

34. Smith, B., and Kurama, Y. (2009). "Design of Hybrid Precast Concrete Walls for Seismic Regions." *Proceedings of the 2009 ASCE Structures Congress*, Austin, TX.

35. Smith, B., and Kurama, Y. (2010a). "Analytical Model Validation of a Hybrid Precast Concrete Wall for Seismic Regions." *Proceedings of the 2010 ASCE Structures Congress*, Orlando, FL.

36. Smith, B., and Kurama, Y. (2010b). "Seismic Behavior of a Hybrid Precast Concrete Wall Specimen: Measured Response versus Design Predictions." *Proceedings of the 9th U.S. National and 10th Canadian Conference on Earthquake Engineering*, Toronto, ON, Canada.

37. Smith, B., McGinnis, M., and Kurama, Y. (2010). "Full-Field Lateral Response Investigation of Hybrid Precast Concrete Shear Walls." *Proceedings of the 3rd International Congress and fib Exhibition Incorporating the PCI Annual Convention and Bridge Conference*, Washington D.C.

38. Smith, B., Kurama, Y., and McGinnis, M. (2011a). "Comparison of Hybrid and Emulative Precast Concrete Shear Walls for Seismic Regions." *Proceedings of the 2011 ASCE Structures Congress*, Las Vegas, NV.

39. Smith, B., Kurama, Y., and McGinnis, M. (2011b). "Design and Measured Behavior of a Hybrid Precast Concrete Wall Specimen for Seismic Regions." *Journal of Structural Engineering*, 137(10), 1052-1062.

40. Smith, B., Kurama, Y., and McGinnis, M. (2011c). "Design and Measured Behavior of a Perforated Hybrid Precast Concrete Shear Wall for Seismic Regions." *Proceeding of the 2011 PCI Annual Convention and Exhibition*, Salt Lake City, UT.

41. Smith, B., Kurama, Y., and McGinnis, M. (2012a). "Hybrid Precast Wall Systems for Seismic Regions." Structural Engineering Research Report #NDSE-2012-01, University of Notre Dame, IN, Notre Dame, IN.

42. Smith, B., Kurama, Y., and McGinnis, M. (2012b). "Behavior of Precast Concrete Shear Walls for Seismic Regions: Comparison of Hybrid and Emulative Specimens." J*ournal of Structural Engineering*, In-Review.

43. Smith, B., Kurama, Y., and McGinnis, M. (2012c). "Comparison of Solid and Perforated Precast Concrete Shear Walls for Seismic Regions." *Proceeding of the 2012 ASCE Structures Congress*, Chicago, IL.

44. Smith, B., Kurama, Y., and McGinnis, M. (2012d). "Hybrid Precast Concrete Shear Walls for Seismic Regions: Solid and Perforated Walls." *Proceedings of the 9$^{th}$ International Conference on Urban Earthquake Engineering and 4$^{th}$ Asia Conference on Earthquake Engineering*, Tokyo, Japan.

45. Walsh, K. and Kurama, Y. (2010). "Behavior of Unbonded Post-Tensioning Monostrand Anchorage Systems Under Monotonic Tensile Loading." *PCI Journal*, 55(1), 97-117.

46. Walsh, K. and Kurama, Y. (2012). "Effects of Loading Conditions on the Behavior of Unbonded Post-Tensioning Strand-Anchorage Systems." *PCI Journal*, 57(1), 76-96.

# CHAPTER 8

## DEFINITIONS

<u>Base Joint</u> - Horizontal joint between the base panel and the foundation. Gap opening is designed to occur at the base joint and be the primary mode of lateral displacements for hybrid precast concrete shear walls.

<u>Emulative</u> - Precast concrete systems that are designed and detailed such that their behavior under earthquakes is similar to the behavior of conventional monolithic cast-in-place reinforced concrete structures.

<u>Energy Dissipating (E.D.) Steel</u> - Non-prestressed Grade 60 reinforcement crossing the base joint and designed to yield over a specified unbonded length.

<u>Mild Steel Reinforcement</u> - Non-prestressed Grade 60 reinforcement designed not to yield or dissipate energy. Mild steel reinforcement crossing the upper panel-to-panel joints is designed to prevent significant gap opening at the upper panel-to-panel joints.

<u>Non-Emulative</u> - Precast concrete systems that are designed and detailed such that their behavior under earthquakes is not similar to the behavior of conventional monolithic cast-in-place reinforced concrete structures, but rather governed by the opening and closing of gaps at the joints between the precast members.

<u>Panel Perforation</u> - Opening within the precast concrete wall panel to allow for window, doors, or other functions.

<u>Self-Centering</u> - Action by which a wall returns towards its original undeformed position following deformations beyond the linear-elastic range.

<u>Upper Joint</u> - Horizontal joint between the wall panels (i.e., panel-to-panel joint). No significant gap opening is allowed at the upper panel-to-panel joints.

<u>Wall Drift</u> - Relative lateral displacement at the top of the wall divided by the wall height from the top of the foundation. All lateral deformations and rotations of the structure due to flexure, shear, horizontal shear slip, and gap opening are included in the calculation of the wall drift. However, since the design of a hybrid wall includes provisions to prevent significant shear slip at the horizontal joints and gap opening across the upper panel-to-panel joints, these displacement components can be ignored.

This page intentionally left blank.

# CHAPTER 9

# NOTATIONS

$a_d$ = length of ACI 318 (2011) equivalent rectangular concrete compression stress block at $\Delta_{wd}$

$a_m$ = length of ACI ITG-5.2 (2009) equivalent rectangular concrete compression stress block at $\Delta_{wm}$

$A_{gross}$ = gross area of wall cross section (taken at section with perforations in case of perforated walls)

$A_p$ = total post-tensioning (PT) steel area

$A_s$ = total energy dissipating (E.D.) steel area

$A_{s,c}$ = area of horizontal or vertical chord mild steel reinforcement around panel perforations

$A_{s,u}$ = tension mild steel area crossing upper panel-to-panel joint at panel end

$A'_{s,u}$ = compression mild steel area crossing upper panel-to-panel joint at panel end

$A_{sh}$ = effective shear area of wall cross section

$c$ = neutral axis length (i.e., contact length) at horizontal joint

$c_d$ = neutral axis length at base joint at $\Delta_{wd}$

$c_m$ = neutral axis length at base joint at $\Delta_{wm}$

$c_{m,u}$ = neutral axis length at upper panel-to-panel joint at $\Delta_{wm}$

$C_d$ = ASCE-7 (2010) deflection amplification factor

$\bar{C}_d$ = concrete compressive stress resultant at base joint at $\Delta_{wd}$

$\bar{C}_m$ = concrete compressive stress resultant at base joint at $\Delta_{wm}$

$\bar{C}_{m,u}$ = concrete compressive stress resultant at upper panel-to-panel joint at $\Delta_{wm}$

$d$ = centroid location of tension mild steel bars crossing upper panel-to-panel joint

$d'$ = centroid location of compression mild steel bars crossing upper panel-to-panel joint

$d_s$ = diameter of E.D. bar

$e_p$ = distance of individual PT tendon from wall centerline

$e_s$ = distance of individual E.D. bar from wall centerline

$E_c$ = Young's modulus of unconfined concrete

$E_p$ = Young's modulus of PT steel

$E_s$ = Young's modulus of E.D. (or mild) steel

$f_{c,u}$ = maximum concrete compression stress at upper panel-to-panel joint at $\Delta_{wm}$

$f'_c$ = design compression strength of unconfined panel concrete

$f'_{cc}$ = design compression strength of confined concrete at toes of base panel

$f_{p,loss}$ = stress loss in compression-side PT tendon due to nonlinear material behavior associated with cyclic loading of wall to $\pm\Delta_{wm}$

$f_{pd}$ = PT steel stress at $\Delta_{wd}$

$f_{pi}$ = initial stress of PT steel after all short-term and long-term losses (but before any lateral displacements of wall)

$f_{pm}$ = PT steel stress at $\Delta_{wm}$

$f_{pm,1}$ = stress in tension-side PT tendon at initial and repeated loading to $\pm\Delta_{wm}$

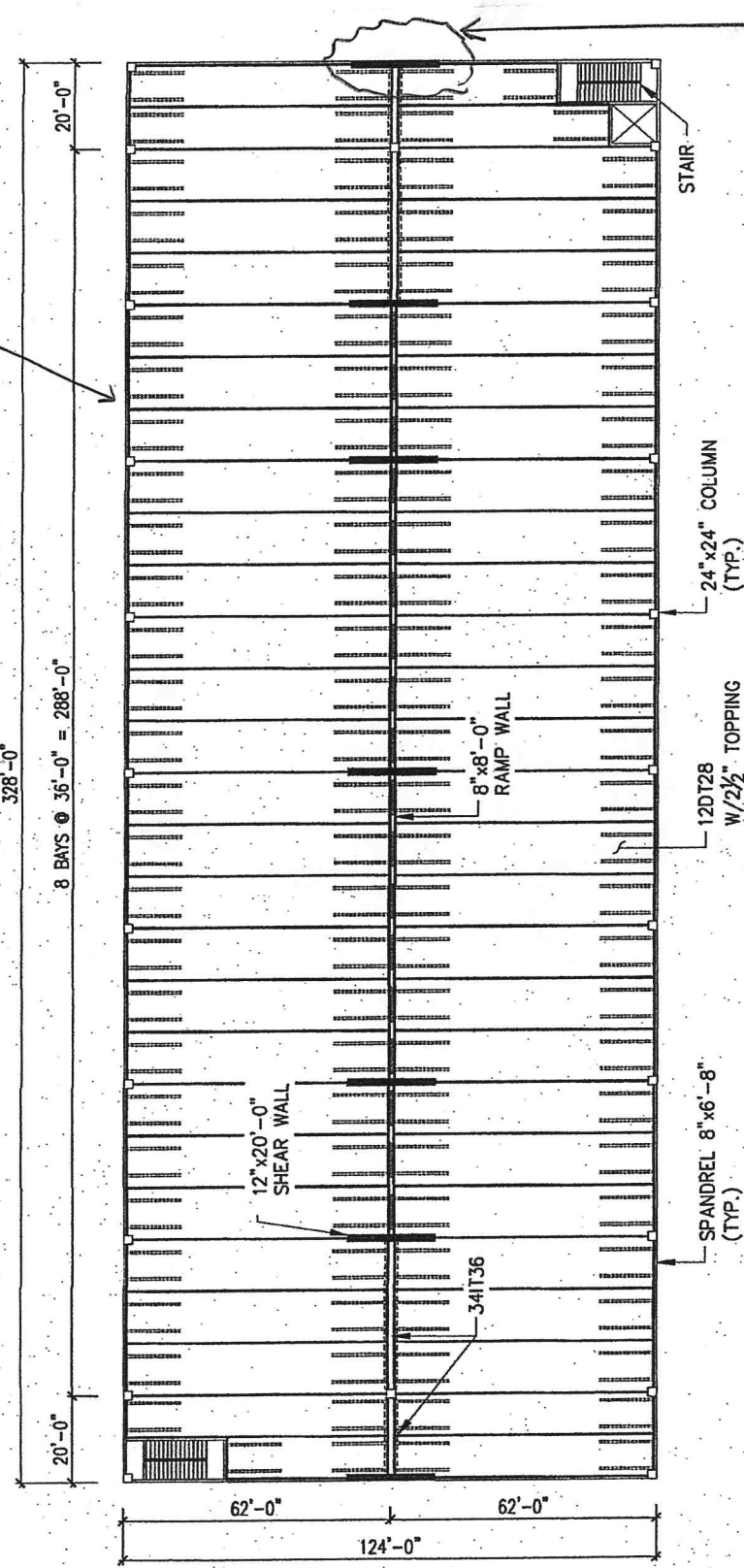$f_{pm,2}$ = stress in compression-side PT tendon at initial loading to $+\Delta_{wm}$

$f_{pm,2r}$ = stress in compression-side PT tendon after repeated loading to $+\Delta_{wm}$

$f_{py}$ = yield strength of PT steel, defined at the limit of proportionality point on the strand stress-strain relationship

$f_{s,u}$ = stress in tension mild steel crossing upper panel-to-panel joint at $\Delta_{wm}$

$f'_{s,u}$ = stress in compression mild steel crossing upper panel-to-panel joint at $\Delta_{wm}$

$f_{sd}$ = E.D. steel stress at $\Delta_{wd}$

$f_{sm}$ = E.D. steel stress at $\Delta_{wm}$

$f_{su}$ = ultimate (maximum) strength of E.D. (or mild) steel

$f_{sy}$ = yield strength of E.D. (or mild) steel

$F$ = applied lateral force at top of wall

$G_c$ = shear modulus of concrete

$h_{cr}$ = height at wall base over which tension strength of concrete fibers is taken as zero within fiber element model

$h_{gap}$ = height used to determine rotation of wall due to gap opening in linear-elastic effective stiffness model

$h_p$ = plastic hinge height over which plastic curvature is assumed to be uniformly distributed at wall base

$H_p$ = wall panel height

$H_w$ = wall height from top of foundation

$I_e$ = reduced linear-elastic effective moment of inertia of wall cross section

$I_{gap}$ = moment of inertia of wall base cross section in compression (i.e., contact region at base joint) in linear-elastic effective stiffness model

$I_{gross}$ = moment of inertia of gross wall cross section (taken at section with perforations in case of perforated walls)

$l_{pu}$ = unbonded length of PT steel strand

$l_{su}$ = total unbonded length of E.D. steel (i.e., wrapped length plus additional debonded length expected under cyclic loading of wall)

$l_{sw}$ = wrapped length of E.D. steel

$L_w$ = wall length

$M_{wd}$ = wall design base moment at $\Delta_{wd}$

$M_{wm}$ = probable base moment strength of wall at $\Delta_{wm}$

$M_{wm,u}$ = upper panel-to-panel joint moment corresponding to $M_{wm}$ at $\Delta_{wm}$

$M_{wn}$ = contribution of wall gravity axial force, $N_w$ to satisfy $M_{wd}$

$M_{wp}$ = contribution of PT steel to satisfy $M_{wd}$

$M_{ws}$ = contribution of E.D. steel to satisfy $M_{wd}$

$N_w$ = design gravity axial force at wall base

$N_{w,u}$ = design gravity axial force at upper panel-to-panel joint

$R$ = response modification factor from ASCE-7 (2010)

$t_w$ = wall thickness

$T_c$ = total horizontal or vertical design tensile force in chord around panel perforations

$V_{jm}$ = maximum shear force at horizontal joint at $\Delta_{wm}$

$V_{ss}$ = shear friction capacity at horizontal joint

$V_w$ = wall base shear force

$V_{wd}$ = design base shear force corresponding to $M_{wd}$ at $\Delta_{wd}$

$V_{wm}$ = maximum base shear force corresponding to $M_{wm}$ at $\Delta_{wm}$

$V_{wm,u}$ = upper panel-to-panel joint shear force corresponding to $V_{wm}$

$z_d$ = distance between tension and compression stress resultants at base joint at $\Delta_{wd}$

$z_m$ = distance between tension and compression stress resultants at base joint at $\Delta_{wm}$

$\alpha_s$ = ACI ITG-5.2 (2009) coefficient to estimate additional E.D. bar debonding that is expected to occur during reversed-cyclic lateral displacements of wall

$\beta_1$ = ACI 318 (2011) factor that relates $c_d$ to length, $a_d$ of equivalent rectangular concrete compression stress block at $\Delta_{wd}$

$\beta_m$ = ACI ITG-5.2 (2009) factor that relates $c_m$ to length, $a_m$ of equivalent rectangular concrete compression stress block at $\Delta_{wm}$

$\delta_p$ = elongation of PT strand due to lateral displacement of wall

$\delta_s$ = elongation of E.D. bar due to lateral displacement of wall

$\delta_w$ = total lateral displacement at top of wall

$\delta_{we}$ = component of $\delta_{w,flex}$ due to linear-elastic flexural deformations over wall height

$\delta_{w,flex}$ = wall displacement due to flexural deformations in linear-elastic effective stiffness model

$\delta_{w,gap}$ = component of $\delta_{w,flex}$ due to gap opening at wall base

$\delta_{w,sh}$ = wall displacement due to shear deformations in linear-elastic effective stiffness model

$\Delta_w$ = wall drift, defined as relative lateral displacement at wall top divided by height from top of foundation

$\Delta_{wc}$ = typical minimum drift capacity of special unbonded post-tensioned precast concrete shear walls based on ACI ITG-5.1 (2007)

$\Delta_{wd}$ = design-level wall drift corresponding to Design-Basis Earthquake (DBE)

$\Delta_{we}$ = linear-elastic wall drift calculated using linear-elastic effective stiffness model

$\Delta_{wm}$ = maximum-level wall drift corresponding to Maximum-Considered Earthquake (MCE)

$\varepsilon_{cm}$ = maximum concrete compression strain at base joint at $\Delta_{wm}$

$\varepsilon_p$ = strain of PT steel

$\varepsilon_{pd}$ = strain in PT steel at $\Delta_{wd}$

$\varepsilon_{pi}$ = initial PT steel strain after all short-term and long-term losses (but before any lateral displacements of wall)

$\varepsilon_{pm,1}$ = strain in tension-side PT tendon at initial and repeated loading to $+\Delta_{wm}$

$\varepsilon_{pm,2}$ = strain in compression-side PT tendon at initial and repeated loading to $+\Delta_{wm}$

$\varepsilon_{py}$ = yield strain of PT steel, defined at the limit of proportionality point on the strand stress-strain relationship

$\varepsilon_s$ = E.D. steel strain

$\varepsilon_{sa}$ = allowable strain in E.D. steel at $\Delta_{wm}$

$\varepsilon_{sd}$ = strain in E.D. steel at $\Delta_{wd}$

$\varepsilon_{sm}$ = strain in E.D. steel at $\Delta_{wm}$

$\varepsilon_{su}$ = strain of E.D. steel at $f_{su}$

$\varepsilon_{sy}$ = yield strain of E.D. (or mild) steel at $f_{sy}$

$\gamma_m$ = ACI ITG-5.2 (2009) factor that relates stress of rectangular confined concrete compression block at toe of base panel to confined concrete strength, $f'_{cc}$

$\kappa_d$ = E.D. steel moment ratio, defining relative amounts of energy dissipating resistance (from $A_s f_{sd}$) and restoring resistance (from $A_p f_{pd}$ and $N_w$) at wall base

$\phi_c$ = capacity reduction factor for design of chord reinforcement around panel perforations

$\phi_f$     = capacity reduction factor for axial-flexural design of base joint

$\phi_{f,u}$     = capacity reduction factor for axial-flexural design of upper panel-to-panel joints.

$\phi_r$     = capacity reduction factor against loss of restoring

$\phi_s$     = capacity reduction factor for shear design

$\varphi_{wm}$     = plastic curvature at wall base at $\Delta_{wm}$

$\rho_h$     = confinement reinforcement ratio at wall toes

$\theta_{gap}$     = rotation of wall due to gap opening at base in linear-elastic effective stiffness model

$\mu_{ss}$     = coefficient of shear friction at horizontal joints

# APPENDIX A

# DESIGN EXAMPLE

**EXAMPLE GARAGE FLOOR PLAN**

LFRS IN LONG. DIRECTION PROVIDED BY FRAME.

DESIGN THIS WALL, ONE OF 7 HYBRID WALLS IN TRANSVERSE DIRECTION.

STAIR

24"x24" COLUMN (TYP.)

8"x8'-0" RAMP WALL

12DT28 W/2½" TOPPING

12"x20'-0" SHEAR WALL

SPANDREL 8"x6'-8" (TYP.)

34T36

20'-0"

8 BAYS @ 36'-0" = 288'-0"

328'-0"

20'-0"

62'-0"     62'-0"

124'-0"

* PROTOTYPE BUILDING CONCEPTUAL DESIGN COURTESY OF CEG-TEXAS

| FLOOR HEIGHTS | |
|---|---|
| LEVEL 1-2 | 12'-0" |
| LEVEL 2-3 | 11'-0" |
| LEVEL 3-4 | 11'-0" |
| LEVEL 4-5 | 11'-0 |

## SECTION 4.1 — SEISMIC DESIGN FORCES:

- ### BUILDING WEIGHT (DEAD LOADS):

    - FLOOR DOUBLE TEES w/ TOPPING = 90 psf
    - LOAD BEARING SPRANDRELS = 780 #/ft
    - NONLOAD BEARING SPRANDRELS = 680 #/ft
    - IT BEAMS = 1000 #/ft
    - COLUMNS = 600 #/ft
    - RAMP WALLS = 800 #/ft
    - STAIRS = 100 psf
    - SHEAR WALLS = 150 psf

- ### LEVEL TWO : (TRIB. HEIGHT = $\frac{12'}{2} + \frac{11'}{2}$ = 11.5')

    | | | |
    |---|---|---|
    | – DOUBLE TEES w/ TOPPING | $= (0.09^{ksf})(328')(124')$ | $= 3660^k$ |
    | – L.B. SPRANDRELS | $= (0.78^{k/ft})(2 \cdot 328')$ | $= 512^k$ |
    | – N.L.B. SPRANDRELS | $= (0.68^{k/ft})(4 \cdot 62' - 2 \cdot 20')$ | $= 141^k$ |
    | – IT BEAMS | $= (1.0^{k/ft})(2 \cdot 34' + 2 \cdot 16')$ | $= 100^k$ |
    | – COLUMNS | $= (0.6^{k/ft})(11.5')(24)$ | $= 166^k$ |
    | – SHEAR WALLS | $= (0.15^{ksf})(20')(11.5')(7)$ | $= 242^k$ |
    | – RAMP WALLS | $= (0.80^{k/ft})(11.5')(18)$ | $= 166^k$ |
    | – STAIRS & ELEVATOR WALLS | $= (0.10^{ksf})(11.5')(40')$ | $= 46^k$ |
    | – STAIRS | $= (0.16 - 0.09^{ksf})(10')(20')(2)$ | $= 28^k$ |

    $$\omega_2 = 5061^k$$

- ### LEVEL THREE & FOUR : (TRIB. HEIGHT = 11')

    | | | |
    |---|---|---|
    | – REDUCE RAMP WALLS | $= (0.8^{k/ft})(0.5')(18)$ | $= 7^k$ |
    | – REDUCE COLUMNS | $= (0.6^{k/ft})(0.5')(24)$ | $= 7^k$ |
    | – REDUCE SHEAR WALLS | $= (0.15^{ksf})(20')(0.5')(7)$ | $= 11^k$ |
    | – REDUCE STAIRS & ELEVATOR WALLS | $= (0.10^{k/ft})(0.5')(40')$ | $= 2^k$ |

    $$\Delta\omega = 27^k$$

    $$\therefore \omega_3 = \omega_4 = 5034^k$$

- ### LEVEL FIVE : (TRIB. HEIGHT = $\frac{11'}{2}$ = 5.5')

    | | | |
    |---|---|---|
    | – REDUCE WALLS & COLUMNS | $= (27^k)(5.5'/0.5')$ | $= -297^k$ |
    | – ADD WALL EXTENSION @ ROOF | $= 70^k$ | $= 70^k$ |

    $$\Delta\omega = 227^k$$

    $$\therefore \omega_5 = 4807^k$$

$$\therefore \text{TOTAL DL} = \omega_2 + \omega_3 + \omega_4 + \omega_5 = 19936^k$$

SEISMIC DESIGN: (ASCE 7-05 EQUIVALENT LATERAL FORCE PROCEDURE)

$$V = C_s W \quad \text{where} \quad W = 19936^k$$

- For Los Angeles, CA, 90045 per ASCE 7-05

$$S_S = 1.500$$
$$S_1 = 0.640$$
$$\text{SITE CLASS} = D$$
$$I = 1.0$$
$$R = 6.0 \quad \text{(Special RC walls w/ Frame System)}$$
$$C_d = 5.0$$

$$\therefore S_{DS} = \tfrac{2}{3} S_{MS} \qquad\qquad \therefore S_{D1} = \tfrac{2}{3} S_{M1}$$
$$S_{MS} = F_a S_a \qquad\qquad\qquad S_{M1} = F_v S_1$$

- For Site Class D:  $F_a = 1.0$
$$F_v = 1.5$$

$$\therefore S_{DS} = 1.000$$
$$S_{D1} = 0.640$$

- Period:  $T = C_t h_n^x = (0.02)(45^{ft})^{0.75} = 0.347 \text{ sec}$

$$\therefore C_s = \frac{S_{DS}}{R/I} = \frac{1.000}{(6/1)} = 0.167$$

$$\therefore C_{s,min} = 0.044 \, S_{DS} \, I = (0.044)(1.00)(1.0) = 0.044$$

$$\therefore C_{s,max} = \frac{S_{D1}}{T(R/I)} = \frac{0.640}{(0.347)(6/1)} = 0.307$$

$$\therefore \underline{\underline{C_s = 0.167}}$$

$$\therefore V = C_s W = (0.167)(19936) = \underline{\underline{3323^k}}$$

VERTICAL DISTRIBUTION OF FORCES: (per ASCE 7-05)

$$F_x = C_{vx} V \quad \text{where} \quad V = 3323^k$$

$$C_{vx} = \frac{w_x h_x^k}{\sum\limits_{i=1}^{n} w_i h_i^k} \quad \text{where} \quad k = 1.0$$

| LEVEL | HEIGHT (h) | WEIGHT (w) | $w \cdot h^k$ | $C_{vx}$ | $F_x$ |
|---|---|---|---|---|---|
| 2 | 12' | $5061^k$ | $60,732^{k-1}$ | 0.108 | $357.8^k$ |
| 3 | 23' | $5034^k$ | $115,782^{k-1}$ | 0.205 | $682.2^k$ |
| 4 | 34' | $5034^k$ | $171,156^{k-1}$ | 0.303 | $1008.5^k$ |
| 5 | 45' | $4807^k$ | $216,315^{k-1}$ | 0.384 | $1274.5^k$ |
| | | $\Sigma = 19936^k$ | $\Sigma = 563,985^{k-1}$ | $\Sigma = 1.00$ | $\Sigma = 3323^k$ |

TORSION:

FRAMES IN LONG. DIRECTION NOT SHOWN. ASSUME $k_{frame} = 7.5 \, k_{wall}$



CM & CR

$F_v$

$\vdash e \dashv$

62'

62'

PROTOTYPE WALL TO BE DESIGNED

$\vdash 56' \dashv 36' \vdash 72' \dashv 72' \vdash 36' \dashv 56' \dashv$
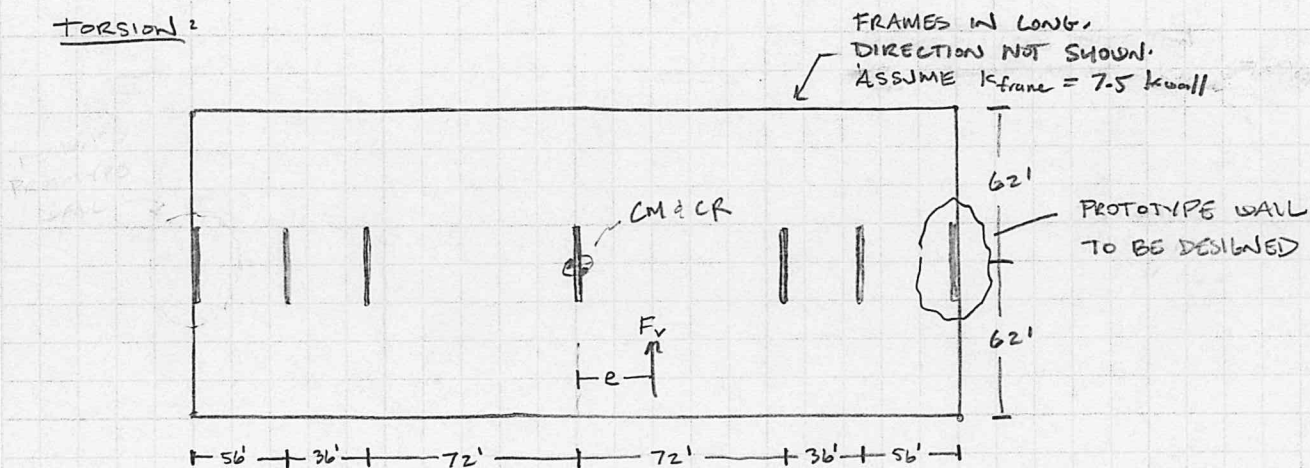
- Assume perfectly rigid diaphragms and all walls have equal rigidity (R)

- Translational component $= V' = \dfrac{k_{wall}}{\Sigma k_{wall}} = \dfrac{k_{wall}}{7 k_{wall}} = \dfrac{1}{7} = 0.1429$

- Rotational component $= V'' = \dfrac{e \cdot d \cdot k_{wall}}{\Sigma d^2 k_{wall} + \Sigma d^2 k_{frame}}$

$e = (0.05)(328') = 16.4^{ft}$

$d =$ distance btwn walls and center of rigidity

$k_{frame} =$ in-plane stiffness of frame (ASSUME $k_{frame} = 7.5 \, k_{wall}$)

$k_{wall} =$ in-plane stiffness of wall

$\therefore V'' = \dfrac{(16.4')(162') k_{wall}}{2 k_{wall} (162^2 + 108^2 + 72^2) + 2(7.5 k_{wall})(62^2)}$

$V'' = 0.0184$

$\therefore V_{total} = V' + V'' = 0.1429 + 0.0184 = 0.1613$

SEISMIC DESIGN CONT'D?

$\therefore F_{x \, wall} = 0.1613 \, F_x$
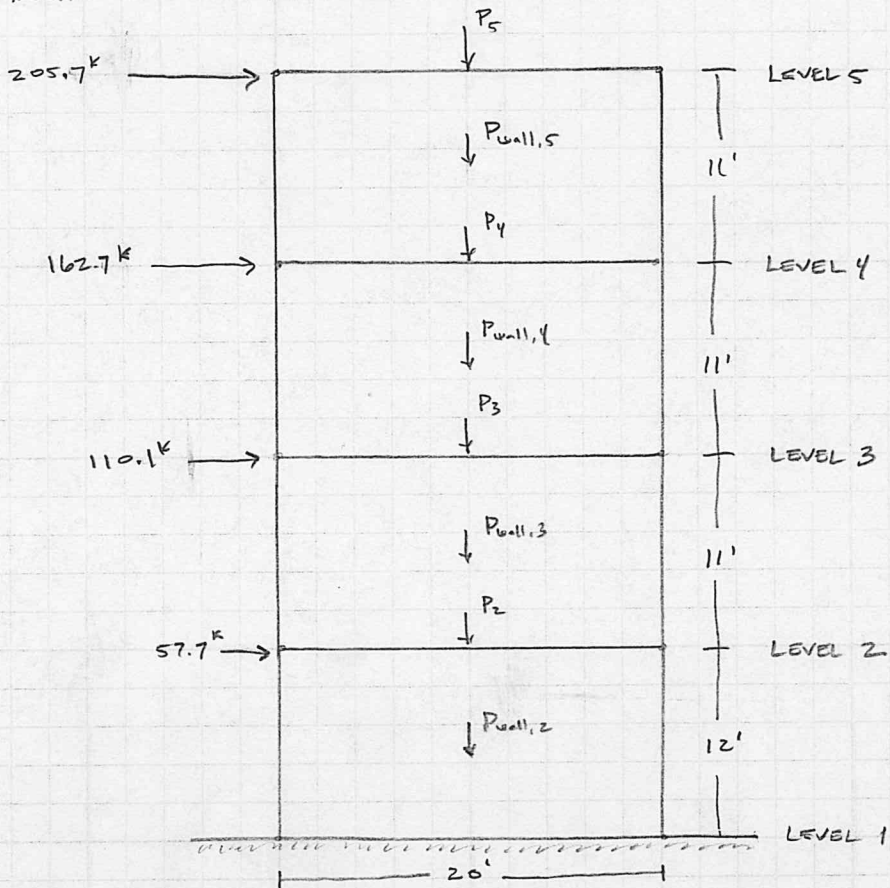


- WEIGHTS:

$P_2 = P_3 = P_4 = P_5 = 1T \text{ Beam } DL = (1.0^{k/ft})(\frac{16'}{2}) + (0.09^{ksf})(\frac{(62')(16')}{2}) = 52.6^k$

$P_{wall,2} = (0.15^{ksf})(20')(12') = 36^k$

$P_{wall,3} = P_{wall,4} = P_{wall,5} = (0.15^{ksf})(20')(11') = 33^k$

- ASCE 7-05 : SECTION 12.4.2 :

LOAD CASE #7: $= 0.9 D_L - 0.2 S_{DS} D_L + \rho Q_E + 1.6H = 0$

$H = 0$ ; $S_{DS} = 1.0$ ;

$\rho = 1.0$ BASED ON ASCE 7-05, SECTION 12.3.4.2(a):

⇒ NO TORSIONAL IRREGULARITY

⇒ LOSS OF SHEAR WALL WOULD HAVE LESS THAN 33% STRENGTH REDUCTION

SHEAR FORCES :

$\therefore LC7 = 0.7 D_L + Q_E$

| LEVEL | SHEAR | MOMENT | GRAVITY LOAD | LOAD CASE #1 |
|---|---|---|---|---|
| 4 | $205.7^k$ | $2262.7^{k-1}$ | $85.6^k$ | $59.9^k$ |
| 3 | $368.4^k$ | $6315.1^{k-1}$ | $171.2^k$ | $119.8^k$ |
| 2 | $478.5^k$ | $11578.6^{k-1}$ | $256.8^k$ | $179.8^k$ |
| 1 | $536.2^k$ | $18013.0^{k-1}$ | $345.4^k$ | $241.8^k$ |

$18,013^{k-ft} = M_{uD}$

** DESIGN EXAMPLE WILL ONLY USE LOAD CASE #7, OTHER LOAD COMBO'S, INCLUDING THE APPROPRIATE APPLICATION OF ORTHOGONAL LOAD COMBINATIONS & OVERSTRENGTH FACTORS, SHOULD BE EXPLORED.

• MATERIAL ASSUMPTIONS:

- CONCRETE: $f_c' = 6^{ksi}$       — NON E.D. STEEL: $f_{sy} = 60^{ksi}$

- E.D. STEEL: $f_{sy} = 65^{ksi}$ ⎫ → USING MEASURED STRESS-STRAIN PROPERTIES
  $f_{su} = 95^{ksi}$ ⎬    OF E.D. STEEL FOR DESIGN EXAMPLE (SEE BELOW)
  $E_s = 29,000^{ksi}$ ⎭   TO DEMONSTRATE USE OF STEEL STRESS-STRAIN RELATIONSHIP

- PT STEEL: $f_{pi} = (0.65)(0.85)(270^{ksi}) = 149.2^{ksi}$

  ↑ ASSUMED FACTOR FOR SHORT-TERM & LONG-TERM PT LOSSES.

  $f_{py} = 235^{ksi}$ → BASED ON MEASURED STRESS-STRAIN PROPERTIES
  $E_{pi} = 28,500^{ksi}$      OF THE PT STRAN (SEE BELOW)



E.D. STEEL
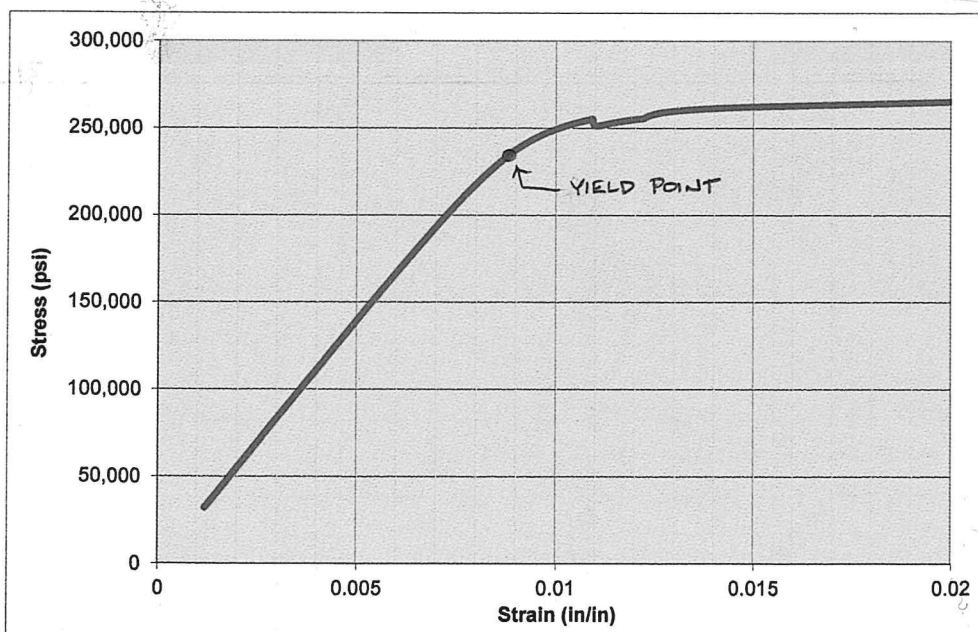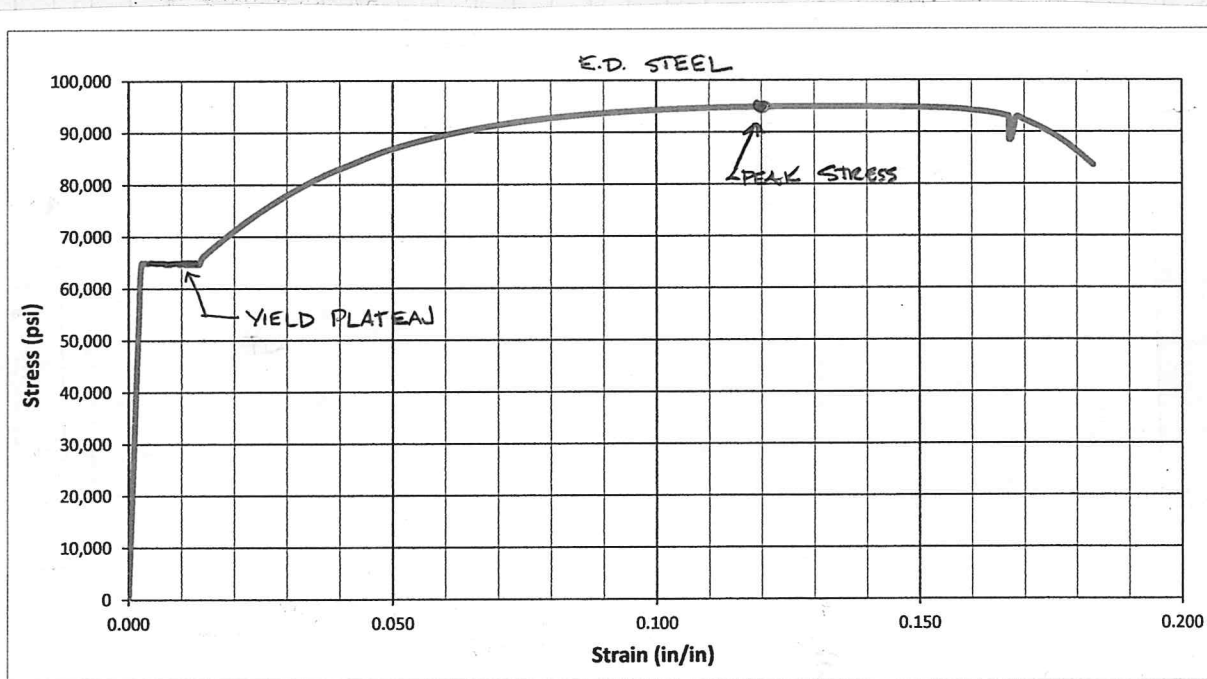
SECTION 4.2 — WALL DRIFT DEMANDS

DRIFTS (per ASCE-7)

$M_{ud} = 18,013^{k-1}$

$V_{ud} = 536.2^{k}$

-FOR POINT LOAD: $h = \dfrac{M_{ud}}{V_{ud}} = \dfrac{18013^{k-1}}{536.2'} = 33.6'$



$H_o = 45^{FT}$
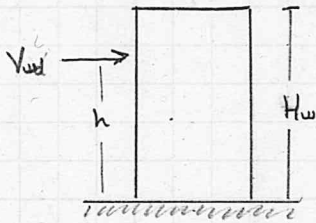
$h = 33.6^{FT}$

$t_w = 15^{in}$ (THICKNESS)

$L_w = 20^{FT}$

$E_c = 57,000 \sqrt{f_c'} = 57000 \sqrt{6000} = 4415^{ksi}$

$I_{gross} = \dfrac{1}{12} b L^3 = \dfrac{1}{12} \left(\dfrac{15"}{12}\right) (20^{FT})^3 = 833.3^{FT^4}$

$I_e = 0.5 \, I_{gross} = 416.67^{FT^4}$

A) DEFLECTION OF CANTILEVER WALL:

$\delta_{w,flex} = \dfrac{V_{ud} \, h^2}{6 E_c I_e} (3H_o - h) = $ DEFLECTION AT TOP OF WALL

$= \dfrac{(536.2^k)(33.6^{FT})^2 (3(45') - 33.6')}{(6)(4415.2^{ksi})(416.67^{FT^4})\left(\dfrac{12^{in}}{ft}\right)^2} = 0.039^{ft} = 0.47^{in}$

B) SHEAR DEFLECTION:

$\gamma = \dfrac{V_{ud}}{G_c A_{sh}}$ where $A_{sh} = 0.8 \, A_{gross}$

$A_{sh} = (0.8)(15")(20 \cdot 12") = 2880 \, in^2$

$G_c = \dfrac{E_c}{2(1+\nu)} = \dfrac{4415.}{(2)(1+0.18)} = 1871^{ksi}$

$\therefore \gamma = \dfrac{536.2^k}{(1871)(2880 \, in^2)} = 9.951 \, e\text{-}5$

$= \delta_{w,sh} = \gamma H_o = (9.951 \, e\text{-}5)(45^{FT}) = 0.05^{in}$

$\therefore \delta_w = \delta_{w,flex} + \delta_{w,sh} = 0.47 + 0.05 = \underline{\underline{0.52^{in}}}$

$\therefore \Delta_{we} = \dfrac{(0.52^{in})}{(45^{FT})(12^{in}/ft)} \times 100 = \underline{\underline{0.096\%}}$  LINEAR-ELASTIC DRIFT

DRIFTS CONT'D:

- PER ASCE-7 (SECT. 12.8.6):

$$\Delta_{wD} = \frac{C_d \delta_{we}}{I} \qquad \text{where} \quad I = 1.0$$
$$C_d = 5.0$$

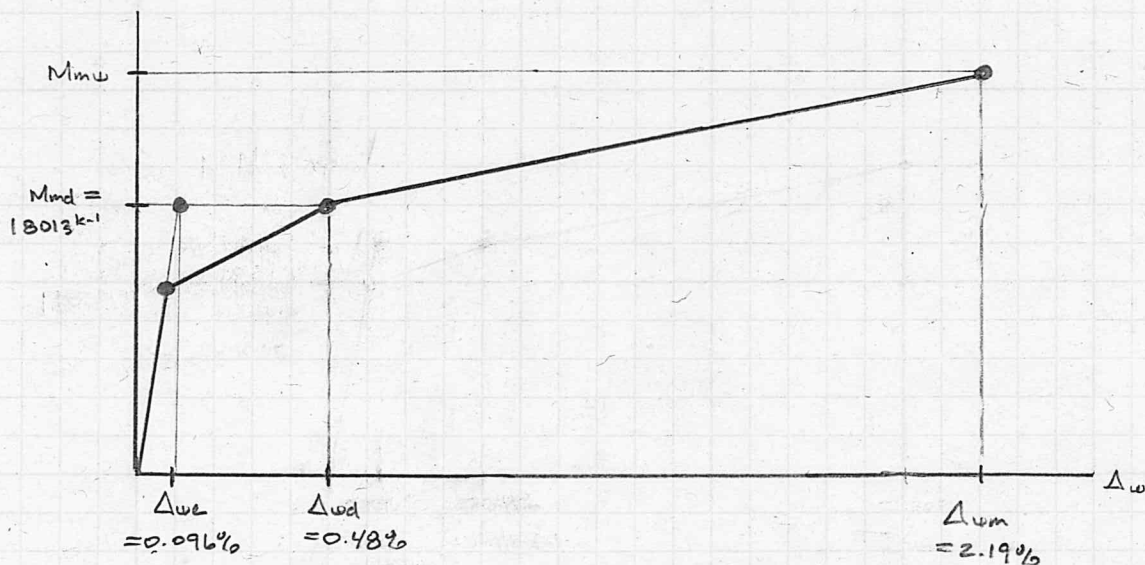$$\therefore d_{wd} = \frac{(5.0)(0.52\text{in})}{(1.0)} = 2.6 \text{ in}$$

$$\Delta_{wd} = \frac{(2.6\text{in})}{(45')(12^{in}/_1)} \times 100 = \underline{\underline{0.48\%}} \qquad \text{DESIGN-LEVEL} \atop \text{DRIFT}$$

- PER ACI ITG-5.1:

$$\Delta_{wc} = 0.9 \leq 0.8\left(\frac{H_w}{L_w}\right) + 0.5 \leq 3.0$$
$$0.8\left(\frac{45}{20}\right) + 0.5 = 2.3\%$$

$$\Delta_{wm} = 0.95 \Delta_{wc} = \underline{\underline{2.19\% = \Delta_{wm}}}$$



MOMENT-DRIFT RELATIONSHIP

SECTION 4.3:

PROPORTIONING OF WALL
CROSS-SECTION GEOMETRY:

$$V_{ud} = 536.2^k$$

$$A_{gross} = L_u t_u = (20')(15'') = 3600^{in^2}$$

$$f_c' = 6000^{psi}$$

$$\therefore \frac{V_{ud}}{A_{gross}} = \frac{536.2^k}{3600^{in^2}} = 0.149^{ksi} = 149 psi$$

$$149 \frac{\sqrt{f_c'}}{\sqrt{f_c'}} = \frac{149\sqrt{f_c'}}{\sqrt{6000}} = 1.94\sqrt{f_c'} < 3\sqrt{f_c'} \quad \underline{OK}$$

     - COULD REVISE WALL CROSS-SECTION,
       AND REDUCE GEOMETRY; HOWEVER
       THIS ISN'T DONE HERE.

## SECTION 4.4 — DESIGN OF BASE JOINT

### DETERMINE AREA OF STEEL (SECTION 4.4.1)

- ASSUME PT STEEL PLACED SYMMETRICALLY OFF $\mathcal{C}_L$
- ASSUME ED STEEL PLACED SYMMETRICALLY OFF $\mathcal{C}_L$

FBD @ $\Delta_{ud}$ :
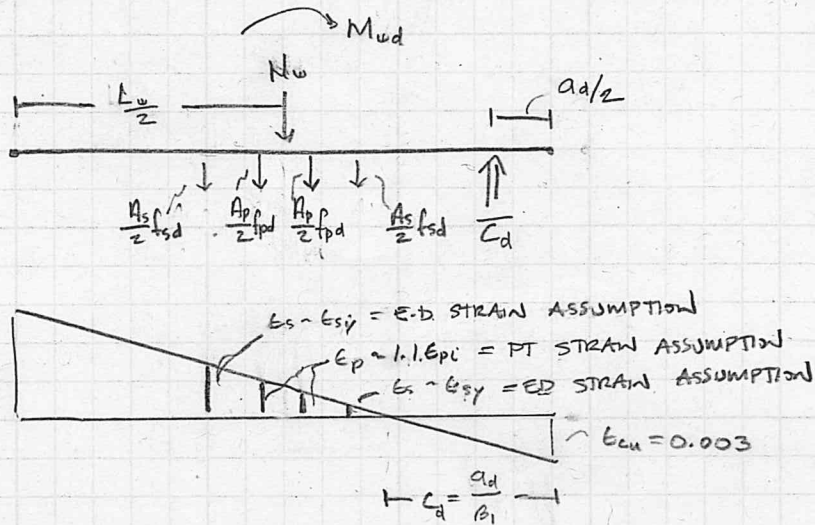


where :  $M_{ud}$ = design moment

$N_u$ = external axial (geometry) load

$A_s$ = E.D. steel area

$A_p$ = PT steel area

$f_{sd}$ = E.D. steel stress

$f_{pd}$ = PT steel stress

$L_u$ = wall length

$a_d$ = depth of equivalent rectangular stress block

$t_u$ = wall thickness

$\therefore \ \Sigma F_x = 0 \rightarrow$ (1)  $\overline{C}_d = A_s f_{sd} + A_p f_{pd} + N_u$   [EQN. 4.5 IN DOCUMENT]

(2)  $\overline{C}_d = 0.85 f_c' \, a_d t_u$   [EQN. 4.6 IN DOCUMENT]

$\Sigma M = 0 \rightarrow$ (3)  $\dfrac{M_{ud}}{\phi_f} = \overline{C}_d \left( \dfrac{L_u}{2} - \dfrac{a_d}{2} \right)$   [EQNS. 4.7 & 4.8 IN DOCUMENT]

(4)  $K_d = \dfrac{M_{us}}{M_{up} + M_{un}}$   [EQN 4.13 IN DOCUMENT]

$\longrightarrow \dfrac{A_s f_{sd}}{A_p f_{pd} + N_u}$   [EQN 4.14 DOCUMENT]

where  $K_D$ = E.D. Steel Moment Ratio

– WITHIN SYSTEM OF EQ'NS:

UNKNOWNS: $A_s$
$A_p$
$\overline{C_d}$

$C_d \rightarrow$ WHERE $a_D = \beta_1 C_d = 0.75 C_d$

KNOWNS: $N_u = 241.8^k$

$M_{ud} = 18013^{k\text{-}ft} = 216156^{k\text{-}in}$

$L_u = 20 ft = 240^{in}$

$t_w = 15^{in}$

$f'_c = 6^{ksi}$

$\phi_f = 0.90$ (per ACI-318)

$\chi_d = 0.5$ (SELECTED BY DESIGNER)

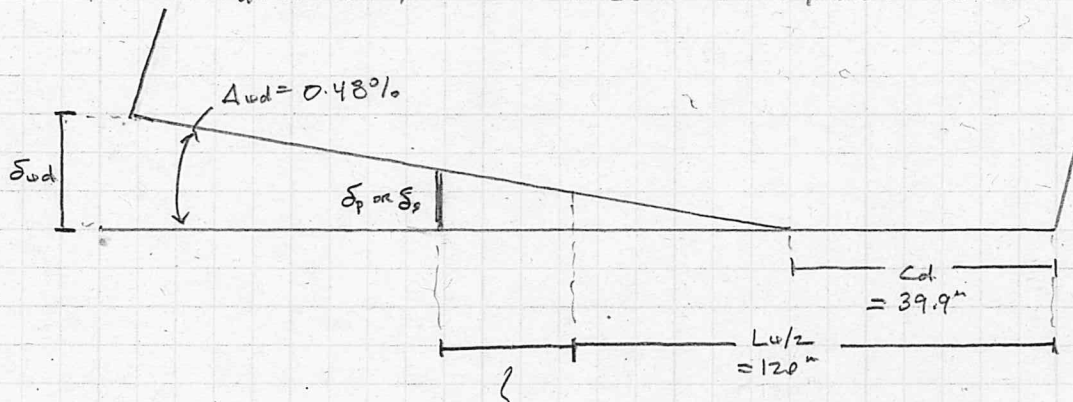INITIAL ASSUMPTIONS: – FOR PT : $l_{pu} = 50' = 600''$
$e_p = \pm 8''$

– FOR ED : $l_{sw} = 32''$ (@ $A_{wo}$ $l_{su} = l_{sw}$ b/c $\alpha_s = 0$)
$e_s = \pm 22''$

SOLVING EQ'NS:

[EQN 4.6] : $\overline{C_d} = (0.85)(6) a_d (15)$

[EQNS. 4.7 & 4.8] : $\dfrac{216156}{0.9} = \overline{C_d}\left(\dfrac{240}{2} - \dfrac{a_d}{2}\right)$

$$\therefore \overline{C_d} = 2286^k$$
$$a_d = 29.9^{in}$$
$$C_d = \frac{a_d}{\beta_1} = \frac{29.9}{0.75} = 39.9^{in}$$

– USING $C_d = 39.9^{in}$, FIND BAR ELONGATIONS w/ FIGURE BELOW:
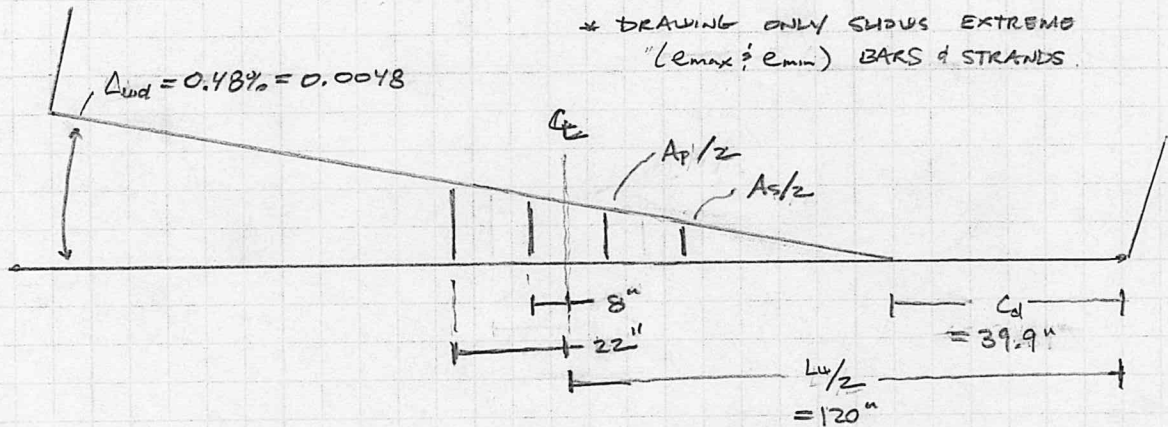


$e_p$ or $e_s$ = ECCENTRICITY OF BAR OR DISTANCE FROM WALL CENTERLINE

– NEED TO ASSUME ECCENTRICITY & UNBONDED LENGTH
– FOR SIMPLICITY, LUMP PT & ED INTO TWO GROUPS
– FOR LUMPED STEEL AREAS, EQNS. 4.6-4.8 FROM THE DESIGN PROCEDURE DOCUMENT CAN BE SOLVED DIRECTLY FOR $\overline{C_D}$ & $C_D$.

— DETERMINE STRAINS & STRESSES :      $(A_{wd} = 0.48\%)$



$\Delta_{wd} = 0.48\% = 0.0048$

* DRAWING ONLY SHOWS EXTREME "($e_{max}$ & $e_{min}$) BARS & STRANDS.

$\mathbb{C}_{\mathbb{L}}$

$A_p/2$

$A_s/2$

$8"$

$22"$

$C_d = 39.9"$

$L_u/2 = 120"$

PT:   $\Delta_{wd} = \dfrac{\Delta_{wd}}{L_u - C_d} = \dfrac{\delta_p}{L_u/2 - C_d \pm e_p}$

$= 0.0048 = \dfrac{\delta_{p-min}}{120" - 39.9" - 8"} = \dfrac{\delta_{p-max}}{120" - 39.9" + 8"}$

$\therefore \delta_{p-min} = 0.346 \text{ in}$
$\delta_{p-max} = 0.423 \text{ in}$

— FOR STRANDS : $L_{pu} = 50^{FT}$ ( WALL HEIGHT + FOUNDATION DEPTH)

$E_p = 28500 \text{ psi}$

$f_{pi} = (0.35)(0.65)(270^{ksi}) = 149.2 \text{ ksi}$

$\therefore f_{pd} = E_p \dfrac{\delta_p}{L_{pu}} + f_{pi} \implies$
$f_{pd-min} = 28500 \left[\dfrac{0.346}{600}\right] + 149.2 = 165.6 \text{ ksi}$
$f_{pd-max} = 28500 \left[\dfrac{0.423}{600}\right] + 149.2 = 169.3 \text{ ksi}$

$f_{pd} = f_{pd-avg} = \underline{\underline{167.5 \text{ ksi}}}$

ED:   $\Delta_{wd} = 0.0048 = \dfrac{\delta_{s-min}}{120" - 39.9" - 22"} = \dfrac{\delta_{s-max}}{120" - 39.9" + 22"}$

$\therefore \delta_{s-min} = 0.28 \text{ in}$
$\delta_{s-max} = 0.49 \text{ in}$

— FOR E.D. BARS :   $l_{su} = 32"$

$E_s = 29000 \text{ ksi}$

$\therefore t_{sd} = \dfrac{\delta_s}{l_{su}} \implies$
$t_{sd-min} = \dfrac{0.28"}{32"} = 0.0088 \text{ in/in}$
$t_{sd-max} = \dfrac{0.49"}{32"} = \underline{\underline{0.0153 \text{ in/in}}}$

* W/IN YIELD PLATEAU, THEREFORE
FROM $\sigma-\varepsilon$ CURVE :   $f_{sd} = f_{sy} = 65 \text{ ksi}$

— SOLVE FOR $A_s$ & $A_p$ w/ ASSUMED $f_{sD}$ & $f_{pD}$:

[EQN. 4.14] $\quad K_d = \dfrac{A_s f_{sd}}{A_p f_{pd} + N_\omega} \quad \longrightarrow \quad \therefore A_s = \dfrac{K_d(A_p f_{pd} + N_\omega)}{f_{ps}}$

[EQN. 4.5] $\quad \overline{C}_d = A_s f_{sD} + A_p f_{pd} + N_\omega$

$$= \frac{K_d(A_p f_{pd} + N_\omega)\cancel{f_{sd}}}{\cancel{f_{sd}}} + A_p f_{pd} + N_\omega$$

$$\overline{C}_d = (K_d + 1)(A_p f_{pd} + N_\omega)$$

$\therefore$ [EQN 4.5] $\quad 2286 = (0.5 + 1)\big[A_p(167.5) + 241.8\big]$

$\therefore$ [EQN. 4.14] $\quad A_s = \dfrac{(0.5)\big[A_p(167.5) + 241.8\big]}{(65)}$

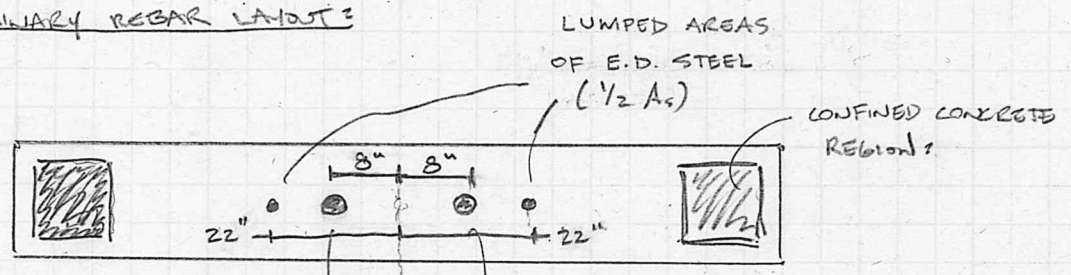$\therefore A_p = 7.66\,\text{in}^2$
$A_s = 11.02\,\text{in}^2$

— FINAL SOLUTION AFTER ITERATIONS:

$A_s = 11.02\,\text{in}^2 \;\longrightarrow\;$ USE (14) #8's $\;(A_{prov} = 11.06\,\text{in}^2)$
$A_p = 7.66\,\text{in}^2 \;\longrightarrow\;$ USE (36) 0.6-in STRANDS $\;(A_{prov} = 7.81\,\text{in}^2)$
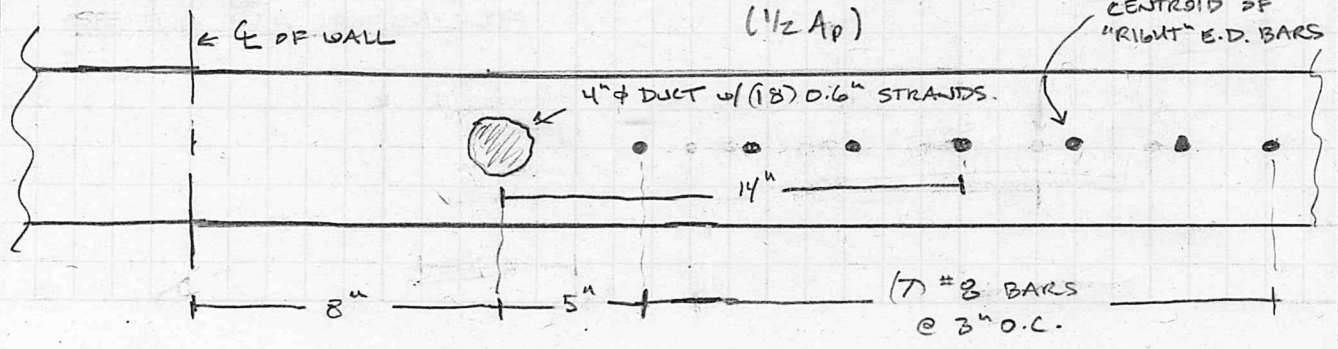$\overline{C}_d = 2286^k$
$a_d = 29.9\,\text{in}$

$\therefore C_d = \dfrac{a_d}{\beta_1} = \dfrac{29.9^{in}}{0.75} = 39.9\,\text{in}$

NOTE: MAY NEED TO REVISE
IF ASSUMED $l_{su}$, $l_{pu}$,
$e_s$ OR $e_p$ ARE MODIFIED.

PRELIMINARY REBAR LAYOUT:

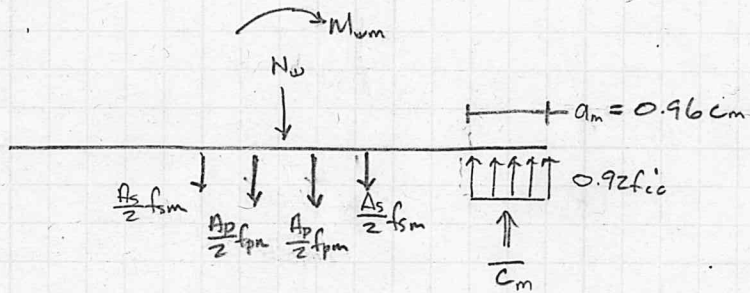LUMPED AREAS
OF E.D. STEEL
$(\frac{1}{2} A_s)$

CONFINED CONCRETE
REGION:



SPECIFIC REBAR
LAYOUT:

LUMPED AREAS
OF P.T. STEEL
$(\frac{1}{2} A_p)$

CENTROID OF
"RIGHT" E.D. BARS



4"⌀ DUCT w/ (18) 0.6" STRANDS.

(7) #8 BARS
@ 3" O.C.

SECTION 4.4.2:
PROBABLE-LEVEL STRENGTH:

FBD:



$$N_w$$
$$M_{wm}$$
$$\frac{A_s}{2} f_{sm} \qquad \frac{A_p}{2} f_{pm} \quad \frac{A_p}{2} f_{pm} \qquad \frac{A_s}{2} f_{sm}$$
$$a_m = 0.96\,c_m$$
$$0.92 f'_{cc}$$
$$\overline{C_m}$$

- KNOWNS: $A_s = 11.06\ in^2$
$$A_p = 7.81\ in^2$$
$$N_w = 241.8^k$$

- ASSUME: $C_m = 0.9\,C_d = (0.9)(39.9) = 35.9''$

- FIND PT & ED STRANS USING DIAGRAM ON P. A12 EXCEPT w/ $c = c_m$
@ $\Delta_{um} = 2.19\%$

PT: $\Delta_{um} = 0.0219 = \dfrac{\varepsilon_p}{120 - 35.9'' \pm 8''} \Rightarrow \begin{array}{l} \delta_{p\,min} = 1.67'' \\ \delta_{p\,max} = 2.02'' \end{array}$

$$\varepsilon_p = \frac{f_{pi}}{E_p} + \frac{\delta_p}{l_{pu}} \Rightarrow \frac{149.2}{28500} + \frac{1.67}{600} = 0.0080\ in/in$$

$$\frac{149.2}{28500} + \frac{2.02}{600} = 0.0086\ in/in$$

- FROM $\sigma$-$\varepsilon$ CURVE $\Rightarrow f_{p\,min} = 217.9\ ksi$
$$f_{p\,max} = 230.4\ ksi$$

E.D. $\Delta_{um} = 0.0219 = \dfrac{\delta_s}{120'' - 35.9'' \pm 22''} \Rightarrow \begin{array}{l} \delta_{s\,min} = 1.36'' \\ \delta_{p\,min} = 2.32'' \end{array}$

$$\varepsilon_s = \frac{\delta_s}{l_{su} + \alpha_s d_s} \qquad \text{where} \quad \alpha_s = 2.0$$
$$\delta_s = 1.0'' \quad (\#8\ BAR)$$

$$\therefore \varepsilon_s = \frac{1.36''}{32'' + (2)(1'')} = 0.040\ in/in \rightarrow f_{s\,min} = 84.9\ ksi$$

$$\frac{2.32''}{32'' + (2)(1'')} = 0.068\ in/in \rightarrow f_{s\,max} = 91.8\ ksi$$

$$\boxed{\begin{array}{l} \therefore f_{pm\text{-}avg} = 224.2\ ksi \\ f_{sm\text{-}avg} = 88.4\ ksi \end{array}}$$

$\Sigma F_y = 0$ :

$$\therefore \overline{T}_m = A_s f_{sm} + A_p f_{pm} + N_w$$
$$= (11.06)(88.4) + (7.81)(224.2) + 241.8$$
$$= 2970.5^k$$

$\Sigma M = 0$ :

$$\therefore M_{um} = \overline{C}_m \left( \frac{L_w}{2} - \frac{a_m}{2} \right)$$
$$= (2970.5)\left( \frac{240}{2} - \frac{(0.96)(35.9)}{2} \right)$$
$$= 305272.3^{k\cdot "} = 25,439^{ksi}$$

$$\text{OVERSTRENGTH} = \frac{M_{um}}{M_{uD}} = \frac{25439}{18013} = 1.41$$

NOTE: $\Sigma M = 0$ EQUATION ASSUMES STEEL
IS LUMPED @ CENTERLINE FOR SIMPLICITY.
WOULD NEED TO CONSIDER INFLUENCE
OF PT & ED STEEL ON BASE MOMENT
STRENGTH IF STEEL IS LOCATED
AWAY FROM CENTERLINE.

SECTION 4.4.3:
  CONFINEMENT REGION:



$d_s$ = HOOP BAR DIAMETER

$c_c$ = CLEAR COVER

$b_c$ = WIDTH OF CONFINED REGION

$c_c$ = CLEAR COVER

$t_w$

$\leftrightarrow$ $d_c$ = CLEAR DISTANCE
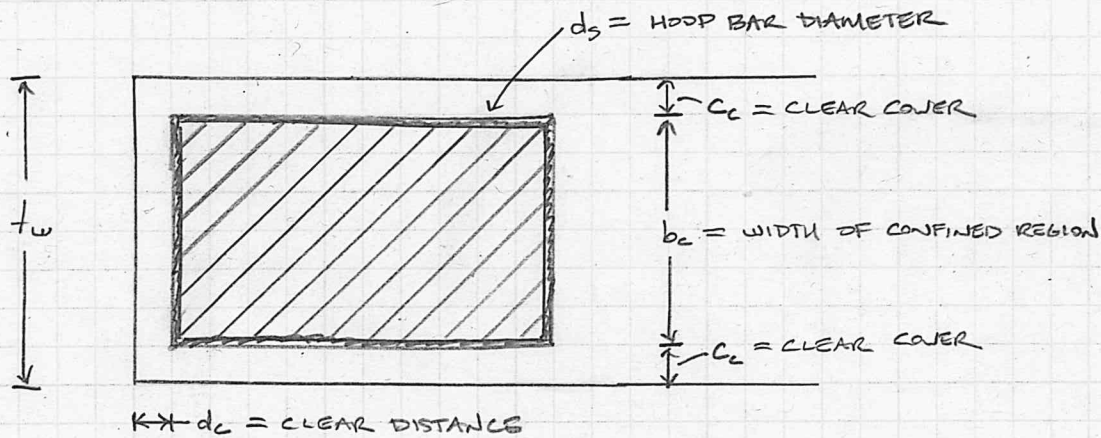
$$t_w = 15.0 \text{ in}$$
$$c_c = 1.0 \text{ in}$$
$$b_c = 13.0 \text{ in}$$
$$d_c = 1.0 \text{ in}$$

DESIGNER SELECTED PARAMETERS

$$\Delta_{vm} = 2.19\%$$

~ USE SECTION 5.6.3.5 - 5.6.3.9 IN ACI ITG-5.2

$$h_p = 0.06 H_w = 0.06 (45^{FT}) = 2.7^{FT} = 32.4 \text{ in}$$

$$\varepsilon_{cm} = \phi_{um} c_m = \frac{\Delta_{vm}}{h_p} c_m$$

* FOR INITIAL ASSUMPTION:   $c_m = 0.9 c_d$

$$\therefore c_m = (0.9)(39.9 \text{ in}) = 35.9 \text{ in}$$

$$\therefore \varepsilon_{cm} = \frac{(0.0219)(35.9 \text{ in})}{(32.4 \text{ in})} = 0.0242 \text{ in/in}$$

$$\varepsilon_{cm} = 0.004 + 4.6 \, \varepsilon_{sut} \left( \frac{f_c'}{f_{cc}'} \right)$$

$$\varepsilon_{sut} = \text{ULTIMATE STRAIN OF CONFINEMENT STEEL} = 0.08 \text{ in/in} \quad \left( \begin{array}{c} \text{DIFFERENT THAN} \\ \text{E.D. STEEL} \\ \text{ULTIMATE STRAIN} \end{array} \right)$$
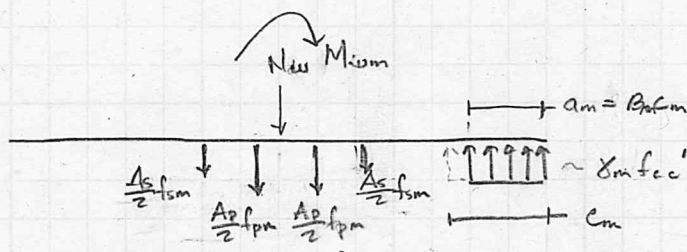
$$\therefore \frac{f_c'}{f_{cc}'} = 0.055$$

CONFINEMENT REGION CONT'D:

- USE ACI ITG-5.2 TABLE 5-1 :

$$\text{-FOR}\quad \frac{f_L'}{f_{cc}'} = 0.055 \quad ; \quad \frac{f_{cc}'}{f_c'} = 1.48$$

$$\therefore f_{cc}' = (1.48)f_c' = (1.48)(6) = \underline{\underline{8.88^{ksi}}}$$

- CHECK "$C_m$" BASED ON EQUILIBRIUM @ $\Delta_{um} = 2.19\%$ :



- KNOWNS :  $A_s = 11.06 \text{ in}^2$
            $A_p = 7.81 \text{ in}^2$
            $N_w = 241.8^k$

- ASSUMPTIONS :  $f_{sm} = 88.4^{ksi}$
                 $f_{pm} = 224.8^{ksi}$
                 $f_{cc}' = 8.88 \text{ ksi}$

- ACI ITG-5.2 :  $\beta_m = 0.96$
                 $\gamma_m = 0.92$

- UNKNOWNS :  $C_m = ?$

$\Sigma F_y = 0 : T_m = \overline{C}_m$  where  $T_m = A_s f_{su} + A_p f_{py} + N_w$
$$= (11.06)(88.4) + (7.81)(224.2) + 241.8$$
$$= 2970.5^k$$

$$\overline{C}_m = \gamma_m f_{cc}' b_c a_m = \gamma_m f_{cc}' b_c \beta_m C_m$$
$$= (0.92)(8.88)(13)(0.96) C_m$$
$$= 101.9 C_m$$

$$\therefore C_m = \frac{2970.5^k}{101.9} = 29.2 \text{ in} < 0.9 C_D = \underline{35.9 \text{ in}}$$

- IF ITERATED ON SOLUTION, USE $C_m = 29.2 \text{ in}$ FOR $\varepsilon_{cm}$
  RE-SOLVE FOR $f_{cc}'$ AND $C_m$

- AFTER ITERATIONS :  $\boxed{\begin{array}{l} C_m = 32.2 \text{ in} \\ f_{cc}' = 8.46 \text{ ksi} \end{array}}$

CONFINEMENT REINFORCEMENT:

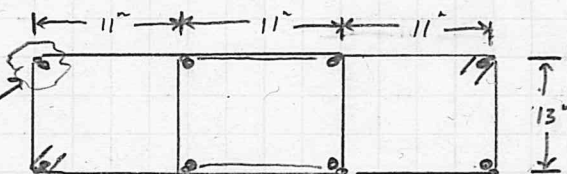- LENGTH OF CONFINEMENT $\geq 0.95 c_m = (0.95)(32.2") = 30.6"$

- TRY $L_{cc} = 33"$
  $b_{cc} = 13"$
  $A_s = 0.2 \text{ in}^2$ (#4 BAR)
  $f_{yt} = 60 \text{ ksi}$

- TRY HOOP DESIGN:



#4 VERT. BAR
(SAME SIZE AS
DISTRIBUTED
PANEL REINF.)

(2) HOOPS 13" × 22" $\rightarrow \dfrac{22}{13} = 1.69 < 2.50$ OK
WHICH OVERLAP

- FROM PREVIOUS STEPS:  $f_c' = 6 \text{ ksi}$
  $f_{cc}' = 8.46 \text{ ksi}$

- FROM TABLE 5.6.3.9 IN ACI ITG-5.2: $\dfrac{f_{cc}'}{f_c'} = 1.41$

$$\therefore \frac{f_\ell'}{f_c} = 0.069$$

$$\therefore f_\ell' = (0.069)(6) = 0.414$$

$$\therefore \rho_s = \frac{f_\ell'}{0.35 f_{yt}} = \frac{0.414}{(0.35)(60)} = 0.020$$

$$\rho_s = \frac{A_s [4 b_c + 4 h_c]}{s b_c L_c}$$

$$0.020 = \frac{(0.20)[(4)(13") + (4)(22")]}{s (13)(33)}$$

$$\therefore s = 3.26"$$

$\therefore$ USE #4's @ 3¼" w/ (2) OVERLAPPING
13" × 22" HOOPS

- HOOPS SHOULD EXTEND VERTICALLY
  A DISTANCE $= h_p = (0.06)(45') = 2.7'$
  $= 32.4"$ (MIN.)

$\therefore$ USE #4's @ 3¼" OVER 32.5"
TOTAL OF (11) HOOPS PER TOE.

CONFINEMENT REINFORCEMENT CONT'D:

- CHECK ACI REQUIREMENTS:

    - ACI 318-11  SECT. 21.9.6.4 (c) =

    - SECTION REFERENCES  21.6.4.2 — 21.6.4.4

    - PER 21.6.4.2 : SPACING OF LEGS $\leq$ 14"    OK    PROVIDING 11"

    - PER 21.6.4.4 : MUST USE EQ'N 21-5
                      FOR RECTANGULAR HOOPS

        - EQ'N 21.5 :

        $$A_{sh,min} = 0.09 \frac{s b_c f_c'}{f_{yt}}$$

        $$= \frac{(0.09)(3.00)(13)(6)}{(60)} = 0.35 in^2 > 0.40 in^2 \; OK$$

    - PER 21.6.4.3 :

        $$s_{min} = \left(\frac{1}{3}\right) t_c = (0.33)(15") = 5" > 3.25 in \; OK$$

        $$s_{min} = (6)(1.0) = 6" > 3.25" \; OK$$
        $\hookrightarrow$ ASSUMES #8 BAR IS SMALLEST
        LONGITUDINAL REBAR
        BASED ON E.D. STEEL

        $$s_{min} = 4 + \frac{14 - h_x}{3}$$

        $$= 4 + \frac{14 - 11}{3} = 5" > 3.25" \; OK$$

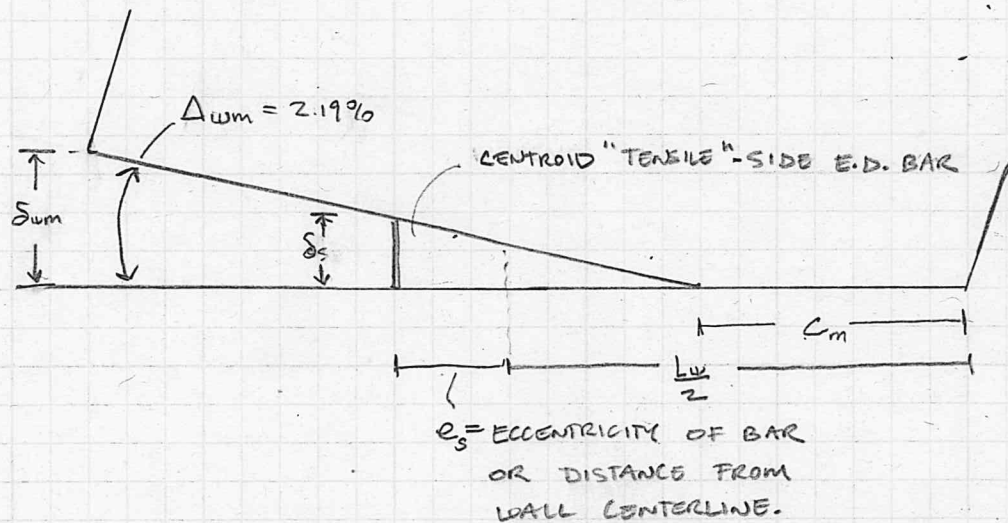        - SATISFIES ALL CHECKS

SECTION 4.4.4:

E.D. STEEL UNBONDED LENGTH:

- CHECK INITIAL ASSUMPTION OF $l_{su} = 32"$



$\Delta_{wm} = 2.19\%$

CENTROID "TENSILE"-SIDE E.D. BAR

$\delta_{wm}$

$\delta_s$

$C_m$

$\frac{Lw}{2}$

$e_s$ = ECCENTRICITY OF BAR OR DISTANCE FROM WALL CENTERLINE.

- DETERMINE ELONGATION OF BAR:

$$\therefore \Delta_{wm} = \frac{\delta_{wm}}{Lw - C_m} = \frac{\delta_s}{\frac{Lw}{2} - C_m + e_s}$$

where $C_m = 32.2$ in

$e_s = 22$ in (CENTROID OF TENSILE-SIDE E.D. BARS)

$$\therefore 0.0219 = \frac{\delta_s}{\frac{240}{2} - 32.2 + 22} \rightarrow \delta_s = 2.40 \text{ in}$$

- DETERMINE UNBONDED LENGTH:

$$\varepsilon_s = \frac{\delta_{sm}}{l_{su} + \alpha_s d_s}$$

where

SELECTED BY DESIGNER

$\varepsilon_{sa} = 0.60 \varepsilon_{su}$
$\varepsilon_{su} = 0.12$ in/in
$\alpha_s = 2.0$
$d_s = 1.0$ (FOR #8 BAR)

- SET $\varepsilon_s = \varepsilon_{sa}$

$$\therefore (0.60)(0.12) = \frac{2.40}{l_{su} + (2.0)(1.0)} \rightarrow l_{su} = 31.3"$$

$\therefore$ USE $\boxed{l_{su} = 32"}$ $\rightarrow$ OK  ✳ DON'T NEED TO ITERATE ON PT & ED STRESS @ $\Delta_{wD}$.

$$\therefore \varepsilon_s = \frac{2.40}{32 + (2)(1)} = 0.071 \text{ in/in} = \underline{\underline{0.59 \varepsilon_{su}}} \quad \text{OK}$$

- NOTE THAT THE UNBONDED LENGTH CAN BE VARIED BETWEEN THE INDIVIDUAL E.D. BARS BASED ON THEIR LOCATIONS; HOWEVER THE UNBONDED LENGTHS WILL BE CONSTANT AMONG ALL E.D. BARS IN THIS EXAMPLE.

SECTION 4.4.5:

<u>DEVELOPMENT LENGTH OF BARS:</u>

- USE ACI 318, SECTION 21.9.2.3:
  - REFER BACK TO SECTION 12.2 w/ 1.25 FACTOR

$$L_d = (1.25) \frac{f_y \, \Psi_t \, \Psi_e}{20 \lambda \sqrt{f_c'}} d_s$$

- FOR STRUCTURE:  $\Psi_t = 1.0$
  $\Psi_e = 1.0$
  $\lambda = 1.0$
  $f_c' = 6^{ksi}$
  $f_{yt} = 65^{ksi} \longrightarrow$ FOR ED STEEL
  DESIGN WILL BE CONSERVATIVE
  # FOR OTHER REINFORCEMENT

$$L_d = (1.25) \frac{(65000)(1.0)(1.0)}{(20)(1.0)\sqrt{6000}} d_s$$

$$= (1.25)(42) d_b = \underline{52.5 \, d_s} \qquad \text{where } d_s = \text{ED BAR DIAMETER}$$

- FOR <u>#8 BAR, $L_d = 52.5"$</u>

- IF BAR GROUTED IN CORRUGATED METAL DUCT

$$L_d = 25 d_s = 25" \text{ FOR #8 BAR}$$

SECTION 4.4.4 & 4.4.6.

- __CHECK STRAINS__ @ __MAXIMUM-LEVEL DRIFT__

  - SAME DIAGRAM EXCEPT $C_m = 32.2$ in @ $\Delta_{um} = 2.19\%$

__PT:__   $\Delta_{um} = 0.0219 = \dfrac{\delta_{p-min}}{120 - 32.2 - 8} = \dfrac{\delta_{p-max}}{120 - 32.2 + 8}$

$$\therefore \delta_{p-min} = 1.75 \text{ in}$$
$$\delta_{p-max} = 2.10 \text{ in}$$

$\therefore \epsilon_{pm} = \dfrac{f_{pi}}{E_p} + \dfrac{\delta_p}{L_p}$

$\therefore \epsilon_{pm-min} = \dfrac{149.2}{28500} + \dfrac{1.75}{(50)(12)} = 0.0082 \text{ in/in}$

$\epsilon_{pm-max} = \dfrac{149.2}{28500} + \dfrac{2.10}{(50)(12)} = 0.0087 \text{ in/in}$

$\therefore f_{pm-min} = 222.4^{ksi}$  $\Big\}$ From $\sigma$-$\epsilon$ curve
$f_{pm-max} = 233.0$

$f_{pm} = \underline{f_{pm-avg} = 227.7^{ksi}}$  - USED $224.2^{ksi}$

__E.D.:__   $\Delta_{um} = 0.0219 = \dfrac{\delta_{s-min}}{120 - 32.2 - 22} = \dfrac{\delta_{s-max}}{120 - 32.2 + 22}$

$$\therefore \delta_{s-min} = 1.44 \text{ in}$$
$$\delta_{s-max} = 2.40 \text{ in}$$

$\therefore \epsilon_s = \dfrac{\delta_s}{l_{sw} + \alpha_s d_s}$  where $\alpha_s = 2.0$
$d_s = 1.0$ in ($\#8$ BAR)
$l_{sw} = 32"$

$\therefore \epsilon_{s-min} = 0.042 \text{ in/in}$
$\epsilon_{s-max} = 0.071 \text{ in/in}$

$\therefore \epsilon_{su-avg} = 0.057 \text{ in/in}$   $f_{ps} = \underline{f_{s-avg} = 89.8^{ksi}}$  - USED $88.4^{ksi}$

✗✗ ITERATE TO FIND
EXACT $M_{um}$

REVISED PROBABLE-LEVEL STRENGTH:

- SAME FBD ON PAGE A-12, BUT REVISED $f_{sm}, f_{pm}$ & $a_m$

  - $\Sigma F_y = 0$

    $\therefore \bar{C}_m = A_s f_{sm} + A_p f_{pm} + N_w$
    $= (11.06)(89.8) + (7.81)(227.7) + 241.8$
    $= 3013.3^k$

  - $\Sigma M = 0$

    $\therefore M_{om} = \bar{C}_m \left( \dfrac{L_w}{2} - \dfrac{a_m}{2} \right)$   where   $a_m = \beta_n C_m$
    $= (3013.3)\left( \dfrac{240}{2} - \dfrac{(0.96)(32.2)}{2} \right)$
    $= 315022^{k-in} = 26252^{k-ft} = M_{wm}$

- CHECK REVISED $f_{cc}'$

    $\bar{C}_m = \gamma_m f_{cc}' b_c \beta_n C_m$
    $= (0.92) f_{cc}' (13)(0.96)(32.2) = 3013.3^k$

    $\therefore f_{cc}' = 8.15^{ksi} < 8.46^{ksi}$

    - CAN REDESIGN CONFINED STEEL
      FOR $\underline{f_{cc}' = 8.15^{ksi}}$ AND $\underline{C_m = 32.2''}$

    w/ $M_{wD} = \underline{\underline{26,252^{k-ft}}}$

    - FOR CONSERVATIVE DESIGN
      WILL KEEP #4's @ 3¼" O.C.
      $\underline{OK}$

- REVISED OVERSTRENGTH:

    $O.F. = \dfrac{M_{wm}}{M_{wd}} = \dfrac{26252}{18013} = 1.46$

SECTION 4.4.6 :

ESTIMATE PT LOSSES :



$\}$ → PT STRESS @ $\Delta_{wm} = 2.19\%$
AT 1ST CYCLE

$\}$ → PT STRESS @ $\Delta_{wm} = 2.19\%$
AFTER MULTIPLE CYCLES

$\epsilon_{pm,1} = 0.0087$ in/in

$\epsilon_{pm,2} = 0.0082$ in/in

$\epsilon_{pi} = 0.00532$ in/in
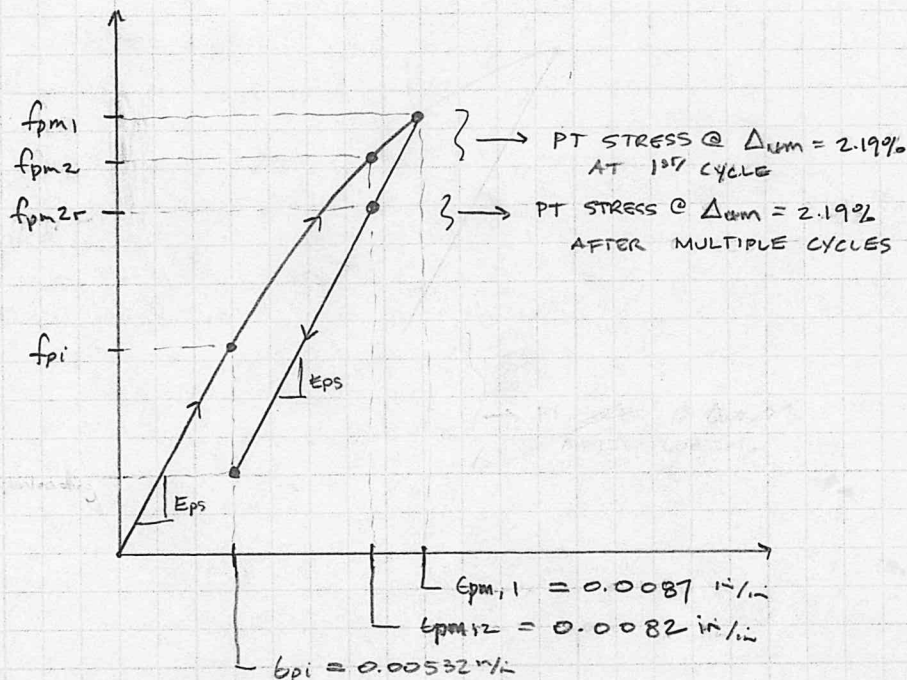
$f_{pm1}$ = STRESS IN TENSION -SIDE PT TENDON WHEN @ 1ST CYCLE @ $\Delta_{wm}$

$f_{pm2}$ = " " COMPRESSION-SIDE " " " " " " "

$f_{pm2r}$ = " " " " " " AFTER MULTIPLE CYCLES
@ $\pm \Delta_{wm}$

$\therefore f_{ps1} = 233.0$ ksi
$f_{ps2} = 222.4$ ksi

$$f_{pm,2r} = f_{pm1} - E_p(\epsilon_{pm,1} - \epsilon_{pm,2})$$
$$= 233.0 - (28500)(0.0087 - 0.0082) = 218.8 \text{ ksi}$$

$$f_{p,loss} = f_{pm2} - f_{pm2r} = 222.4 \text{ ksi} - 218.8 \text{ ksi}$$
$$= 3.6 \text{ ksi}$$

$$\therefore f_{p,loss} = 3.6 \text{ ksi}$$

= CALCULATED LOSSES ARE SMALL
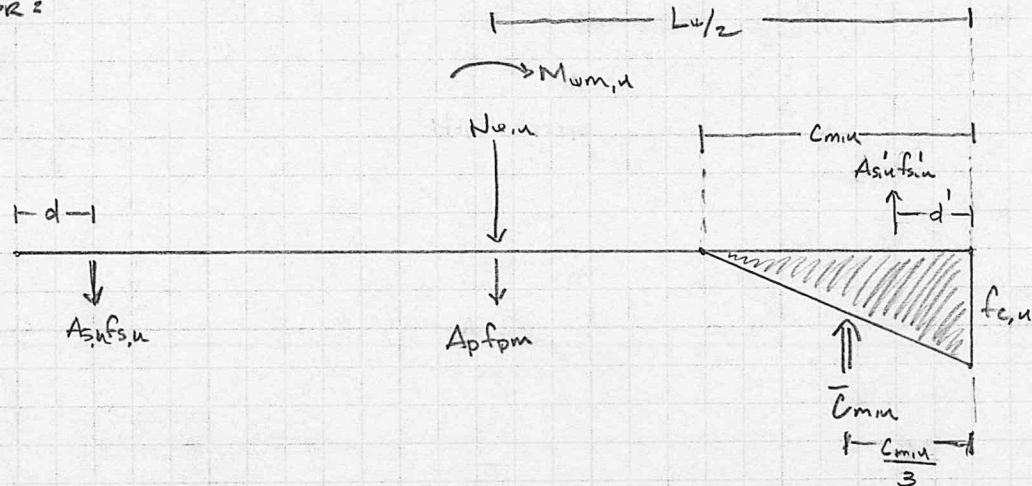AND COULD BE IGNORED, BUT
INCLUDED FOR DEMONSTRATION PURPOSES

## SECTION 4.5:

### DESIGN OF UPPER JOINT:

* BASED ON PRELIMINARY ANALYSIS, GAP WILL OPEN W/O REBAR. REBAR SHOULD BE LOCATED AT ENDS OF WALL.

* MUST CHECK HORIZONTAL SHEAR-SLIP AT JOINT AFTER SELECTING REBAR SIZE & LOCATION

- 2ND FLOOR:



1) CONCRETE STRESS-BLOCK (LINEAR-ELASTIC):

$$1) \qquad \bar{C}_{m,u} = \tfrac{1}{2} f_{c,u} \, t_w \, C_{m,u}$$

2) SUM OF FORCES:

$$2) \qquad \bar{C}_{m,u} = A_{s,u} f_{s,u} - A'_{s,u} f'_{s,u} + A_p \left( f_{pm} - \tfrac{1}{2} f_{p,loss} \right) + N_{o,u}$$

3) SUM OF MOMENTS:

$$3) \qquad M_{om,u} = \phi_{f,u} \left[ \bar{C}_{m,u} \left( \tfrac{L_w}{2} - \tfrac{C_{m,u}}{3} \right) + A_{s,u} f_{s,u} \left( \tfrac{L_w}{2} - d \right) + A'_{s,u} f'_{s,u} \left( \tfrac{L_w}{2} - d' \right) \right]$$

4) STRAIN COMPATIBILITY:

$$\frac{t_{c,u}}{C_{m,u}} = \frac{t_{s,u}}{L_w - C_{m,u} - d} \quad \Rightarrow \quad t_{s,u} = t_{c,u} \left( \frac{L_w - C_{m,u} - d}{C_{m,u}} \right)$$

$$4) \qquad \therefore f_{s,u} = \left( \frac{E_s}{E_c} \right) f_{c,u} \left[ \frac{L_w - C_{m,u} - d}{C_{m,u}} \right]$$

$$\frac{t_{c,u}}{C_{m,u}} = \frac{t'_{s,u}}{C_{m,u} - d'} \quad \Rightarrow \quad t'_{s,u} = t_{c,u} \left( \frac{C_{m,u} - d'}{C_{m,u}} \right)$$

$$5) \qquad \therefore f'_{s,u} = \left( \frac{E_s}{E_c} \right) f_{c,u} \left[ \frac{C_{m,u} - d'}{C_{m,u}} \right]$$

- BASED ON SYSTEM OF EQUATIONS #1 - #6:

    <u>KNOWNS:</u>

$$E_s = 29,000 \text{-ksi}$$
$$E_c = 4415.2 \text{ ksi}$$
$$N_{w,u} = 241.8^k - \left(\begin{array}{c}\text{BASE PANEL}\\ \text{SELF WEIGHT}\end{array}\right)(0.7) = 241.8 - 0.7\left[(150\text{pcf})(20)(12)\left(\frac{15}{12}\right)\right]$$
$$= 210.3^k$$

(LOAD COMBO FACTOR)

$$A_p = 7.81 \text{ in}^2$$
$$f_{pm} = 227.7 \text{ ksi}$$
$$f_{p,loss} = 3.6^{ksi}$$
$$L_u = 240 \text{ in}$$
$$t_u = 15^{in}$$
$$\phi_{f,u} = 0.90$$
$$M_{um,u} @ \text{ LEVEL TWO} = (O.F.)(M_{wp,u})$$
$$= (1.46)(11578.6^{k\text{-}ft}) = 16905^{k\text{-}ft}$$
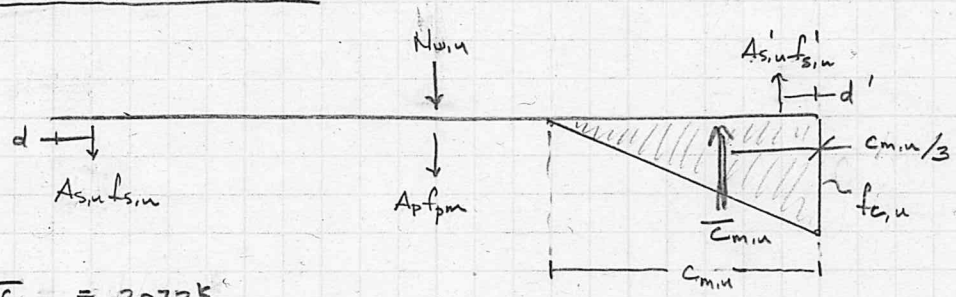
    <u>UNKNOWNS:</u>

$$\overline{C}_{m,u}$$
$$C_{m,u}$$
$$f_{c,u} \rightarrow \text{LIMIT TO } 0.5 f_c' \quad (3^{ksi})$$
$$f_{s,u} \rightarrow \text{LIMIT TO } f_{sy}$$
$$f_{s,u}' \rightarrow \text{ " " "}$$

    <u>DESIGNER SELECTIONS:</u>

$$A_{s,u} = A_{s,u}' = 3.16 \text{ in}^2 \quad (4 \text{-} \#8 \text{ BARS})$$
$$d = d' = 6 \text{ in}$$

- SOLVE SYSTEM OF EQUATIONS:

    <u>FBD @ $\Delta_{um}$ @ 2ND LEVEL:</u>



*NOTE: PROCEDURE WOLD BE REPEATED @ EACH JOINT IN FULL-DESIGN

$$\overline{C}_{m,u} = 2073^k$$
$$\therefore \quad C_{m,u} = 73.6^{in}$$
$$f_{c,u} = 2.75^{ksi} < 0.5 f_c' \quad \underline{\underline{OK}}$$

$$f_{s,u}' = 22.7^{ksi} \text{ (COMPRESSION)}$$
$$f_{s,u} = 53.7^{ksi} \text{ (TENSION)} < f_{sy} \quad \underline{\underline{OK}}$$

> CAN USE (4) #8's
> @ EACH SIDE
> @ EACH JOINT

SECTION 4.62

<u>SHEAR DESIGN ACROSS JOINTS</u> :

$$\phi_s V_{ss} > V_{jm}$$

— AT BASE JOINT :

$$\phi_s \mu_{ss} \left( \overline{C}_m - 0.5 A_p f_{p,loss} \right) > V_{um}$$

where   $\phi_s = 0.75$
$\mu_{ss} = 0.50$
$\overline{C}_m = 3013.3^k$
$A_p = 7.81 \, in^2$
$f_{p,loss} = 3.6^{ksi}$
$V_{um} = (536.2^k)(1.46) = 782.9^k$

$$\therefore (0.75)(0.5)\left[(3013.3) - (0.5)(7.81)(3.6)\right] > 782.9^k$$
$$(0.75)(0.5)(2999.2^k) > 782.9^k$$

$$\therefore 1124.7^k > 782.9^k \qquad \underline{\underline{OK}}$$

— AT 2ND FLOOR JOINT :

$$\phi_s \mu_{ss} \left[ (A_{su}' + A_{su}) f_{sy} + A_p \left( f_{pm} - 0.5 f_{p,loss} \right) + N_{u,u} \right] > V_{um,u}$$

where :   $\phi_s = 0.75$
$\mu_{ss} = 0.60$
$A_{su}' = A_{su} = 3.16 \, in^2$
$f_{sy} = 60^{ksi}$   (NON-ED STEEL)
$A_p = 7.81^{ksi}$
$f_{pm} = 227.7^{ksi}$
$f_{p,loss} = 3.6^{ksi}$
$N_{u,u} = 210.3^k$
$V_{u,u} = (478.5^k)(1.46) = 698.6^k$

$$\therefore (0.75)(0.60)\left[(3.16 + 3.16)(60) + (7.81)\left[227.7 - (0.5)(3.6)\right] + 210.3\right] > V_{um,u}$$

$$(0.75)(0.60)\left[2353.8^k\right] > 698.6^k$$

$$1059.2^k > 698.6^k \qquad \underline{\underline{OK}}$$

* PROCEDURE WOULD BE REPEATED
  @ EACH JOINT IN FULL-DESIGN

SECTION 4.7: DESIGN OF PANEL REINFORCEMENT

DISTRIBUTED REINFORCEMENT @ BASE PANEL : (SECT. 4.7.1)

— PER ACI 318 SECT. 21.9.4

$$V_{wm} = \phi V_n$$

$$= \phi A_{cu} (\alpha_c \lambda \sqrt{f_c'} + \rho_t f_y)$$

WHERE
$\phi = 0.75$
$\alpha_c = 2.0$
$\lambda = 1.0$
$A_{cu} = L_w t_w$

$\therefore A_{cu} = (20^{FT})(12^{in/FT})(15^{in}) = 3600 \ in^2$

$f_y = 60^{ksi}$

$V_{wm} = 782.9^k$

$f_c' = 6^{ksi}$

$\therefore 782900^k = (0.75)(3600 \ in^2)[(2.0)(1.0)\sqrt{6000} + \rho_t(60000)]$

$\therefore \rho_t = 0.0023 \ in/in$

$V_{n,max} = 8 A_{cu} \sqrt{f_c'} = (8)(3600)\sqrt{6000} = 2230.8^k$

$V_{wm} = \phi V_{n,max} = (0.75)(2230.8) = 1673.1^k > 782.9^k$ OK

— TRY #4's @ 12" O.C. @ EACH FACE :

$A_{t,prov} = (0.20 \ in^2/ft)(2) = 0.40 \ in^2/ft$

$A_{t,req'd} = (0.00230)(15 \ in)(12^{in}/ft) = 0.41 \ in^2/ft \sim 0.40 \ in^2/ft$ OK

— CHECK ACI REQUIREMENT: (SECTION 21.9.2.1)

$\rho_{l,min} = \rho_{t,min} = 0.0025 < A_{s,prov}$

→ — TRY #4's @ 10" O.C. @ EACH FACE

$\therefore A_{t,prov} = (0.20)(2)(\frac{12}{10}) = 0.48 \ in^2/ft$

NOTE: ACI 318-11 SECTION 21.9.6.4(e) SHOULD ALSO BE SATISFIED FOR THE DEVELOPMENT OF HORIZONTAL BARS IN CONFINED BOUNDARIES.

$A_{t,req'd} = (0.0025)(15)(12) = 0.45 \ in^2/ft$ OK

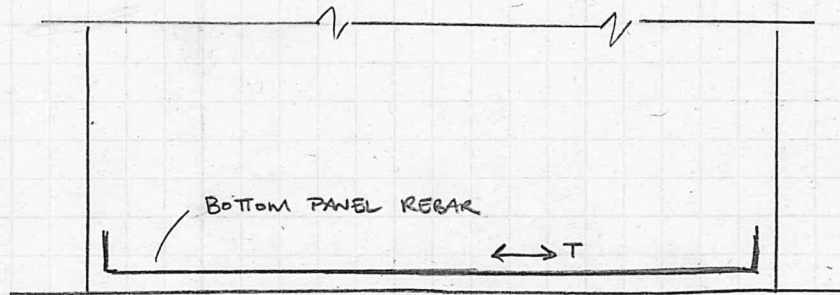$\therefore$ USE #4's @ 10" O.C., EACH FACE, EACH WAY

* PROCESS CAN BE REPEATED FOR UPPER PANELS USING SECTION 16.4.2 WHERE $\rho = 0.001$.

SECTION 4.7.2:

    PANEL EDGE REINFORCEMENT:

                            - BOTTOM OF BASE PANEL:
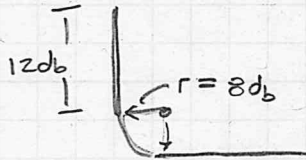


$$L_u = 20'$$

$$T_{req'd} = (6000 \,\#/_{FT})(20') = 120^K$$

$$T = A_s f_y \implies A_s = \frac{T}{f_y} = \frac{120^K}{60^{ksi}} = 2.0\, in^2$$

          USE (2) #9's  $A_{sprov} = 2.0\, in^2 = A_{s,req}$

                  ∴ USE (2) #9's FOR
                       BASE PANEL BOTTOM
                       REINFORCEMENT.

- HOOK DESIGN: (PER ACI 318 SECTION 7.1 + 7.2)



                   ∴ HOOKED END  $= 12 d_b + 8 d_b$
                    TOTAL LENGTH
                             $= 20 d_b = 20(9/8) = \underline{\underline{22.5''}}$

- DEVELOPMENT LENGTH : - PER ACI 318 SECTION 21.9.2.3

$$L_d = \frac{0.02\, \psi_e\, f_y}{\lambda \sqrt{f_c'}} d_b \quad \text{where} \quad \psi_e = \lambda = 1.0$$

$$= \frac{(0.02)(60000)}{\sqrt{6000}} d_b = 15.5 d_b = 15.5(9/8) = \underline{\underline{17.4''}}$$

$$L_d = 17.4'' < C_m = 32.2''$$

NOTE: DESIGN OF OTHER EDGE
REINFORCEMENT NOT
DONE IS THIS EXAMPLE

∴ BAR WILL BE DEVELOPED
BEFORE REACHING CRITICAL
LENGTH OF $C_m$.

## SECTION 4.8 : DESIGN CHECKS

- SELF-CENTERING TO E.D. RATIO?

$$\phi_r \left[ A_p \left( f_{pm} - 0.5 f_{p,loss} \right) + N_u \right] > A_s \left( f_{sm} + f_{sy} \right)$$

where
$\phi_r = 0.90$
$A_p = 7.81 \text{ in}^2$
$f_{pm} = 227.7 \text{ ksi}$
$f_{p,loss} = 3.6 \text{ ksi}$
$N_u = 241.8^k$

$A_s = 11.06 \text{ in}^2$
$f_{sm} = 89.8 \text{ ksi}$
$f_{sy} = 65 \text{ ksi}$

$$\therefore (0.90) \left[ (7.81) \left[ (227.7) - (0.5)(3.6) \right] + 241.8 \right] > 11.06 (65 + 89.8)$$

$$(0.9)(2006^k) > 1712^k$$

$$1805^k > 1712^k \quad \underline{\underline{OK}}$$
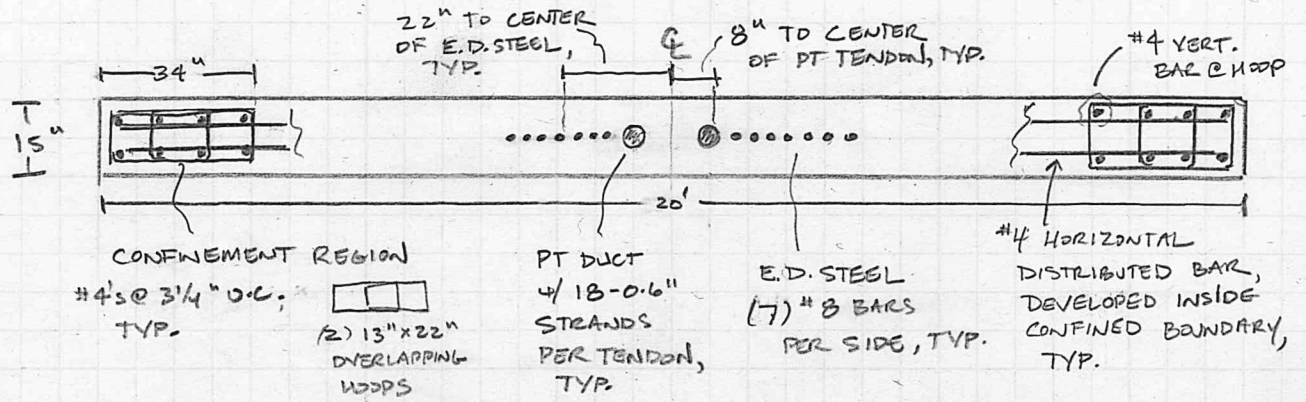
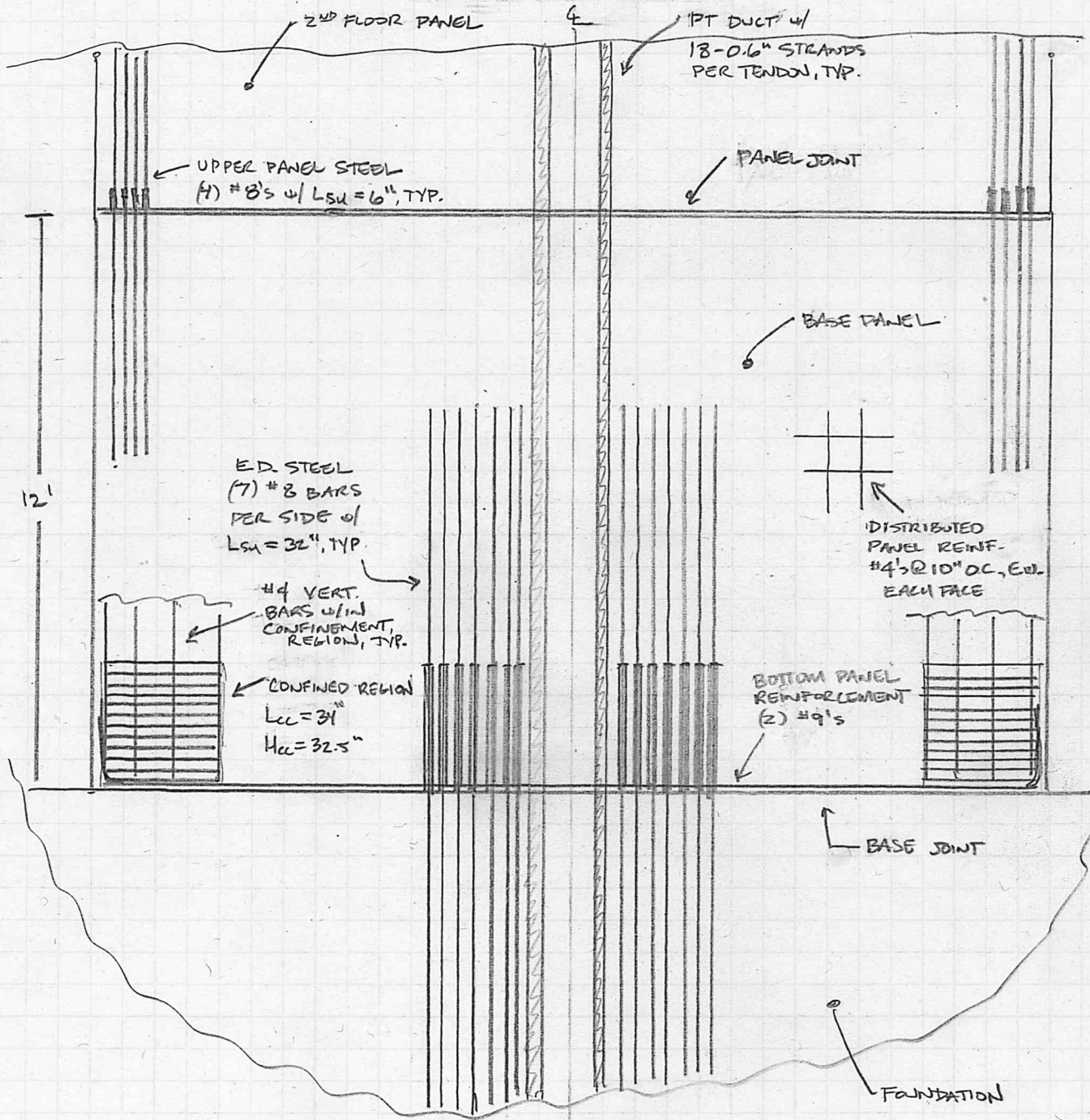- YIELDING OF E.D. BARS :

- @ $A_{uD}$ $\rightarrow$ $f_{sD} = f_{sy}$

$$f_{pD} = 168.5 < 0.95 f_{py} = (0.95)(235) = 223.3 \text{ ksi}$$

$\therefore$ ED BARS WILL YIELD WELL BEFORE
PT STRANDS WILL APPROACH YIELD.

$\underline{\underline{OK}}$

34"

T
15"

22" TO CENTER
OF E.D. STEEL,
TYP.

℄  8" TO CENTER
OF PT TENDON, TYP.

#4 VERT.
BAR @ HOOP

20'

CONFINEMENT REGION
#4's @ 3¼" O.C.
TYP.

(2) 13"×22"
OVERLAPPING
HOOPS

PT DUCT
w/ 18-0.6"
STRANDS
PER TENDON,
TYP.

E.D. STEEL
(7) #8 BARS
PER SIDE, TYP.

#4 HORIZONTAL
DISTRIBUTED BAR,
DEVELOPED INSIDE
CONFINED BOUNDARY,
TYP.

CROSS-SECTIONAL VIEW

2ND FLOOR PANEL

℄

PT DUCT w/
18-0.6" STRANDS
PER TENDON, TYP.

UPPER PANEL STEEL
(7) #8's w/ Lsu = 6", TYP.

PANEL JOINT

12'

E.D. STEEL
(7) #8 BARS
PER SIDE w/
Lsu = 32", TYP.

BASE PANEL

DISTRIBUTED
PANEL REINF-
#4's @ 10" OC, EW.
EACH FACE

#4 VERT.
BARS w/in
CONFINEMENT,
REGION, TYP.

CONFINED REGION
$L_{cc} = 34$"
$H_{cc} = 32.5$"

BOTTOM PANEL
REINFORCEMENT
(2) #9's

BASE JOINT

FOUNDATION

ELEVATION VIEW